Technische Universität München

TUM School of Medicine and Health

Modelling hyperactivated CXCR4 signaling in murine models of indolent and aggressive B cell lymphoma

Richard Ian Lewis

Vollständiger Abdruck der von der TUM School of Medicine and Health der Technischen Universität München zur Erlangung eines

Doktors der medizinischen Wissenschaften (Dr. med. sci.)

genehmigten Dissertation.

Vorsitz: apl. Prof. Dr. Sylvie Lorenzen

Prüfende der Dissertation:

1. Prof. Dr. Ulrich Keller

2. Prof. Dr. Maximilian Reichert

3. apl. Prof. Dr. Katharina Simone Götze

Die Dissertation wurde am 05.04.2024 bei der Technischen Universität München eingereicht und durch die TUM School of Medicine and Health am 05.11.2024 angenommen.

Parts of this work, including the results and figures, have been previously published ahead of this dissertation in:

Lewis R, Habringer S, Kircher M, Hefter M, Peuker CA, Werner RA, Ademaj-Kospiri V, Gäble A, Weber W, Wester H-J, Buck A, Herhaus P, Lapa C, Keller U, *Investigation of spleen CXCR4 expression by [^{68}Ga]Pentixafor PET in a cohort of 145 solid cancer patients*. **EJNMMI Research 11, 77 (2021)** (Lewis, Habringer, et al. 2021)

Lewis R, Maurer HC, Singh N, Gonzalez-Menendez I, Wirth M, Schick M, Zhang L, Isaakidis K, Scherger AK, Schulze V, Lu J, Zenz T, Steiger K, Rad R, Quintanilla-Martinez L, Espeli M, Balabanian K, Keller U*, Habringer S*. *CXCR4 hyperactivation cooperates with TCL1 in CLL development and aggressiveness.* **Leukemia. 35 2895-2905 (2021)** (Lewis, Maurer, et al. 2021)

Content

List of Abbreviations

ABC-type DLBCL	Activated B cells type diffuse large B-cell lymphoma
AKT	Akt kinase / protein kinase B
ALL	Acute lymphocytic leukemia
AML	Acute myeloid leukemia
AMD3100	Drug AMD3100 / Plerixafor
BCR	B-cell receptor
BL	Burkitt's lymphoma
B-NHL	B-cell non-Hodgkin lymphoma
BSA	Bovine serum albumine
BTK	Bruton's tyrosine kinase
C57BL/6J	C57 black 6 J inbred mouse strain
Ca^{2+}	Calcium ion Ca^{2+}
cAMP	Cyclic adenosine monophosphate
CD19	Cluster of differentation 19 / B-lymphocyte antigen CD19
cDNA	Complementary desoxyribonucleic acid (DNA)
CLL	Chronic lymphatic leukemia
CML	Chronic myeloid leukemia
CXCR4	C-X-C motif chomokine receptor 4
CXCR4	Gene coding for C-X-C motif chomokine receptor 4
$CXCR4^{C1013G}$	C-X-C motif chomokine receptor 4 with truncating mutation C1013G
$CXCR4^{C1013G}$	Gene coding for C-X-C motif chomokine receptor 4 with truncating mutation C1013G
CXCL12	C-X-C motif chemokine 12
DAPI	4',6-diamidino-2-phenylindole
DEG	Differentially expressed gene
DLBCL	Diffuse large B-cell lymphoma
DNA	Desoxyribonucleic acid
EDTA	Ethylenediaminetetraacetic acid
EGTA	Ethylene glycol-bis(β-aminoethyl ether)-*N*,*N*,*N*′,*N*′tetraacetic acid)
ERK1	Extracellular-regulated kinase 1
ERK2	Extracellular-regulated kinase 2
Eμ-Myc	Eμ-Myc mouse model
Eμ-TCL1	Eμ-TCL1 mouse model

FACS	Fluorescence-activated cell sorter
FBS	Fetal bovine serum
FDR	False discovery rate
FELASA	Federation of European Laboratory Animal Science Associations
FOXM1	Forkhead box protein M1
GCB-type DLBCL	Germinal center B cells type diffuse large B-cell lymphoma
GPCR	G protein-coupled receptor family
GRK	G protein-coupled receptor kinase
GSEA	Gene set enrichment analysis
H&E	Hematoxylin and eosin stain
Hepes	4-(2-hydroxyethyl)-1-piperazineethanesulfonic acid
HL	Hodgkin lymphoma / Morbus hodgkin
HPV	Human papilloma virus
Ki-67	Antigen Ki-67
MAPK	Mitogen-activated protein kinase
MBL	Monoclonal B-cell lymphocytosis
MDSCs	Myeloid derived suppressor cells
mTOR	mTOR kinase / mammalian target of rapamycin
MYC	MYC gene
MYD88	Myeloid differentiation primary response 88
NaCl	Sodium chloride
NaF	Sodium fluoride
$NaVO_4$	Sodium orthovanadate
NF-κB	Nuclear factor ‘kappa-light-chain-ehancer’ of activated B cells
NHL	Non-Hodgkin lymphoma
NOTCH	NOTCH protein
pAKT	Phosphorylated Akt
pERK	Phosphorylated extracellular-regulated kinase
PI	Propidium iodide
PI3K	Phosphoinositide 3-kinase
PKA	Protein kinase A
PLC	Phospholipase C
PLK-1	Polo-like kinase 1
PMSF	Phenylmethylsulfonyl fluoride

PTLD	Posttransplant lymphoproliferative disorders
Raf	RAF proto-oncogene serine/threonine-protein kinase
Ras	Ras (rat sarcoma virus) GTPase
RIN	RNA integrity number
RNA	Ribonucleic acid
RPMI-medium	Roswell park memorial institute medium
RT	Richter's transformation
SD	Standard deviation
SDS PAGE	Sodium dodecyl sulfate polyacrylamide gel electrophoresi
TCL1	TCL1 gene
Tween	Polysorbate 20
USA	United States of America
WHIM Syndrome	Warts, hypergammaglobulinemia, immunodeficiancy and myelokathexis syndrome
WHO	World Health Organization
WM	Waldenström's macroglobulinemia
WT	Wild type

1 Introduction

1.1 Lymphoid neoplasms / lymphomas

1.1.1 Definition of lymphoid neoplasms / lymphomas

Lymphoid neoplasms are defined as malignant diseases which arise from cells derived from the lymphoid line within the hematopoietic system. These diseases develop from a multitude of different cells of origin, on each step of the physiological development of lymphoid cells. Thus, they represent a biologically and clinically very heterogenous group of entities. The World Health Organization's (WHO) classification is the internationally most recognized form of classification for tumors. The latest updated version of classification for lymphoid neoplasms was published in 2016. Herein the WHO classifies lymphoid neoplasms based on cell of origin into mature B cell neoplasms, mature T cell and NK cell neoplasms, Hodgkin lymphoma, posttransplant lymphoproliferative disorders (PTLD) and histiocytic and dendritic cell neoplasms. For further subclassification morphology, immunophenotype, pathology, genetics, and clinical presentation are considered for diagnosis (Swerdlow et al. 2016).

In a clinical context, the terms lymphoid neoplasm and lymphoma are used close to synonymously and lymphomas are separated into Hodgkin lymphoma (HL) and non-Hodgkin lymphoma (NHL) for further categorization. However, acute lymphocytic leukemia (ALL) and chronic lymphocytic leukemia (CLL) which biologically likewise represent lymphoid malignancies, yet manifest with leukemic infiltration of tumor cells to the peripheral blood, are also frequently referred to separately as leukemias, together with acute myeloid leukemia (AML) and chronic myeloid leukemia (CML). Nonetheless, especially CLL biologically represents a leukemic form of an indolent NHL. Thus, in many recent publications, including the WHO classification, CLL is specified as a low-malignant form of NHL, rather than being grouped with leukemias of myeloid origin (Swerdlow et al. 2016). Due to the large extent of the topic and multitude of different entities, the rest of this thesis will focus on NHL and specifically those NHL of B cell origin (B-NHL), only.

1.1.2 Clinical features and epidemiological significance of B-NHL

Of all lymphoid neoplasms B-NHL account for approximately 80-85% of all NHL cases, while only 15-20% are of T cell or NK cell origin (Armitage et al. 2017). In general, NHL represent approximately 3% of all cancer patients. In the USA, NHL are the overall 7th most common cancer and exhibit the 6th highest mortality rate of all cancers (Thandra et al. 2021).

Prognosis of patients and intent of treatment show great differences between the diverse entities of B-NHL. Thus, regarding their clinical presentation and biology, B-NHL can clinically be separated into aggressive and indolent NHL. In general, aggressive B-NHL typically present with rapid cell growth and high rates of cell turnover as compared to low-malignant / indolent lymphomas. However, due to their relatively high cell turnover and rate of progression, aggressive B-NHL generally exhibit a higher susceptibility to treatment with chemotherapeutics compared to indolent B-NHL. For this reason, in most cases upon diagnosis for most aggressive lymphomas the treatment intention is curative, even in more advanced stages of disease, whereas in the case of advanced stage indolent lymphomas, treatment intention is frequently palliative. However, in some entities, due to critical advances over the last decades and the slow growth of indolent lymphomas, treatment has become somewhat comparable to the management of chronic disease in some patients.

In the following, diffuse large B cell lymphoma (DLBCL) and chronic lymphocytic leukemia (CLL), each as an example of aggressive B-NHL and indolent B-NHL, respectively, will be elaborated in more detail for better understanding of the subsequent results and discussion section.

1.1.3 Diffuse large B cell lymphoma (DLBCL)

Resembling approximately 30-40% of all B-NHL, diffuse large B cell lymphoma is the most common form of aggressive B-NHL, and overall form of lymphoid neoplasm (Li, Young, and Medeiros 2018). Large epidemiological data from the USA show an incidence across all ethnicities of around 7 per 100,000 per year (Li et al. 2015). DLBCL mainly manifests

symptomatically with lymph node enlargement and such symptoms caused by the compression of surrounding structures by this growth. Further patterned symptoms include weight-loss, night sweats and fever, loss of appetite and overall reduction of general well-being.

Biologically DLBCL arises from mature B cells which have undergone germinal center reaction and may develop *de novo* or as a malignant transformation from indolent lymphomas such as follicular lymphoma or CLL. On a molecular and genetic basis, the large majority of DLBCL may be separated into patients harboring tumors with transcriptional signatures more closely related to germinal center B cells (GCB-type) and such more closely resembling activated, post germinal center reaction B cells (ABC-type). Approximately 10-15% of DLBCLs cannot be fully sorted into any of the aforementioned (Pasqualucci and Dalla-Favera 2018).

In principle, upon primary diagnosis intention of therapy for most patients is curative and depending on risk factors success rates of first-line therapies are between 50-90%, with GCB-type tumors exhibiting significantly better prognosis than patients with ABC-type DLBCL (Pasqualucci and Dalla-Favera 2018; Lenz et al. 2008). However, even within GCB-type and ABC-type patient cohorts, subgroups with favorable and unfavorable outcomes exist. Especially those patients with therapy refractory or relapsed DLBCL show unfavorable outcomes and new therapeutic options and better molecular stratification will be needed to more effectively determine prognosis and treatment protocols and overcome these adversities in future (Susanibar-Adaniya and Barta 2021).

1.1.4 Chronic lymphocytic leukemia (CLL)

CLL is the most common form of leukemia in the western hemisphere (Siegel et al. 2022) and most frequently diagnosed in elderly patients above the age of 60 (Delgado and Villamor 2014). Recurring symptoms may include lymphocytosis, lymphadenopathy, hepatosplenomegaly, weight loss, night sweats, exhaustion, and a reduction of overall fitness. Biologically, as mentioned above, CLL represents a mature B cell neoplasm / B-NHL which clinically manifests

with a leukemic dissemination to the peripheral blood. In recent years it has moreover become clear that CLL almost always develops from monoclonal B-cell lymphocytosis (MBL) (Landgren et al. 2009). The transition from MBL to CLL is fluid. By definition, CLL is distinguished from MBL by a lymphocyte count of > 5000/µl and/or symptoms of disease in combination with the presence of small morphologically mature lymphocytes (Swerdlow et al. 2016). Multiple studies show the prevalence of MBL and CLL increases with age of patients and approximately one to two per cent of patients per year with MBL progress to CLL requiring treatment (Rawstron et al. 2008; Strati and Shanafelt 2015). This also helps to understand why tumor cells of CLL are genetically highly heterogeneous, as many different genetic mutations may accumulate over the rather long period of disease development. However, some mutations/genetic aberrations occur with an increased frequency and include deletions 13q14, 11q22 and 17p13, trisomy 12 as well as a multitude of mutations affecting major signaling pathways such as NOTCH, MAPK, NF-κB and p53 (Gaidano and Rossi 2017).

Clinically, apart from blood smears and lab results, flow cytometry plays an essential role in the diagnosis of CLL. In flow cytometry, CLL cells are defined as a clonal population co-expressing surface markers of mature B cells (CD19, CD20 and CD23) together with the T cell marker CD5 (Hallek 2019).

1.2 The C-X-C motif chemokine receptor (CXCR4) in B-NHL

1.2.1 Overview over chemokine receptors and their role in cancer

Chemokines are a subgroup of cytokines - small signaling molecules secreted by cells - which are distinguished from other cytokines by their function to induce a chemotactic reaction, a concentration dependent directional movement. Chemokines and their receptors play an essential role in the pathology of many diseases, such as asthma, multiple sclerosis, rheumatoid arthritis, HIV/AIDS and many more (Proudfoot 2002). They bind to a specific group of receptors on a vast set of different effector cells. These chemokine receptors are all part of the G protein-coupled receptor family (GPCR) and can be distinguished by their structure into

different groups: CC chemokine receptors, CXC chemokine receptors, C chemokine receptors and CX3C chemokine receptors. Most of these bind multiple chemokines, with only some restricted to a single chemokine. Overall there are approximately 50 chemokines and 20 chemokine receptors that have been described (Proudfoot 2002). As in other diseases, in cancer, dysregulation of chemokine signaling has been related to cancer progression and prognosis. Chemokines here play an integral and multifaceted role in the tumor biology of many different cancers, such as tumor growth and proliferation, metastasis and complex interactions within the tumor microenvironment (Do, Lee, and Cho 2020). Understanding chemokine signaling and therapeutically targeting dysregulated signaling have thus become an interesting field of study in many pathologies, especially cancer.

1.2.2 CXCR4 – Its physiological function and downstream signaling targets

C-X-C-motif chemokine receptor 4 (CXCR4) is a G-protein-coupled receptor with pivotal functions in hematopoietic stem cell homeostasis, myelopoiesis, lymphopoiesis, and homing of immune cells towards its ligand C-X-C motif chemokine 12 (CXCL12) (also known as stromal cell-derived factor 1 (SDF-1)) (Nagasawa et al. 1996; Freitas et al. 2017; Ding and Morrison 2013). CXCR4 is further essential for cardiovascular development and morphogenesis of different areas of the central nervous system (Doring et al. 2014; Odemis et al. 2005; Ma et al. 1998). The importance of CXCR4 for the aforementioned multitude of different systems is underscored by the fact, that $CXCR4^{-/-}$ mice die perinatally (Ma et al. 1998). When CXCL12 binds to CXCR4, it induces a multitude of G-protein-dependent and -independent signaling pathways including PI3K/AKT/mTOR, Ras/Raf/MAPK/ERK, PLC/Ca2+ and cAMP/PKA signaling (Figure 1) (Scala 2015). After binding of CXCL12, as a form of self-regulation, CXCR4 is phosphorylated at the C-terminus by G protein-coupled receptor kinase (GRK) and rapidly internalized after binding of the protein arrestin to the then phosphorylated C-terminus (Figure 3) (Busillo and Benovic 2007). CXCR4 is expressed at different stages of B cell development and critical for homeostasis of different B cell compartments as well as humoral immunity (Allen

et al. 2004) and moreover indispensable for the organization of dark and light zones in germinal centers (Allen et al. 2004). Furthermore, data indicates an intense receptor cross talk of CXCR4 with the B cell receptor (BCR) (Becker et al. 2017) and some data even suggests CXCR4 may promote B cell viability under hypoxic conditions (Jang et al. 2021). Hence, CXCR4 expression is not surprisingly known to be highest on B cells, as compared to any other tissue in the human body, as data from the Human Protein Atlas confirms (Figure 2) (Uhlen et al. 2015).

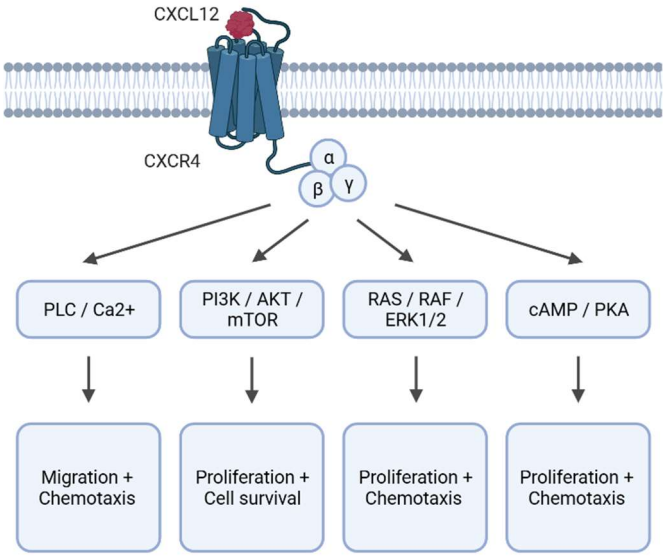

Figure 1. Downstream targets of CXCR4

Upon binding of CXCL12, multiple pathways are activated in a G-protein and G-protein independent manner. CXCR4 modulates migration and chemotaxis via PLC/Ca2+ signaling, as well as proliferation and cell survival via the PI3K/AKT/mTOR pathway. Furthermore, proliferation and chemotaxis are mediated through RAS/RAF/ERK1/2 signaling as cAMP and PKA. Adapted from Scala et al., 2015 (Scala 2015). Created using BioRender.com.

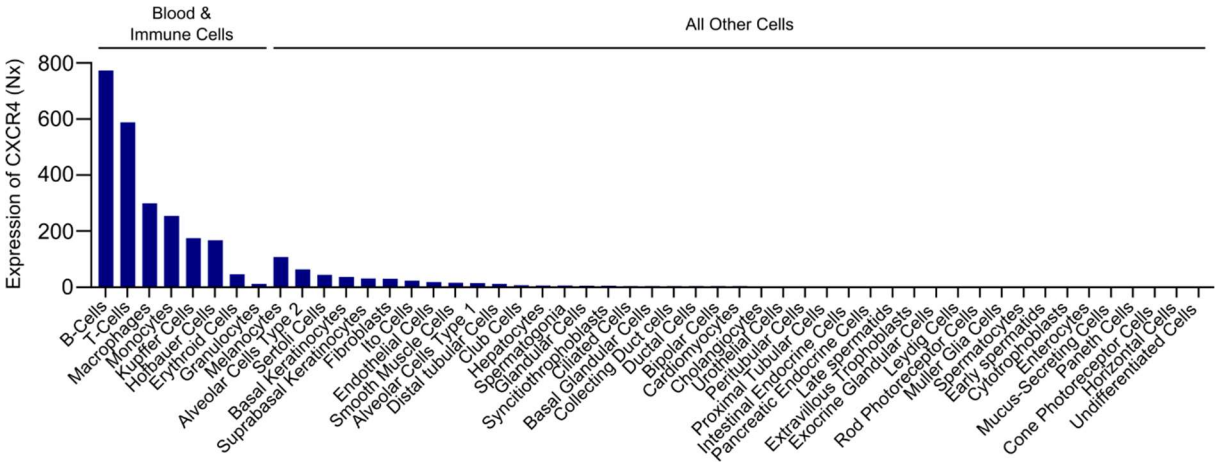

Figure 2. Physiologic expression of CXCR4 in different tissues

Comparison of physiologic expression levels of CXCR4 mRNA among different cell types obtained from the Human Protein Atlas, shown as Nx expression scores of single cell transcriptomic data (Uhlen et al. 2015).

1.2.3 CXCR4 in the context of oncology

CXCR4 has been shown to be overexpressed on malignant cells, as compared to non-malignant control tissue and furthermore to be associated with adverse prognosis in many different types of cancer (Zhao et al. 2015; Su et al. 2005; Speetjens et al. 2009; Muller et al. 2001; Scala et al. 2005), which suggests a role of CXCR4 as a tumor driver. Furthermore, extensive data links CXCR4 with crucial functions within tumor supportive microenvironments, metastasis, and dissemination of tumors and has been reviewed before (Burger and Kipps 2006; Balkwill 2004; Scala 2015; Tulotta et al. 2019). Summarizing, tumor cells utilize the CXCR4/CXCL12 axis to directly drive tumor growth as well as indirectly drive tumorigenesis by promoting angiogenesis. Furthermore, dysregulation of CXCR4 signaling within tumor cells facilitates homing to immune evasive microenvironments. E.g., suppression of anti-tumor immunity is, along with other complex mechanisms, majorly regulated through immunosuppressive myeloid-derived suppressor cells (MDSCs) and tumor infiltrating MDSCs are known to express high levels of CXCR4 and to migrate towards a CXCL12 gradient (Benedicto, Romayor, and Arteta 2018; Jiang et al. 2019).

1.2.4 CXCR4 in hematopoietic malignancies and especially B-NHL

Given the many crucial roles in the hematopoietic system and its known association with adverse outcomes in many different cancer entities, especially hematopoietic malignancies, the role of CXCR4 has been extensively studied in lymphomas and leukemia. Therein, molecularly targeted imaging studies, including those from our own group, have revealed enhanced CXCR4 expression in various B cell non-Hodgkin lymphomas (B-NHL) (Wester et al. 2015; Mayerhoefer et al. 2018; Herhaus et al. 2020). Also, in the aforementioned entities CLL and DLBCL, clinical data hints towards a possible role of CXCR4 as a tumor driver, as CXCR4 expression levels have been associated with adverse prognosis (Moreno et al. 2015; Ganghammer et al. 2016) (also refer to 3.4.1 and 3.5.1). Here it is noteworthy, that in CLL specifically, CXCR4 was demonstrated to be overexpressed and involved in multiple interactions of CLL cells with the respective microenvironment (Burger, Burger, and Kipps 1999; Burger et al. 2000; Mohle et al. 1999). E.g., CLL cells are directly protected from apoptosis by the CXCR4/CXCL12-axis as nurse-like cells (tumor associated macrophages) secrete CXCL12, which directly inhibits apoptosis via MAPK/ER1/2-signaling (Burger et al. 2000). In DLBCL, CXCR4 expression is associated with bone marrow infiltration (Recasens-Zorzo et al. 2019), which itself is linked to adverse prognosis. Also, CXCR4 upregulation is an indicator of susceptibility to B cell receptor (BCR) and PI3K inhibitor treatment in DLBCL (Chen et al. 2020) and *in vitro* the CXCR4 antagonist plerixafor synergistically increased the anti-proliferative/pro-apoptotic effect of rituximab on DLBCL cells (Reinholdt et al. 2016). Similarly, *in vivo* data demonstrated enhanced efficacy of rituximab treatment in B-NHL xenograft models (Beider et al. 2013).

1.2.5 Truncating mutations of CXCR4 in lymphoma and WHIM syndrome

There are known frequently recurring mutations, which truncate the C-terminus and lead to increased activity of CXCR4 signaling, upon binding of the receptor's ligand CXCL12 by impairing receptor desensitization and internalization without reduced overall receptor

expression levels (compare with Figure 3) (Haribabu et al. 1997; Hernandez et al. 2003; Balabanian et al. 2005). Such mutations have most frequently been studied in patients diagnosed with Waldenström's macroglobulinemia (WM) or warts, hypogammaglobulinemia, immunodeficiency and myelokathexis syndrome (WHIM syndrome).

Waldenström's macroglobulinemia is an indolent lymphoma derived from plasma cells and almost all tumors have somatic mutations of MYD88. Approximately 25-30% of all patients with WM further carry truncating mutations of CXCR4. Those patients harboring somatic CXCR4 mutations are associated with unfavorable outcomes (Varettoni et al. 2017).

WHIM syndrome is a rare genetic disorder etiologically caused in almost all cases by nonsense or frame shift mutations causing a truncated CXCR4 protein and may be inherited autosomal dominantly or occur as a *de novo* mutation (Hernandez et al. 2003). Clinically WHIM syndrome manifests as an immunodeficiency caused by an impaired release of mature hematopoietic cells to the peripheral blood, causing a retention of these cells in the bone marrow (myelokathexis) and thus leading to peripheral neutropenia and lymphopenia and associated hypogammaglobulinemia with congenital recurrent infections. In many cases of WHIM syndrome especially immune reactions to viruses of the human papilloma virus (HPV) family are impaired. Hence, such patients may present with excessive HPV-associated warts (Heusinkveld et al. 2019).

1.3 *CXCR4^{C1013G}* - Functionally modelling activated CXCR4 signaling *in vivo*

Since the discovery of WHIM syndrome as well as recurring mutations of CXCR4 in hematopoietic malignancies, such as WM, there has been further interest in studying the consequences of activated CXCR4 signaling *in vivo*. A team around Karl Balabanian for this reason created the genetically engineered mouse model *CXCR4^{C1013G}*. Transgenic mice express CXCR4 with a truncated C-terminus caused by a nonsense mutation at position 1013, equivalent to the effects of the human mutations in WM and WHIM syndrome mentioned above. This results in an aforementioned CXCR4 protein lacking critical phosphorylation sites,

required for G protein-coupled receptor kinase (GRK) and arrestin mediated internalization and degradation of CXCR4 upon binding of CXCL12 (Figure 3) (Balabanian et al. 2012; Busillo and Benovic 2007). Hence, the *CXCR4*^{C1013G} model represents a pivotal tool to investigate the physiological and pathological functions of CXCR4 signaling.

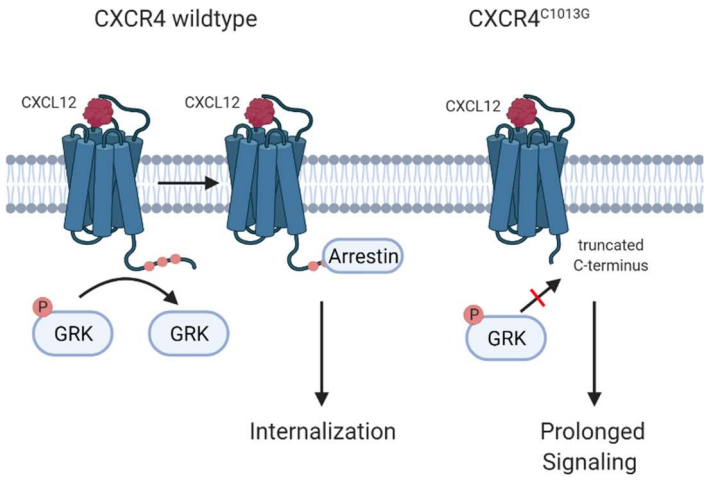

Figure 3. The murine model *CXCR4*^{C1013G} of activated CXCR4 signaling
Upon binding of CXCL12, G protein-coupled receptor kinases phosphorylate phosphorylation sites on the C-terminus of CXCR4. Consecutively, arrestin binds and CXCR4 is internalized and degraded. *CXCR4*^{C1013G} exhibits a truncated C-terminus lacking the necessary phosphorylation sites for GRK and therefore cannot be internalized and effectively causes prolonged signaling upon binding of CXCL12. Adapted from Busillo et al, 2007 (Busillo and Benovic 2007). Created using BioRender.com.

1.4 Modelling B cell lymphoma in murine models

1.4.1 Functionally modelling CLL / indolent lymphoma – *Eμ-TCL1*

To model indolent lymphoma, different murine models exist. One of the most well studied is the *Eμ-TCL1* transgenic murine model in which B cell-directed TCL1 expression drives spontaneous development of a CLL-like disease. This was achieved by placing the oncogene TCL1/TCL1A under control of a V_H promotor immunoglobulin heavy chain (IgH)-Eμ enhancer and first described by Bichi and colleagues. Clinically, transgenic mice present with extensive hepatosplenomegaly with a median overall survival of approximately one year (Bichi et al. 2002). Since its establishment it has become the most used murine model of high-risk CLL /

indolent lymphoma (Kohlhaas et al. 2021; Knittel et al. 2017). In the context of CXCR4 and CLL, in humans Tcl1 has been shown to be involved directly in CLL pathogenesis (Pekarsky et al. 2008). Furthermore, using the *Eμ-TCL1* model, Chen et al. e.g., showed that downregulation of surface CXCR4 expression and inhibition of CXCR4 downstream signaling in CLL cells can be observed upon treatment with the Bruton's tyrosine kinase (BTK) inhibitor ibrutinib (Chen et al. 2016), which is currently the first-line standard of CLL treatment (Andritsos et al. 2019). Moreover, Kashyap et al. demonstrated promising anti-tumor activity applying a CXCR4 antibody to patient derived CLL cells *in vitro* and in murine xenografts (Kashyap et al. 2017). Hence, there may be a potential of targeting CXCR4 in CLL patients and data from CLL patients demonstrates its potential of mobilizing CLL cells (Andritsos et al. 2019).

1.4.2 Functionally modelling aggressive B cell lymphoma – *Eμ-Myc*

Likewise to indolent lymphoma models, models to study aggressive B cell lymphoma *in vivo* exist. The *Eμ-Myc* model was first published in the 1980s and has since been an indispensable tool for the investigation of lymphomagenesis and -biology, especially of aggressive B cell lymphomas. Similarly, to the *Eμ-TCL1* model, in this transgenic model the transcription factor c-Myc was brought under control of the immunoglobulin heavy chain (IgH) enhancer, hence representing a tool for B cell specific enhanced MYC activity. Mice harboring the Eμ-Myc transgene develop lethal lymphoma within half a year of age with almost complete penetrance (Adams et al. 1985; Harris et al. 1988). Even though *Myc* translocation is most associated with Burkitt's lymphoma (BL), as almost all BL patients present with *Myc* translocations (Molyneux et al. 2012), MYC is also known to be highly expressed, mutated or translocated in a significant number of DLBCL patients. Furthermore, those DLBCL patients with high MYC expression were associated with unfavorable outcomes (Reddy et al. 2017). In previous studies with DLBCL patients MYC and CXCR4 expression was positively associated and patients with high CXCR4 expression were more likely to present with bulky tumor, high Ki67 index and high levels of MYC expression (Chen et al. 2015).

1.5 Objectives of the study

As described above, many previous studies have shown CXCR4 to be frequently mutated or highly expressed in different hematopoietic malignancies. Most commonly, truncating mutations of *CXCR4* can be found in Waldenström's macroglobulinemia, with approximately 25% of all patients harboring mutations of *CXCR4*. However, recurring mutations of *CXCR4* can also be found in a fewer, but significant number of DLBCL patients (Reddy et al. 2017; Chapuy et al. 2018) (also refer to 3.5.1). In CLL, recent data shows CXCR4 is expressed especially high on proliferating CLL cells and higher levels of CXCR4 expression can be found in patients with progressive disease (Friedman et al. 2023). In line with this, data showed mutations in regulatory regions of *CXCR4* in patients with aggressive transformation of CLL (Richter's syndrome (RT)) (Klintman et al. 2021). Moreover, in both diseases higher CXCR4 mRNA expression is linked to an unfavorable outcome, hinting towards a major role of CXCR4 and its downstream targets for these diseases (also refer to 3.4.1 and 3.5.1) (Aguirre-Gamboa et al. 2013). It is however not resolved if and how these affect CXCR4 pathway activity and disease progression. Of especial importance, to this point no study has elaborated the effects of activated CXCR4 signaling *in vivo.*

Hence, in this study we aimed to hyperactivate CXCR4 signaling in two very commonly used murine models of aggressive B cell lymphoma (*Eμ-Myc*) and indolent lymphoma/chronic lymphocytic leukemia (*Eμ-TCL1)*. To achieve CXCR4 hyperactivation we aimed to crossbreed these tumor models with a further transgenic model harboring $CXCR4^{C1013G}$. As elaborated above, mice harboring this transgene express CXCR4 with a truncated C-terminus missing critical phosphorylation sites for CXCR4 internalization, thus consequently leading to enhanced downstream signaling of CXCR4.

Through the establishment of these two new models - *Eμ-Myc;*$CXCR4^{C1013G}$ and *Eμ-TCL1;*$CXCR4^{C1013G}$ - we aimed to shed light on the role of CXCR4 signaling in pathogenesis of B cell lymphoma. For this reason, we aimed to collect clinical data, histopathology, immunohistochemistry, and flow cytometry data of these mice and closely characterize these

new models in a first step. In a second step we planned to employ large-scale RNA-sequencing of premalignant and malignant B cells to further elaborate the transcriptomic effects of activated CXCR4 signaling on B cells. And lastly, in a third step we aimed to correlate our generated transcriptomic data with clinical data sets and investigate the effects of generated transcriptional signatures on clinical outcomes of patients in a translational approach to further validate our findings (Figure 4).

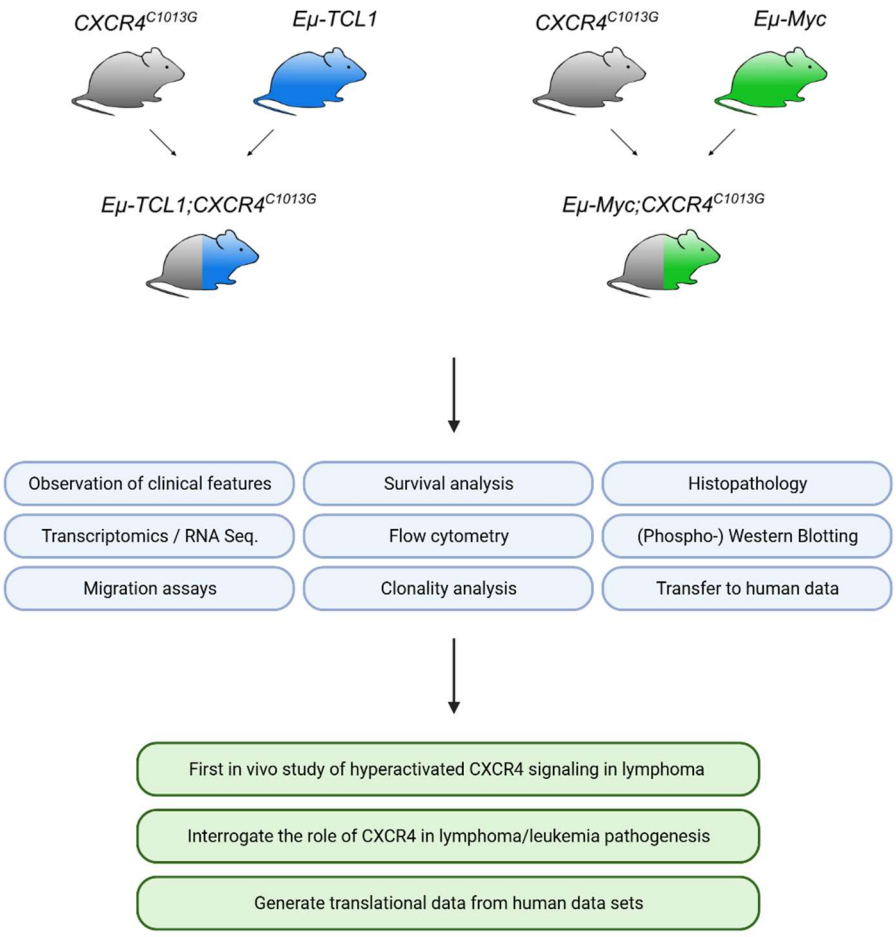

Figure 4. Objectives of the study

Illustration of the generation of *Eμ-TCL1;CXCR4*^{C1013G} and *Eμ-Myc;CXCR4*^{C1013G} by crossbreading *CXCR4*^{C1013G} mice with *Eμ-TCL1* and *Eμ-Myc* mice, respectively, the techniques used in the study and the aims. Generated using BioRender.com.

2 Materials and Methods

2.1 Materials

2.1.1 Consumables, chemicals, and reagents

2-Mercaptoethanol, 50 mM	ThermoFisher Scientific
6 well-plates	Greiner Bio-One GmbH
12 well-plates	Greiner Bio-One GmbH
Acetic acid	Carl Roth GmbH
ACK Lysis buffer	ThermoFisher Scientific
Acrylamide/Bis-acrylamide solution [30%]	Carl Roth GmbH
Agarose NEEO ultra-quality Roti®Garose	Carl Roth GmbH
Ammonium persulfate (APS)	Sigma-Aldrich
Aprotinin Roth Bovine Serumalbumin (BSA)	Sigma-Aldrich
BD PlastipakTM 1 ml Sub-Q insulin syringes	BD Biosciences
Blood lancets supra	Megro GmbH & Co KG
Bromphenol blue	Sigma-Aldrich
Cell culture dishes	TPP
Cell culture flasks T125, T75, T25	Greiner Bio-One GmbH
Cell strainers 100 µm	BD Bioscience
Combitips advanced® 10 ml	Eppendorf AG
Complete Mini (Protease Inhibitor Cocktail)	Roche
CoolCell™ FTS30 Freezing container	Sigma Aldrich
Cryo TubesTM	Corning
Deionized water	B. Braun Melsungen AG
Dimethyl sulfoxide (DMSO)	Serva
DiscarditTM II disposable syringes	BD Biosciences
dNTP Mix, 10 mM	Fermentas
Dithiothreitol (DTT)	Sigma-Aldrich

Dulbecco’s phosphate buffered saline (DPBS)	ThermoFisher Scientific
Dulbecco’s Modified Eagle Medium (DMEM)	ThermoFisher Scientific
Eppendorf tubes, 1.5 ml and 2 ml	Sarstedt
Ethanol	Carl Roth GmbH
Ethidiumbromid (EtBr) solution [1%]	Carl Roth GmbH
Ethylendiamintetraacetate (EDTA)	Carl Roth GmbH
FACS tubes, 5 ml	BD Biosciences
Fetal Calf Serum (FCS)	PAA Laboratories GmbH
Filter vacuum driven bottle top filter	Millipore
Formalin solution [10%]	Sigma-Aldrich
Glycine	Carl Roth GmbH
Hank’s Balanced Salt Solution, 10x (HBSS)	ThermoFisher Scientific
4-(2-hydroxyethyl)-1-piperazineethanesulfonic acid (HEPES)	ThermoFisher Scientific
Isoflurane CP® [1 mg/ml]	CP-Pharma
Isopropanol	Carl Roth GmbH
Leupeptin AppliChem Lipofectamin® 2000	ThermoFisher Scientific
L-Glutamin, 200 mM	ThermoFisher Scientific
MACS LS Columns	Miltenyi Biotech
Magnesium chloride (MgCl2)	Sigma-Aldrich
Methanol	J.T. Baker
Microvette tubes	Sarstedt
Oligo(dT)12-18 Primer	ThermoFisher Scientific
Osteosoft®	Sigma-Aldrich
PCR-Strips Single Cap 8er-Soft-Strips 0.2 ml	Biozym Scientific GMBH
Penicillin/Streptomycin (Pen/Strep)	ThermoFisher Scientific
Phenylmethylsulphonyl fluoride (PMSF)	Sigma-Aldrich

Phosphate buffered saline (PBS)	ThermoFisher Scientific
Pipette tips	Sarstedt
Pipette filter tips	Starlab
S-Monovette®, EDTA	Sarstedt
Skim milk powder	Sigma-Aldrich
Sodium dodecylsulfate (SDS)	Sigma-Aldrich
Sodium chloride (NaCl)	Carl Roth GmbH
Sodium fluoride (NaF)	Sigma-Aldrich
Sodium orthovanadate (Na3VO4)	Sigma-Aldrich
Sodium tetraborate decahydrate (Borax)	Sigma-Aldrich
Sterican® disposable needles	B. Braun Melsungen AG
N,N,N′,N′-Tetramethylethan-1,2-diamin (TEMED)	Sigma-Aldrich
Tris(hydroxymethyl)aminomethane (TRIS)	Carl Roth GmbH
Trypan blue stain solution [0.4%]	ThermoFisher Scientific
Trypsin-EDTA-Solution, 10x	ThermoFisher Scientific
Tween 20	Sigma-Aldrich
Ultra Pure Distilled Water (Aqua dest.)	ThermoFisher Scientific
Whatman® Paper	Biometra

2.1.2 Antibodies

Epitope:	Clone:	Fluorochrome:	Manufacturer:	Ref. Nr:
CD3e	(145-2C11)	PerCP-Cyanine5.5	Invitrogen	35-0031-82
CD4	GK1.5	PE-Cy7	Invitrogen	25-0041-82
CD5	53-7.3	eFluor 450	Invitrogen	48-0051-82
CD8a	53-6.7	PE	BD Biosciences	553032
CD19	eBio1D3 (1D3)	PerCP-Cyanine5.5	Invitrogen	35-0193-82
CD19	eBio1D3 (1D3)	eFluor 450	Invitrogen	48-0193-82
CD19	eBio1D3 (1D3)	PE-Cy7	Invitrogen	25-0193-82
CD19	eBio1D3 (1D3)	FITC/Alexa Fluor 488	Invitrogen	11-0193-82
CD19	eBio1D3 (1D3)	PE	Invitrogen	12-0193-82
CD19	eBio1D3 (1D3)	APC	Invitrogen	17-0193-82
CD19	eBio1D3 (1D3)	APCcy7/APC-eFluor 780	Invitrogen	47-0193-82
CD21/35	Clone 7G6 (RUO)	PE	BD Biosciences	552957
CD23	B3B4	PE-Cy7	Invitrogen	25-0232-82

CD25	PC61.5	PE-Cyanine5	Invitrogen	15-0251-82
CD38	90	APC	Invitrogen	17-0381-81
CD45	30-F11	APC	Invitrogen	17-0451-82
CD45	30-F11	APCcy7/APC-eFluor 780	Invitrogen	47-0451-82
CD45	30-F11	PE	Invitrogen	12-0451-82
CD45	30-F11	PE-Cy5	Invitrogen	15-0451-82
CD45	30-F11	PE-Cy5.5	Invitrogen	35-0451-82
CD45	30-F11	PE-Cy7	Invitrogen	25-0451-82
CD45	30-F11	ef450	Invitrogen	48-0451-82
CD45	30-F11	FITC/Alexa Fluor 488	Invitrogen	11-0451-82
CD45R (B220)	RA3-6B2	APCcy7/APC-eFluor 780	Invitrogen	47-0452-80
CD45R (B220)	RA3-6B2	PE-Cy7	Invitrogen	25-0452-82
CD80	16-10A1	PE	Invitrogen	12-0801-81
CD93	AA4.1	PerCP-Cyanine5.5	Invitrogen	45-5892-82
CD95	Jo2	PE-Cy7	BD Biosciences	557653
CD117 (c-Kit)	2B8	APCcy7/APC-eFluor 780	Invitrogen	47-1171-82
CD138	Clone 281-2 (RUO)	PE	BD Biosciences	553714
CD184 (CXCR4)	2B11	FITC/Alexa Fluor 488	Invitrogen	53-9991-80
CD184 CXCR4	2B11	APC	Invitrogen	17-9991-82
GL7	GL7	PerCP-Cyanine5.5	Biolegend	144609
IgD	11-26c	eFluor 450	Invitrogen	48-5993-82
IgG2b kappa	eB149/10H5	APC	Invitrogen	17-4031-82
IgM	eB121-15F9	PE	Invitrogen	12-5890-82
IgM	II/41	APC	Invitrogen	17-5790-82
MHCII	M5/114.15.2	APCcy7/APC-eFluor 780	Invitrogen	47-5321-80

Table 1: All antibodies used for flow cytometry in this study.

Epitope:	**Clone:**	**Manufacturer:**	**Reference Number:**
CD19	(LE-CD19)	Zytomed	MSK043-05
Ki67	-	abcam	ab15580
Pax5	-	abcam	ab109443
TCL-1	-	BIOZOL	ABX201114
B220	(RA3-6B2)	BD Pharmingen	550286

Table 2: All antibodies used for immunohistochemistry in this study.

Target:	**Manufacturer:**	**Reference Number:**
Akt	Cell Signaling	9272
Phospho-Akt (Ser473)	Cell Signaling	9271
p44/42 MAPK (Erk1/2)	Cell Signaling	9102
Phospho-p44/42 MAPK (Erk1/2) (Thr202/Tyr204)	Cell Signaling	9101
beta-Actin	Sigma-Aldrich	A1978

Table 3: All antibodies used for immunoblotting in this study.

2.1.3 Technical Equipment

Analytical balance Kern 770	Kern & Sohn GmbH
Automated immunostrainer	Ventana Medical Systems Inc.
Axioskop 2 plus microscope	Carl Zeiss AG
Cage systems IVC Tecniplast Cell incubator	Heraeus
CyAn ADP Lx P8	Beckman Coulter
Electrophoresis chamber	Bio-Rad Laboratories
Elphoscan ES2000 Plus device	Sarstedt
FACSAria™ III cell sorter	BD Biosciences
Fridges and lab freezers	Liebherr Hausgeräte GmbH
Dissecting instruments	Fine Science Tools GmbH
Epson Perfection 4990 Photo Scanner	Epson
GelDoc System Universal Hood II	Bio-Rad Laboratories
Glas ware Labware	SCHOTT AG
Infrared lamp	Breuer GmbH
ProgRes C10 plus microscope camera	Jenoptic AG
Liquid nitrogen tank	Biosafe®
MACS MultiStand	Miltenyi Biotec
Microfuge	Heraeus
Biofuge fresco Heraeus Microfuge	Heraeus
Megafuge 16 RS Heraeus Microfuge	Heraeus
Multifuge 3s	Heraeus
Microfuge MiniSpin	Eppendorf AG
Microcentrifuge Mikro22R	Hettich Zentrifugen
MidiMACSTM Separator	Miltenyi Biotec
Multi-Channel Pipettes Research Plus®	Eppendorf AG
NanoDrop 2000c	ThermoFisher Scientific

Neubauer hemocytometer	Paul Marienfeld GmbH
OPTIMAX X-ray Film Processor	PROTEC GmbH & Co KG
pH-meter SevenEasyTM	Mettler Toledo
Pipetboy	Integra Biosciences AG
Pipettes Research Plus®	Eppendorf AG
Power Pac 200	Bio-Rad Laboratories
Power Pac P25T	Biometra
Precision balance Kern EG 2200-2NM	Kern & Sohn GmbH
Repeater 4780 and M4	Eppendorf AG
qRT-PCR Cycler (ABI Prism 7900 HT)	Applied Biosystems
Safety cabinet HERAsafe® HSP18	Heraeus
Scil Vet ABC Blood Counter	ScilAnimal Care
SDS-Gelelectrophoresis chamber	Biometra GmbH
Smart Spec PlusTM Spectrophotometer	Bio-Rad Laboratories
SONOPLUS Homogenisator (HD 2070)	Bandelin electronic
Sunrise Microplate Reader Tecan	Life Sciences
Thermal Cycler VeritiTM 96-well	ThermoFisher
Scientific Thermal Cycler BIOER Gene Touch	Biozym Scientific GmbH
Thermomixer comfort	Eppendorf AG Vortex
Water bath	Memmert
Water bath SUB for Instruments Wet-transfer	Bio-Rad Laboratories

2.1.4 Software

Adobe Photoshop CS6	Adobe Inc.
Excel	Microsoft Office
EndNote 20	Clarivate Analytics
FlowJo Version 10	Tree Star Inc.

GraphPad Prism Version 7	GraphPad Inc
Inkscape Version 0.92	Inkscape Community
Word	Microsoft Office

2.2 Methods

The methods have been previously published in the main publication of this thesis (Lewis, Maurer, et al. 2021). However, they have been adapted to at points to give more specifications and detail for this thesis.

2.2.1 Animal experiments

Genotyping was performed as previously described (Balabanian et al. 2012; Bichi et al. 2002; Adams et al. 1985). All analyses included heterozygous female and male animals on a C57BL/6J background. Animal caretakers, but not researchers performing experiments were blinded for genotypes. Mice were allocated to groups based on genotype; thus, no randomization was performed. All animal experiments were performed in accordance with Federation of European Laboratory Animal Science Associations (FELASA) guidelines and with permission of the respective authorities (Regierung von Oberbayern, Munich, Germany & Landesamt für Gesundheit und Soziales, Berlin, Germany).

2.2.1.1 The *CXCR4^{C1013}* mouse model

The *CXCR4^{C1013G}* mouse model was obtained as a gift by the group of Karl Balabanian and Marion Espeli. These mice express a genetically modified version of CXCR4 with a truncated C-terminus induced by a nonsense mutation at position 1013 (Balabanian et al. 2012).

2.2.1.2 The *Eμ-TCL1* mouse model

The *Eμ-TCL1* mouse model was obtained from Jackson Laboratory. These mice harbor a transgene, in which the oncogene TCL1/TCL1A was brought under control of immunoglobulin

heavy chain (IgH)-Eμ enhancer and is thus expressed B cell specifically. Clinically, transgenic mice develop a slowly proliferating lymphoproliferative disease mimicking human indolent B cell lymphoma / CLL (Bichi et al. 2002).

2.2.1.3 The *Eμ-Myc* mouse model

The *Eμ-Myc* mouse model was obtained from Jackson Laboratory. These mice have been genetically modified to induce B cell specific overexpression of the transcription factor c-Myc, by bringing it under control of the immunoglobulin heavy chain (IgH) enhancer. Hence, transgenic mice develop an aggressive B cell lymphoma disease, beginning from a young age of only a few weeks (Adams et al. 1985; Harris et al. 1988).

2.2.2 Flow cytometry

2.2.2.1 Preparation of samples and protocol for flow cytometry

Organs were collected and kept on ice in HF2 buffer until further processing. After collection of all organs, bones were flushed with cold HF2 buffer. Spleens were mashed through a 70μm cell strainer. Extracted bone marrow was resuspended repeatedly and flushed through a 30μm Syringe Falcon to achieve single cell suspensions. These suspensions were centrifuged at 350g for 5 minutes at room temperature. For red blood cell depletion, the supernatant was discarded, and pellets resuspended in ACK lysis buffer and consequently incubated for 5 minutes at room temperature. To fully remove residual ACK lysis buffer, cells were washed once with HF2 and then resuspended in HF2 for counting. Each $1x10^6$ cells per sample were separated for staining with flow cytometry antibodies. To achieve most efficient binding of antibodies, the consequent staining was performed in flow cytometry buffer (PBS containing 0.5% BSA) for 45 minutes in the dark on ice in a volume of 50-100μl. After staining, 2ml of flow cytometry buffer were added to each sample and samples were centrifuged at 350g for 5 minutes. Cells were then resuspended in 200-400μl of staining buffer to perform flow cytometry. To exclude dead cells from further analyses, dependent on the interaction profile of

the fluorochromes in each stain, live dead-staining was performed by adding PI, or DAPI to the flow cytometry buffer used during flow cytometry. In some stains, alternatively Invitrogen Fixable Aqua Dead Cell Stain Kit was used prior to the staining with antibodies according to the manufacturer's protocol. The actual flow cytometry was performed on a Cyan ADP LX P8 or a CytoFLEX S flow cytometer.

2.2.2.2 Flow cytometry gating strategies for immunophenotyping

After data collection, the analysis was performed with FlowJo™ Version 10.6.0 software. Hereby all samples were primarily gated visually in a first step to exclude events of very low side scatter and forward scatter. In a second step, to exclude doublets, events were plotted by forward scatter height against forward scatter area and outliers were excluded. In all samples, in a third step, plotting of the respective fluorochrome for live-dead staining was plotted against the forward scatter to exclude dead cells from further analyses. After these steps for further analyses gating of the respective fluorochromes linked to the specific antibodies was used to distinguish distinct subsets of cells. A summary of the gating strategies used for immunophenotyping in different experiments can be found in Figure 5.

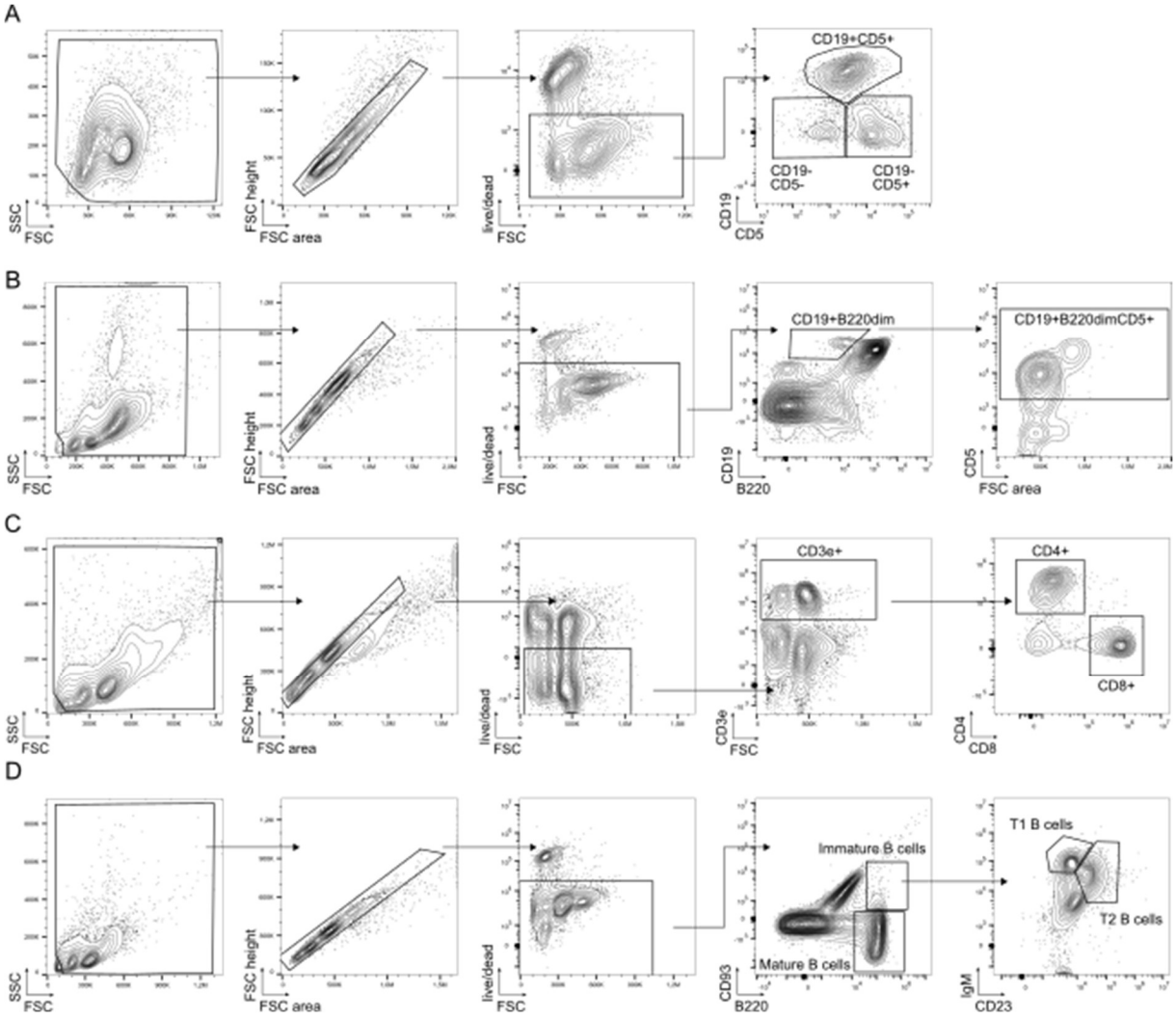

Figure 5: Flow cytometry gating strategies.

(**A**) Gating strategy for CD19+CD5+ cells. (**B**) Gating strategy for CD19+B220dim cells and CD19+B220dimCD5+ B1 B cells. (**C**) T cell gating strategy to measure frequency of all T cells (CD3e+) and to distinguish between CD4+ and CD8+ cells. (**D**) Gating strategy for transitional T1 (IgM+CD23-) and T2 (IgM+CD23+) cells gated on B220+CD93+. Generated using FlowJo. Previously displayed in Lewis et al.

2.2.3 Histopathology and immunohistochemistry (IHC)

2.2.3.1 Fixation and preparation of organ tissue

From sacrificed mice lymphatic tissues, liver, spleen and - if present - visually enlarged tumor material was collected and transferred to biopsy cassettes. To better facilitate the introduction of formaldehyde to the bone marrow we punctured the corticalis of the bones with three small holes along the side of each bone before continuing with the fixation step. Tissue samples

were then fixed in 4% formaldehyde for 48 hours, paraffin embedded, sectioned, and stained using H&E. Samples of bone marrow however were decalcified after fixation by a further incubation for 14 days in Osteosoft®.

2.2.3.2 Immunohistochemistry

Immunohistochemistry on murine tissues was performed on an automated immunostainer according to the company's protocols for open procedures with slight modifications. Appropriate known positive and negative controls were used to confirm the adequacy of the staining. The histologic samples were then analysed by an experienced pathologist, with especially extensive experience in murine oncologic pathology (Prof. Dr. Leticia Quintanilla-Martinez, Tübingen, Germany). Photomicrographic images were acquired with an Axioskop 2 *plus* Zeiss microscope equipped with a Jenoptik ProgRes C10 *plus* camera and software. Objectives Plan-Neofluar used were: 1.25/0,035, 2.5x/0.075, 10x/0.30, 20x/0.50, and 40x/0.75. Final image preparation was performed with Adobe Photoshop CS6.

2.2.3.3 Scoring of immunohistochemistry

To compare different biological samples against each other we decided to establish a scoring system to be able to quantify the immunohistochemistry and assess the tumor infiltration for each organ (scoring system described below). All samples were then scored by an experienced hematopathologist (Prof. Dr. Leticia Quintanilla-Martinez), accordingly and statistical analysis performed as described in the respective materials section below.

Spleen:

Score 1: Preserved white pulp and beginning of infiltration in the red pulp.

Score 2: Decreased white pulp and increase in red pulp infiltration.

Score 3: Loss of white pulp and complete red pulp infiltration.

Liver:

Score 1: Isolated positive cells.

Score 2: Intrasinusoidal infiltration or few portal small groups of lymphoid cells.

Score 3: Intrasinusoidal and portal infiltration with large groups of lymphoid cells.

Bone marrow:

Score 1: Isolated positive cells.

Score 2: Interstitial infiltration or few small groups of lymphoid cells.

Score 3: Interstitial infiltration and large groups of lymphoid cells.

2.2.4 RNA sequencing

2.2.4.1 Preparation of samples for RNA-Sequencing

Single cell suspensions of spleen and bone marrow were produced from sacrificed animals as described above. As the aim of the project was to address B cell intrinsic effects of activated CXCR4 signaling we performed magnetic bead separation. For this matter after production of single cell suspensions of spleen and bone marrow of *WT, CXCR4^{C1013G}, Eμ-TCL1,* and *Eμ-TCL1;CXCR4^{C1013G}*, B cells were isolated with CD19 directed magnetic beads by Miltenyi Biotec following the manufactures protocol. However, as we noticed the efficacy of purification could be enhanced by elongating the staining time with the magnetic beads to 40 minutes and adding an additional rinse of the column before eluting the cells, we adjusted the protocol accordingly.

To ensure sample purity we took a small specimen of the purified and stained cells with a CD19-directed antibody and discarded all samples of not at least 90% B cell purity. Samples were then snap frozen using liquid nitrogen and stored at -80°C until further preparation.

To isolate RNA, we applied the RNeasy Plus Mini Kit of Qiagen according to the manufacturers protocol, including the elimination of gDNA by the use of the gDNA eliminator column.

Due to the frequently observed disruption of RNA integrity by high levels of RNases, especially in splenic tissue, a measurement of the RNA integrity number (RIN) was performed and only

RNA samples with a RIN > 7 were used for RNA-sequencing. RIN was determined using Agilent RNA 6000 Nano Kit and the Agilent 2100 Expert software, as recommended by the fabricator. Library preparation and single-end sequencing was subsequently performed by Novogene (UK) on a HiSeq2500 with a sequencing depth of more than 20 M reads/sample. Fastq files were subsequently mapped to the murine reference genome GRCm38 with STAR. Reads and transcripts per million (TPM) were estimated for each transcript using the transcript sequences from the GENCODE Release 25 (GRCm38) and the Salmon software (v1.3.0). Counts and TPM were summarized at the gene level by summing up the transcript values for each corresponding gene.

The sequencing of *Eμ-Myc* and *Eμ-Myc;CXCR4*^{C1013G} samples was performed on a NextSeq 500 (Illumina, San Diego, CA) in a collaboration with Roland Rad's lab as described by Parekh, Ziegenhein et al. and using the adjusted protocol as described previously by Scherger, Al-Maarri et al. (Scherger et al. 2019; Parekh et al. 2016). Mapping and further analysis was performed by H. Carlo Maurer.

The RNA-Seq data was made accessible to the public through the National Center for Biotechnology Information's Gene Expression Omnibus. The accession code is GSE178959.

2.2.4.2 Differential gene expression analysis

Genome-wide differential gene expression analysis for RNA-Seq count data was carried out using a negative binomial generalized linear model (GLM) as implemented in the DESeq2 R package (Love, Huber, and Anders 2014; R-Core-Team 2018) to test for differentially expressed genes between experimental conditions. For dispersion estimation we considered genotype and organ site as covariates. For individual comparisons a false discovery rate (FDR) < 0.1 was considered significant. Select differentially expressed genes were illustrated in a heatmap after rescaling to have a minimum of -1 and a maximum of +1 using the *pheatmap* R package (Kolde 2019).

2.2.4.3 Gene Set Enrichment Analysis

Gene set enrichment analysis (GSEA) was carried out on individual differential gene expression signatures between two conditions using the *fgsea* R package (Korotkevich G. et al. 2021) and using Wald statistics from the aforementioned GLM as gene-level statistics. Gene sets were retrieved from the MSigDb v7.3 (Liberzon et al. 2011; Subramanian et al. 2005) Enrichment results for select pathways were illustrated using custom R code. Gene set enrichment analysis was conducted by H. Carlo Maurer in a collaborative effort.

2.2.4.4 Derivation and application of CXCR4 associated gene signatures

First we carried out differential gene expression (DEG) analysis on *WT, CXCR4*^{C1013G}, *Eμ-TCL1* and *Eμ-TCL1;CXCR4*^{C1013G} B cells as described. Next, we applied the following thresholds to the DEG results: baseMean > 50, absolute $\log_2$ fold change > 0.5 and adjusted p-value < 0.05. The remaining genes were ordered by their absolute Wald test statistic for up- (i.e. induced by CXCR4 activation) and downregulated (i.e. repressed by CXCR4 activation) genes, respectively, to represent the CXCR4 activation signature (CXCR4a) (Supplemental Table 1). Its enrichment on gene expression signatures derived from comparing other experimental conditions was computed using analytic rank-based enrichment analysis (aREA) (Alvarez et al. 2016) as implemented in the viper R package (Alvarez MJ., Giorgi F., and Califano A. 2014) considering both tails of the CXCR4a activation signature. Similarly, we applied differentially expressed genes between Richter transformed lymphocytes and peripheral blood chronic lymphocytic leukemia (Klintman et al. 2020) to gene expression signatures derived from our experimental conditions. DEG analysis was conducted in a collaboration by H. Carlo Maurer.

2.2.4.5 Application of upregulated genes from CXCR4 associated gene signatures to a data set of CLL patients

Simple sample gene set enrichment analysis (ssGSEA) using GSVA R/Bioconductor package (Hänzelmann, Castelo, and Guinney 2013) was performed on a previously published RNA sequencing dataset derived from a cohort of 210 CLL patients (Dietrich et al. 2018). For each patient sample, an enrichment score was calculated based on the upregulated genes from our CXCR4a (*CXCR4*^{C1013G} vs. *WT*) and *Eμ-TCL1;CXCR4*^{C1013G} vs. *Eμ-TCL1* signature and patients were dichotomized into two equally sized groups of high and low enrichment along the median. Groups were compared regarding their overall survival and time to treatment using log-rank test and the difference was visualized by Kaplan-Meier plots. The application of upregulated genes to CLL patients was performed in a collaborative effort with Thorsten Zenz and Junyan Lu.

2.2.4.6 Overlapping DEGs with known datasets of oncogenes

DEGs, as described above, of 6 week old *Eμ-TCL1* and *Eμ-TCL1;CXCR4*^{C1013G} were generated and pre-selected for protein coding genes with exclusion of Riken-cDNA genes using the MGI database (Bult et al. 2019). We then overlapped the DEGs with the Cancer Gene Census dataset (Sondka et al. 2018) of known cancer oncogenes and two data sets of published B cell oncogenes (Reddy et al. 2017; Chapuy et al. 2018).

2.2.4.7 Clonality Analysis from transcriptomic data

Transcriptomic data generated from RNA-Sequencing of CD19+ B cells from 6-week-old mice was used to profile V(D)J rearrangement using MiXCR and VDJtools as previously published (Shugay et al. 2015; Bolotin et al. 2015). Briefly, adapters were trimmed using Trim Galore (RRID:SCR_011847). Subsequently the paired-end set of reads were loaded into the MiXCR analysis pipeline (shotgun analysis) using a built-in mouse library (Bolotin et al. 2015). Finally,

clonotype results from MiXCR were analyzed and visualized using VDJtools. Clonality was analyzed in a lab internal collaboration by Matthias Wirth.

2.2.5 Immunoblotting upon stimulation with CXCL12

To analyze the response of purified B cells to stimulation of CXCR4 by CXCL12, after purification by magnetic beads, in a first step, B cells were starved of serum by incubating them for 1 hour in RPMI containing 2% of FBS. After this process, B cells were counted and each $2x10^6$ cells were distributed to FACS tubes. After a centrifugation process at 350g for 5 minutes, a subset of the cells was treated with 1µM of AMD3100 in RPMI with 2% FBS at room temperature for 40 minutes, while the others were further incubated in RPMI with 2% FBS only. After a washing step, cells were then resuspended in 37°C pre-tempered RPMI with 2% FBS and with/without 50nM of CXCL12 and incubated at 37°C for 5 minutes for stimulation, before another step of washing. Cells were then pelleted and snap frozen by the use of liquid nitrogen. Protein extracts were prepared by incubating cell pellets in lysis buffer (50 mM Hepes, 150 mM NaCl, 1 mM EDTA, 2.5 mM EGTA and 0.1% Tween) supplemented with NaF, PMSF and $NaVO_4$ followed by sonification. Protein lysates were fractioned on SDS PAGE gels, transferred to Immobilon-P (Millipore, Burlington, MA) membranes and incubated with specific antibodies and developed with Chemostar PC ECL & Fluorescence Imager (Intas Science Imaging, Göttingen, Germany). A list of antibodies used can be found in methods and materials section. Quantification of protein expression levels was performed using ImageJ software (https://imagej.nih.gov/ij). Immunoblotting was performed within a lab internal collaboration with Nikita Singh.

2.2.6 Migration Assay

Splenocytes were extracted from freshly collected spleen, by a 100µm cell separator and resuspended in RPMI-medium. Cells were then counted, and equal cell numbers were resuspended in RPMI-medium with or without 1µM AMD3100 and incubated at room

temperature for 40 minutes. Cells were then washed and loaded onto a Corning® Transwell® 96-well plate with 5µm pore size, with the other side of the membrane containing RPMI-medium with/without 50nM of CXCL12. The fully loaded Transwell® plates were then incubated in a cell culture incubator for 4h at 37°C to facilitate the migration process. Migration of cells to the lower wells was measured using CountBright™ Absolute Counting Beads, according to the manufacturers protocol, without alterations.

2.2.7 Statistics

Statistical analyses were performed using GraphPad Prism Version 9.0. (GraphPad Software, La Jolla, CA). Error bars represent standard deviation (SD). Bar graphs represent the mean. In animal experiments, a single data point represents an individual mouse. No sample size calculations were performed. Data from at least 3 mice per group were reported. In survival analyses, mice were excluded when the cause of death was not transgene-related (e.g. fighting, birth complications). A 2-tailed Student's t test was used to compare quantitative data between 2 independent samples. When comparing 3 or more groups, a one-way ANOVA with Tukey correction for multiple comparisons was used to compare group means. Survival data were compared using a logrank (Mantel-Cox) test. Results with a P value of less than 0.05 were considered significant.

3 Results

3.1 *CXCR4^{C1013G}* mice to study CXCR4 hyperactivation in B cells

In a first step, we aimed to validate our approach of using *CXCR4^{C1013G}* mice to study hyperactivated CXCR4 signaling in B cells. Fort this matter, CD19+ B cells were isolated from *CXCR4^{C1013G}* mice and wild type control mice (*WT*) (Figure 6A) immediately after sacrificing by CD19-directed magnetic bead separation and then stimulated *in vitro* as specified in the methods section. Thereafter, to ensure the presence of the proposed enhanced CXCR4 signaling activity in B cells of *CXCR4^{C1013G}*, immunoblotting for phosphorylation of the downstream effector kinases ERK and AKT (Scala 2015) was performed. For this matter the ratio of phosphorylated ERK (pERK) to ERK and phosphorylated AKT (pAKT) to AKT of B cells from *WT* and *CXCR4^{C1013G}* mice was compared after stimulation with 50nM of CXCL12 among each other, as well as in comparison to respective unstimulated controls. Remarkably higher pERK/ERK ratios and pAKT/AKT ratios were detected in the B cells of *CXCR4^{C1013G}* compared to *WT* controls, indicating an elevated response to CXCL12 and hyperactivation of CXCR4 signaling. To validate that this effect was related to CXCR4 stimulation, we added an additional biological group in which we pretreated the purified B cells with the CXCR4 antagonist AMD3100 before stimulation with CXCL12. Supporting these findings were attributed to stimulation of CXCR4, no significant differences in phosphorylation state of ERK and AKT compared to unstimulated controls were observed after stimulation with CXCL12 when CXCR4 was antagonized by AMD3100 before incubation with CXCL12 (Figure 6B and C). Importantly, as these cells were stimulated *in vitro*, after purification and separation from microenvironmental cells, the effects measured were B cell intrinsic effects.

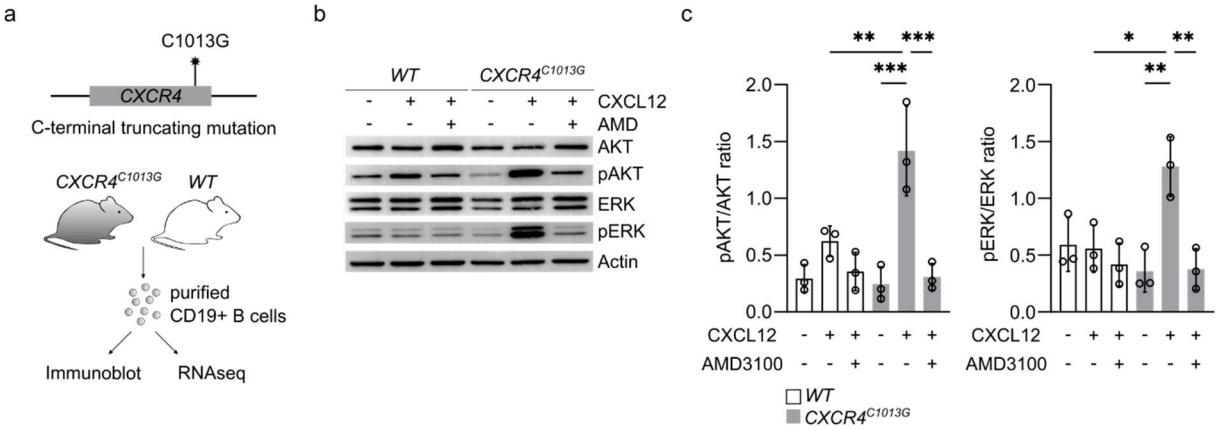

Figure 6: *CXCR4*$^{C1013G+/-}$ B cells exhibit increased phosphorylation of ERK/AKT upon CXCL12 stimulation
(**A**) Illustration of the CXCR4^{C1013G} truncating mutation and outline of experimental setup for immunoblotting and RNA sequencing of splenic and bone marrow CD19+ B cells. (**B**) Representative image of immunoblotting for AKT, pAKT (Ser473), ERK, pERK (Thr202/Tyr204) and Actin of CD19+ B cells treated with/without 50 nM CXCL12 and/or 10 µM CXCR4 inhibitor AMD3100 (AMD) (*WT*, n = 3; *CXCR4*^{C1013G}, n = 3). (**C**) Relative pAKT to AKT and pERK to ERK protein expression by immunoblotting of *WT* and *CXCR4*^{C1013G} CD19+ B cells treated with/without 50nM CXCL12 and/or 10µM CXCR4 inhibitor AMD3100 (*WT*, n = 3; *CXCR4*^{C1013G}, n = 3). Statistical analyses were performed with one-way ANOVA with Tukey correction for multiple comparisons, *P < 0.05, **P < 0.01, ***P < 0.001. Error bars indicate standard deviation (SD).

3.2 CXCR4 activation induces a distinct transcriptomic signature in B cells

As we observed B Cells of *CXCR4*^{C1013G} exhibited activated CXCR4 signaling, we aimed to study the changes this would induce to the B cell transcriptome. Thus, we performed whole transcriptome profiling of CD19+ B cells from *CXCR4*^{C1013G} and *WT* mice, which again we purified by magnetic bead separation (Figure 6A). Strikingly, hyperactivation of CXCR4 vastly changed the transcriptome of B cells and we discovered a set of 199 differentially expressed genes (DEGs, protein coding, $p_{adj} < 0.05$; logFC > 0.5 or < -0.5) in *CXCR4*^{C1013G} compared to *WT* controls (Figure 7A). Importantly, upregulated genes in B cells with hyperactivated CXCR4 signaling were such linked to chemokine signaling, migration and adhesion (*Ccr1*, *Cxcl1*, *Cxcl2*, *Igfn1*, *Cntn2*, *Jaml*), NOTCH signaling (*Sorbs2*), inflammation and cytokine signaling (*Il9r*, *Il7r*, *Csf2rb*, *Trem1*), B cell maturation (*Rag1*, *Rag2*), plasma cell differentiation and proliferation (*Prdm1*), metabolism (*Pdk1*) and cell cycle progression (*Nek6*). Of note, the CXCL12-binding receptor *Ackr3* (encoding CXCR7), known to form heterodimers with CXCR4 (Sanchez-Martin, Sanchez-Mateos, and Cabanas 2013), was upregulated, too.

Having found this large set of dysregulated genes, associated with aforementioned critical cellular functions, known to be pivotal also in tumor biology, we aimed to make our transcriptomic data easily accessible for further analyses. Thus, in a next step, the significantly differentially expressed 199 DEGs in *CXCR4*^{C1013G} vs. *WT*, were used to define a transcriptional profile of hyperactivated CXCR4 signaling (CXCR4a) in B cells (list of genes of signature can be found in Supplemental Table 1).

Subsequently, we applied gene set enrichment analysis (GSEA) using well-established, published transcriptional signatures. Supporting our hypothesis and underscoring the applicability of our CXCR4a signature, B cells of *CXCR4*^{C1013G} mice enriched chemokine receptor signaling, inflammatory response and cytokine signaling pathways (HALLMARK_INFLAMMATORY_REPSONSE, REACTOME_GPCR_LIGAND_BINDING, REACTOME_CYTOKINE_SIGNALING_IN_IMMUNE_SYSTEM). Interestingly, we additionally discovered cancer relevant pathways to be upregulated in CXCR4 hyperactivated B cells (HALLMARK_KRAS_SIGNALING_UP), as well as pathways typically associated with cancer, such as upregulation of glycolysis (HALLMARK_GLYCOLYIS) as well as depletion of DNA repair pathways (HALLMARK_DNA_REPAIR) (Figure 7B).

Summarizing, the data provided resemble the first *in vivo* data of the effects of activated CXCR4 to the transcriptome of B cells and provide a comprehensive database for further hypotheses and mechanistical studies. Moreover, from the set of DEGs we were able to generate a transcriptional signature of hyperactivated CXCR4 signaling in B cells, which represents a valuable tool to assess activity of the CXCR4 pathway. Furthermore, the data proves that enhancing CXCR4 signaling activity leads to an enrichment of several cancer-associated pathways and hyperactivated CXCR4 signaling might predispose B cells for malignant transformation.

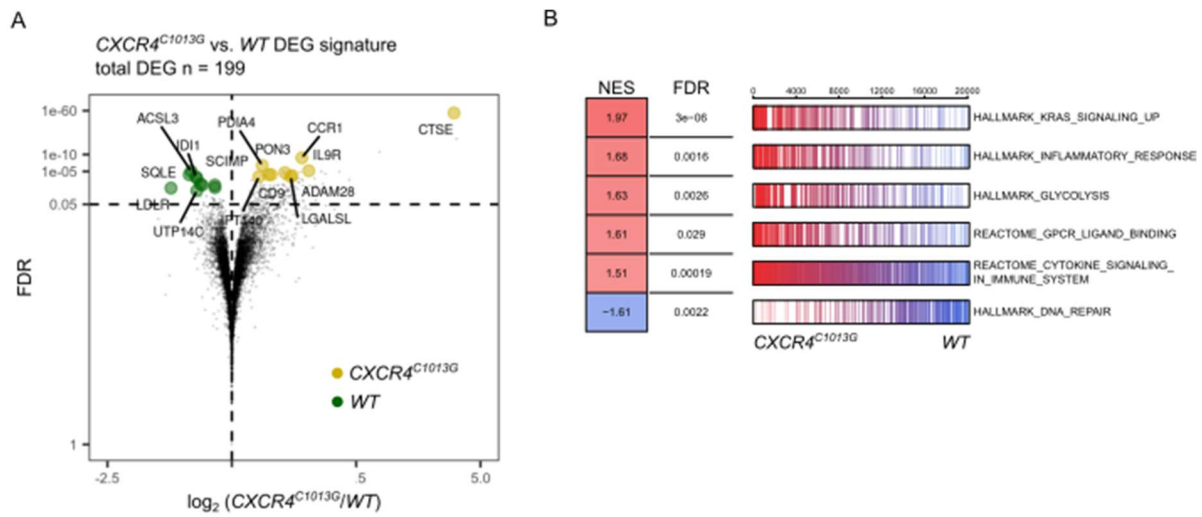

Figure 7: *CXCR4*^{C1013G} B cells display a distinct transcriptomic profile

(**A**) Volcano plot of differentially expressed genes (DEG) of *CXCR4*^{C1013G} vs. *WT* CD19+ B cells (*WT*, n = 5; *CXCR4*^{C1013G}, n = 5). (**B**) Gene set enrichment analysis (GSEA) of *CXCR4*^{C1013G} vs. *WT* CD19+ B cells showing normalized enrichment scores (NES) and false discovery rates (FDR) for curated gene sets listed in MsigDB (Liberzon et al. 2011; Subramanian et al. 2005) of *CXCR4*^{C1013G} compared to *WT* CD19+ B cells. For statistics, please refer to methods. Figure generated in collaboration with H. Carlo Maurer.

3.3 Enhanced CXCR4 signaling predisposes for TCL1 driven leukemia

Having shown that enhanced CXCR4 signaling regulates many cancer-associated pathways on a transcriptomic level, we sought to investigate which effects this would have on the distribution of different B cell compartments. Thus, we carried out an extensive B cell immunophenotyping on young, 3-month-old *CXCR4*^{C1013G} mice focusing on transitional B cells and especially on the population of CD19+/B220dim/CD5+ B1 B cells. We focused on these cells, as a potential mechanism of Eμ-TCL1-driven tumor development includes the accumulation of autoreactive B cells in the transitional T1 population, giving rise to CD19+/B220dim and, to limit autoreactivity, CD5+ B cells, which eventually progress to lethal B cell leukemia (Hippen, Tze, and Behrens 2000; Nganga et al. 2013; Alankus et al. 2021). Herein we discovered that these T1 B cells were significantly increased and concordantly T2 B cells decreased in frequency and total number in the spleens of these healthy young mice

without signs of disease (Figure 8A). Moreover, within the bone marrow compartment and spleen of these *CXCR4*^{C1013G} mice we could discover an increased frequency of CD19+/B220dim and additionally CD5+ cells (Figure 8B - D).

Remarkably this meant that the CD19+B220dim/CD5+ B1 B cell population known from *Eμ-TCL1* mice (Nganga et al. 2013) was already significantly increased in bone marrow and spleen of *CXCR4*^{C1013G} mice at an early age compared to their *WT* littermate controls, which highly suggests an innate increased susceptibility of B cells with CXCR4 hyperactivation for aberrant B cell lymphoproliferation.

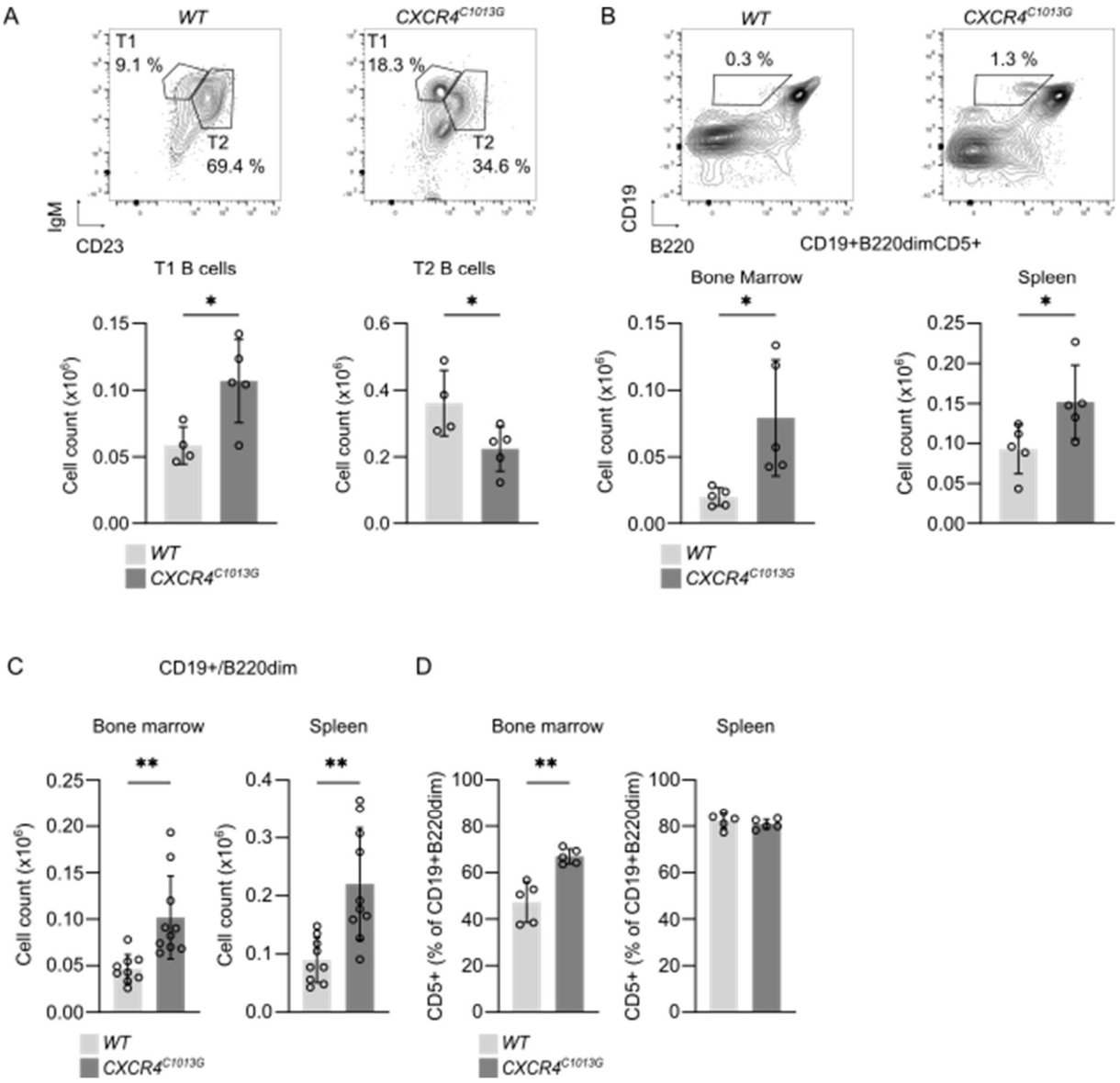

Figure 8: Enhanced CXCR4 signaling creates a predisposition for TCL1 driven leukemia.

(**A**) Quantification and representative contour plots of splenic T1 (IgM+CD23-) and T2 (IgM+CD23+) cells gated on B220+CD93+ B cells by flow cytometry of 3-month-old animals (*WT*, n = 5; *CXCR4*^{C1013G}, n = 5). (**B**) Representative contour plots of splenic CD19+B220dim cells and quantification of total bone marrow and splenic CD19+B220dimCD5+ B1 cells of 3-month-old animals (*WT*, n = 5; *CXCR4*^{C1013G}, n = 5). (**C**) Quantification of total CD19+B220dim cells in bone marrow and spleen of 3-month-old *WT* and *CXCR4*^{C1013G} mice (*WT*, n = 5; *CXCR4*^{C1013G}, n = 5). (**D**) Frequencies of CD5+ cells of CD19+B220dim cells in bone marrow and spleen of 3-month-old *WT* and *CXCR4*^{C1013G} mice (*WT*, n = 5; *CXCR4*^{C1013G}, n = 5). Statistical analyses were performed with Student's t test, *P < 0.05, **P < 0.01. Error bars indicate standard deviation (SD).

3.4 Hyperactivating CXCR4 signaling in TCL1-driven lymphoma / leukemia

3.4.1 Rationale for choosing the *Eμ-TCL1* model organism

No patient or *in vivo* data exist on direct effects of activated CXCR4 signaling on lymphoma genesis and biology. However, when analyzing published data, mRNA-expression of CXCR4 is linked to a reduced overall survival in CLL patients (Figure 9), further hinting to a possible major role of CXCR4 in leukemia / lymphoma biology.

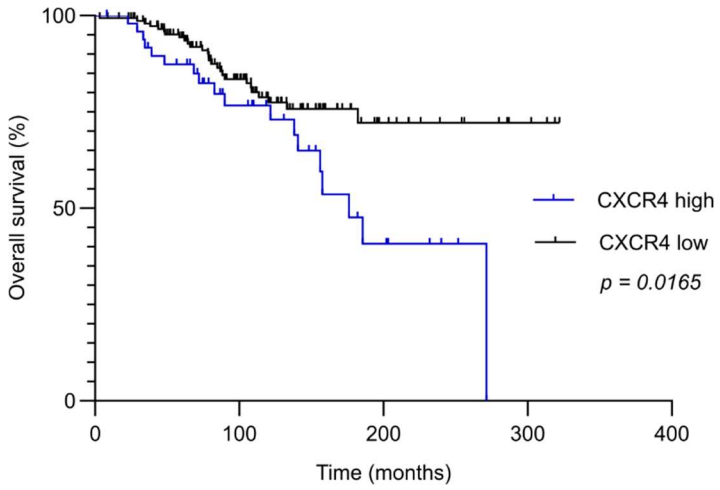

Figure 9. High CXCR4 expression is associated with adverse prognosis in CLL patients.

Kaplan-Meier survival analysis of 201 CLL patients stratified by CXCR4 mRNA expression from the CLL-ES data set of the ICGC database – June 2016, risk-group maximized and analyzed with SurvExpress (Aguirre-Gamboa et al. 2013). P value of log-rank (Mantel-Cox) test is shown.

Hence, we sought to overcome this lack of data, by intercrossing the *CXCR4*^{C1013G} model to a hematopoietic tumor model of CLL / indolent B cell lymphoma. To this end, we chose the well-established *Eμ-TCL1* model of indolent lymphoma / CLL-like disease, which expresses the TCL1 oncogene B cell specifically (Bichi et al. 2002) (also refer to 1.4.1 and 2.2.1.2).

Of note, the model was chosen specifically, as we saw an increased number of CD19+B220dim/CD5+ B1 B cells in the spleens and bone marrow of young mice *CXCR4*^{C1013G}. These are known to be the precursors of Eμ-TCL1-driven disease. Hence, we aimed to investigate whether this observed lymphoproliferation translated to a more profound TCL1-

driven CLL-like disease *in vivo*. Thus, *Eμ-TCL1* mice were intercrossed with *CXCR4*^{C1013G} mice to generate *Eμ-TCL1;CXCR4*^{C1013G} mice, which were both heterogeneous for CXCR4^{C1013G} and Eμ-TCL1 transgenes (Figure 10). Of note, all further experiments were solely performed on mice with double heterogeneous genetic background, not on those homozygously harboring one or both of the mutations.

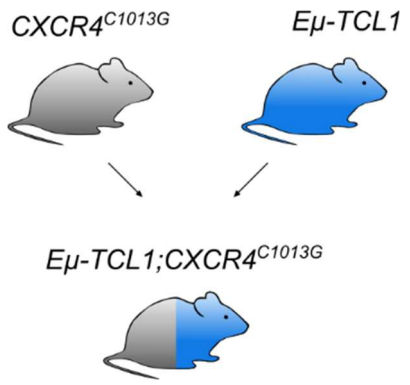

Figure 10: Generation of the *Eμ-TCL1;CXCR4*^{C1013G} mouse model

Outline of the breeding scheme of *CXCR4*^{C1013G} and *Eμ-TCL1* mice to generate double-transgenic *Eμ-TCL1;CXCR4*^{C1013G} mice.

3.4.2 CXCR4 signaling accelerates lymphoproliferation

Many previous studies have shown that even at a young age, clinically healthy *Eμ-TCL1* mice exhibited a steady lymphoproliferation ultimately leading to lethal disease (Nganga et al. 2013). Thus, to analyze the impact of CXCR4 hyperactivation on the lymphomagenesis and early stages of disease, we sacrificed a young age-matched cohort of 6-month-old *Eμ-TCL1* and *Eμ-TCL1;CXCR4*^{C1013G} mice for histopathology and flow cytometry based immunophenotyping.

As anticipated, all mice bearing the Eμ-TCL1 transgene developed a gradually progressing B cell lymphoproliferation with a CD19+CD5+/CD19+B220dim immunophenotype and continuous loss of B220 expression along the course of the disease in line with previous data (Figure 11A) (Bichi et al. 2002). However, in *Eμ-TCL1;CXCR4*^{C1013G} mice, this

lymphoproliferation started earlier as compared to *Eμ-TCL1* littermates. For this matter we sacrificed mice aged 5-6 months and observed not only a significantly increased infiltration of CD19+CD5+/CD19+B220dim cells in bone marrow and spleen (Figure 11A and B) but also an increased spleen weight (Figure 11C). This indicated to us, that CXCR4 may play a role even at early stages of disease development.

Concordantly, these findings were further confirmed by histopathological analysis, as *Eμ-TCL1* mice exhibited enlarged spleens with moderate preservation of the white pulp and clear expansion of the red pulp, which was incipiently infiltrated by B cells, while in *Eμ-TCL1;CXCR4^{C1013G}* mice the white pulp was atrophic with expansion of the red pulp and morphologically more pronounced infiltration (evaluated by Prof. Leticia Quintanilla-Martinez, University of Tübingen; Figure 11D, quantification 11E). These differences could also be observed in the bone marrow, with a significantly increased infiltrative lymphoproliferation in bone marrows of *Eμ-TCL1;CXCR4^{C1013G}* compared to *Eμ-TCL1* (Figure 11D, quantification: Figure 11E).

Having seen the more extensive lymphoproliferation of CD19+CD5+B220dim cells and destruction of regular histology in *Eμ-TCL1;CXCR4^{C1013G}* mice, we aimed to further phenotype these cells and also characterize the T cell compartment.

Underscoring our findings of a further progressed stage of disease in *Eμ-TCL1;CXCR4^{C1013G}* mice, we observed significantly reduced B220 expression at this early stage in *Eμ-TCL1;CXCR4^{C1013G}* compared to *Eμ-TCL1* CD19+CD5+ cells in both bone marrow and spleen (Figure 11F). Importantly when analyzing the T cell compartment, we could not see significant differences in the frequency of CD3e+, CD4+ and CD8+ T cells in spleens of *Eμ-TCL1* and *Eμ-TCL1;CXCR4^{C1013G}* (Figure 11G), hinting towards a B cell intrinsic effect of CXCR4 hyperactivation to lymphoproliferation .

Summarizing these data, Eμ-TCL1-driven lymphoproliferation is accelerated by CXCR4 hyperactivation in young clinically healthy mice. *Eμ-TCL1,CXCR4^{C1013G}* mice showed a histopathologically more advanced stage of disease, including disruption of normal tissue

architecture and reduced expression of B220 on CD19+CD5+ cells. Furthermore, as the lymphoproliferation, known to ultimately progress to Eμ-TCL1-driven leukemia, could be seen in young mice our data hints toward an involvement of CXCR4 in the early stages of disease.

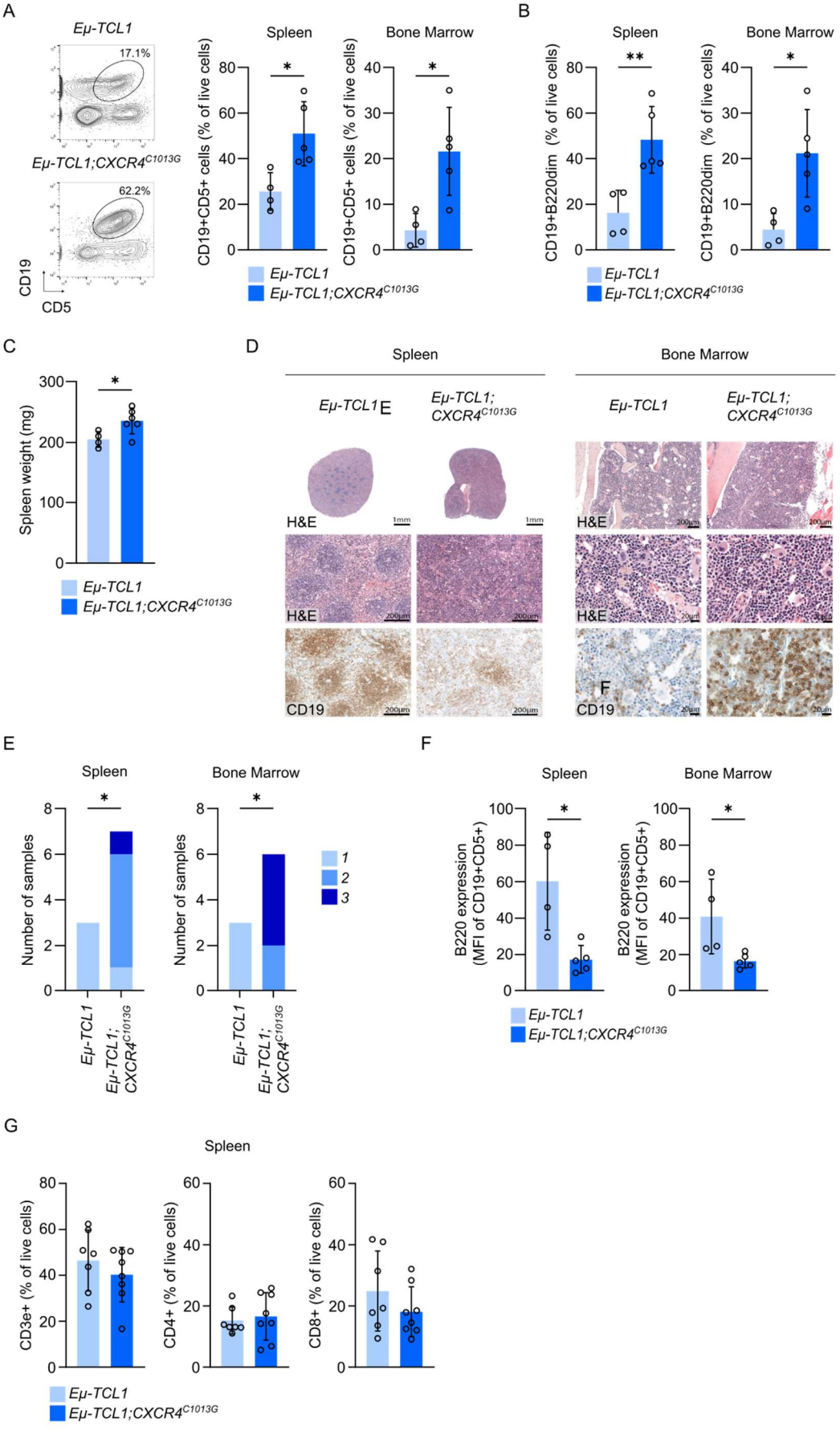
A
Eμ-TCL1
17.1%
Eμ-TCL1;CXCR4C1013G
62.2%
CD19
CD5
Spleen
Bone Marrow
CD19+CD5+ cells (% of live cells)
Eμ-TCL1
Eμ-TCL1;CXCR4C1013G
B
CD19+B220dim (% of live cells)
C
Spleen weight (mg)
D
Spleen
Bone Marrow
Eμ-TCL1
Eμ-TCL1; CXCR4C1013G
H&E
CD19
E
Number of samples
1
2
3
F
B220 expression (MFI of CD19+CD5+)
G
CD3e+ (% of live cells)
CD4+ (% of live cells)
CD8+ (% of live cells)

Figure 11: Hyperactivation of CXCR4 accelerates onset of disease in Eμ-TCL1 driven leukemia

(**A**) Representative contour plots of splenic CD19+CD5+ cells by flow cytometry in 5 - 6 month old animals and quantification of splenic and bone marrow CD19+CD5+ cells (*Eμ-TCL1*, n = 4*; Eμ-TCL1;CXCR4^{C1013G}*, n = 5). **(B**) Frequencies of spleen and bone marrow CD19+B220dim cells by flow cytometry in 5 - 6 month old animals (*Eμ-TCL1*, n = 4; *Eμ-TCL1;CXCR4^{C1013G}*, n = 5). (**C**) Spleen weight of 5 - 6 month old mice (*Eμ-TCL1*, n = 4; *Eμ-TCL1;CXCR4^{C1013G}*, n = 6). (**D**) Representative images of H&E and immunohistochemistry of 5 - 6 month old *Eμ-TCL1* and *Eμ-TCL1;CXCR4^{C1013G}* mice (scale bars spleen: overview = 1mm, detailed images: 200μm, scale bars bone marrow: overview = 200μm, detailed images = 20μm). (**E**) Quantification of histology scores (1-3) of spleen (*Eμ-TCL1*, n = 3; *Eμ-TCL1;CXCR4^{C1013G}*, n = 7) and bone marrow (*Eμ-TCL1*, n = 3; *Eμ-TCL1;CXCR4^{C1013G}*, n = 6) of 5 - 6 month old mice. Scoring system details are shown in Methods section. (**F**) Quantification of spleen and bone marrow B220 expression of CD19+CD5+ cells by flow cytometry in 6 month old animals (*Eμ-TCL1*, n = 4; *Eμ-TCL1;CXCR4^{C1013G}*, n = 5). (**G**) Frequencies of spleen CD3e+, CD4+ and CD8+ T cells by flow cytometry in 5 - 6 month old animals (*Eμ-TCL1*, n = 7; *Eμ-TCL1;CXCR4^{C1013G}*, n = 8). Statistical analyses were performed with Student's t test, *P < 0.05, **P < 0.01. Error bars indicate standard deviation (SD).

3.4.3 CXCR4 hyperactivation reduces survival in TCL1-driven leukemia

With major differences in lymphoproliferation observed in young healthy *Eμ-TCL1;CXCR4^{C1013G}* mice compared to their littermates, the question arose whether this would also translate to an earlier onset of disease and reduced survival of mice. Thus, we observed a cohort of mice until presentation with symptoms of disease fulfilling the termination criteria and requiring euthanasia.

Analyzing the cohort, we found that CXCR4 activation accelerated development of Eμ-TCL1-driven disease. Hence, demonstrating a collaboration of CXCR4 and TCL1 in lymphomagenesis. Enhanced CXCR4 activity reduced the median overall survival of *Eμ-TCL1;CXCR4^{C1013G}* by approximately 100 days compared to their *Eμ-TCL1* littermates (Figure 12A).

Of important note, we furthermore observed a subgroup of *Eμ-TCL1;CXCR4^{C1013G}* mice, which developed an enhanced nodal dissemination of CLL. These mice presented with pronounced lymphadenopathy, which in contrast was not observed in any of the *Eμ-TCL1* mice from this cohort (Figure 12B and C). When investigating the immunophenotype of these tumors, all

tumors in both biological groups expressed the same CD5+CD20+B220dim phenotype, which was already observed in the premalignant cohort, including those tumors with extensive lymphadenopathy. Furthermore, no changes in the grade of splenic infiltration with CD5+CD20+ tumor cells could be observed in those mice fulfilling the termination criteria (Figure 12D).

Also, similarly to the premalignant cohort, the immunophenotype and infiltration of tumors with T cells remained unchanged in mice with symptomatic indolent lympohoma / CLL-like disease requiring euthanasia, as indicated by a non-significant change of tumor infiltrating CD3e+ T cells (Figure 12D).

To quantify tumor burden further, as we observed massive hepatosplenomegaly, which is known to the *Eμ-TCL1* model, we measured the weight of the spleen and liver, when mice required euthanasia. When comparing *Eμ-TCL1;CXCR4*^{C1013G} to *Eμ-TCL1* tumor mice, we could not discover a significant difference of tumor burden as measured by spleen and liver weight (Figure 12E).

Summarizing these data indicate CXCR4 hyperactivation induces a more rapid onset of Eμ-TCL1-driven disease without altering the CLL-like immunophenotype of the disease. Furthermore, a subgroup of *Eμ-TCL1;CXCR4*^{C1013G} mice presented with a pronounced lymphadenopathy not seen in *Eμ-TCL1* mice, indicating CXCR4 hyperactivation may play a role in homing of tumor cells to nodal sites rather than the spleen.

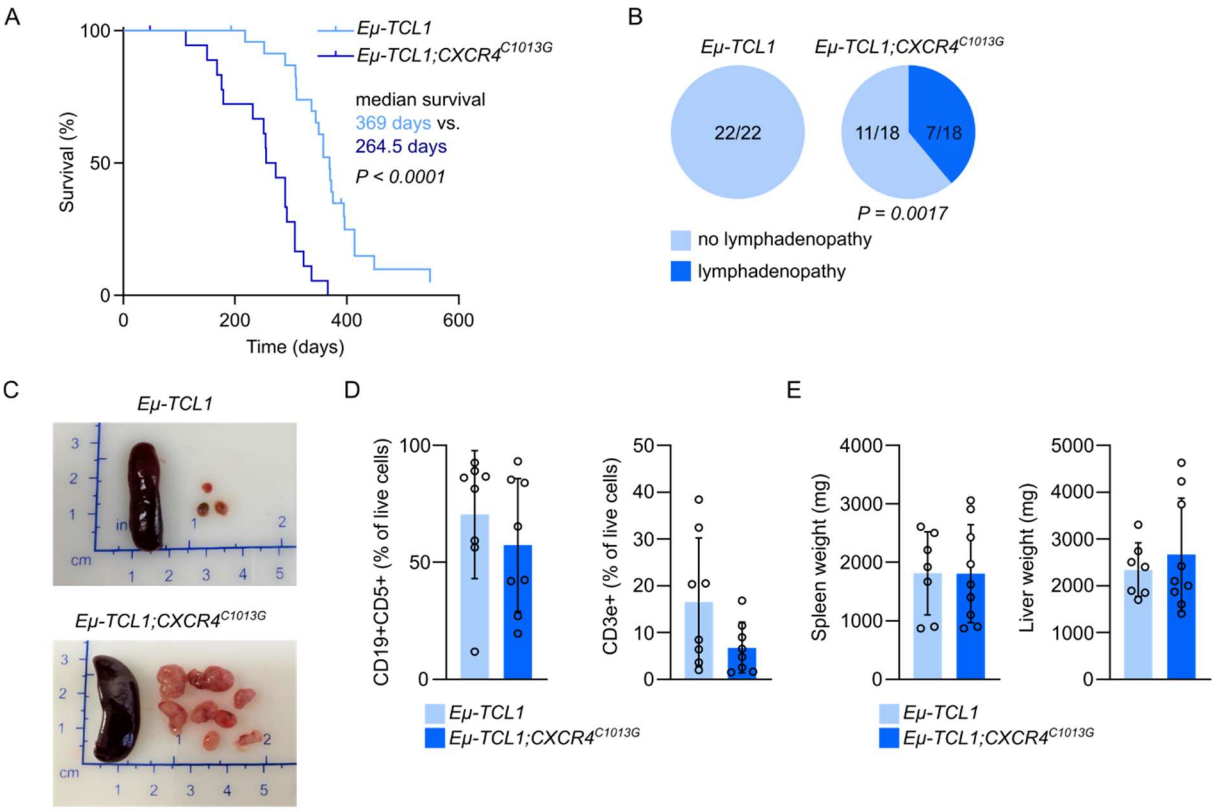

Figure 12: CXCR4 hyperactivation reduces overall survival in TCL1-driven leukemia

(A) Kaplan-Meier survival curves of the indicated cohorts of mice (*Eμ-TCL1*, n = 18; *Eμ-TCL1;CXCR4^{C1013G}*, n = 22). Median survival and P value of log-rank (Mantel-Cox) test is shown. **(B)** Pie charts depicting fractions of animals with overt lymphadenopathy in *Eμ-TCL1* (n = 22) and *Eμ-TCL1;CXCR4^{C1013G}* mice (n = 18). P value of Fisher's exact test is shown. **(C)** Representative images of spleen and lymphatic tissue of mice with symptomatic CLL requiring euthanasia of a *Eμ-TCL1* control and a *Eμ-TCL1;CXCR4^{C1013G}* animal presenting with extensive lymphadenopathy. **(D)** Frequencies of spleen CD19+CD5+ and CD3e+ cells by flow cytometry in mice with symptomatic CLL requiring euthanasia (*Eμ-TCL1*, n = 8; *Eμ-TCL1;CXCR4^{C1013G}*, n = 8). **(E)** Spleen and liver weight of mice with symptomatic CLL requiring euthanasia (*Eμ-TCL1*, n = 7; *Eμ-TCL1;CXCR4^{C1013G}*, n = 9).

3.4.4 CXCR4 hyperactivation promotes a more infiltrative and extranodal pathology

As described above, contrary to the young cohort no differences in the grade of infiltration of tumor cells to bone marrow and spleen could be detected by means of flow cytometry. However, a subgroup of the *Eμ-TCL1,CXCR4^{C1013G}* cohort presented with an aggravated

lymphadenopathy. Thus, we aimed to get a more detailed picture of the disease pattern of our clinically symptomatic mice by evaluating histopathology of diseased mice, too.

When comparing the histopathology of mice presenting with symptomatic CLL-like disease, both genotypes showed extensive infiltration of the red pulp, with complete atrophy of the white pulp in spleens. However, visually evaluated by an experienced hematopathologist (Prof. Leticia Quintanilla-Martinez, University of Tübingen), the bone marrow of *Eμ-TCL1;CXCR4*^{C1013G} mice displayed a more diffuse infiltration pattern, in contrast to a more focal infiltration pattern in *Eμ-TCL1* controls (Figure 13A, scores and quantification Figure 13B).

Interestingly when analyzing the tumor samples some mice exhibited additional features of aggressive transformation. E.g., tumors of 3 out of 7 *Eμ-TCL1;CXCR4*^{C1013G} mice, morphologically resembled features of aggressive transformation of CLL to DLBCL-type Richter's transformation. In line with this, lymphoma cells of *Eμ-TCL1;CXCR4*^{C1013G} mice were larger than typical *Eμ-TCL1* tumor cells, infiltrated surrounding muscle and adipose tissue and showed higher expression of the proliferation marker Ki67 (Figure 13C and D). Furthermore, 3 *Eμ-TCL1;CXCR4*^{C1013G} mice presented with histiocytic sarcoma, a rare transformation of CLL cells to malignant histiocytes (Shao et al. 2011) (Figure 13E).

Summarizing these data show CXCR4 hyperactivation induces a more infiltrative phenotype and moreover promotes aggressive transformation of the CLL-like disease known from *the Eμ-TCL1* mouse.

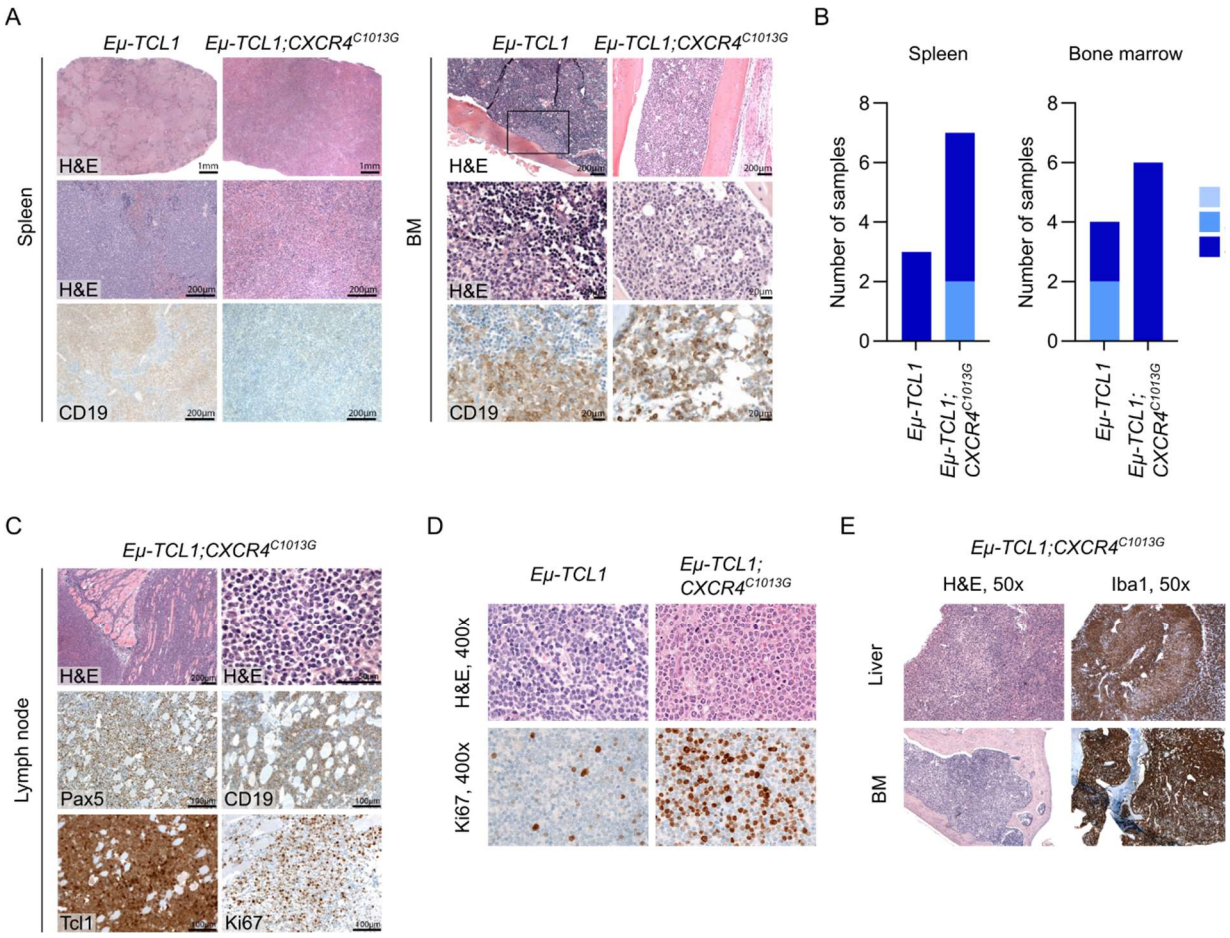

Figure 13: CXCR4 hyperactivation aggravates histopathological phenotype of TCL-driven leukemia

(A) Representative images of H&E and immunohistochemistry of *Eμ-TCL1* and *Eμ-TCL1;CXCR4^{C1013G}* with manifest lymphoma (scale bars spleen: overview = 1mm, detailed images: 200μm, scale bars bone marrow: overview = 200μm, detailed images = 20μm). **(B)** Quantification of histology scores (1-3) of spleen (*Eμ-TCL1*, n = 3; *Eμ-TCL1;CXCR4^{C1013G}*, n = 7) and bone marrow (*Eμ-TCL1*, n = 4; *Eμ-TCL1;CXCR4^{C1013G}*, n = 6) of mice with symptomatic CLL requiring euthanasia. Scoring system details as indicated in the methods section. **(C)** Representative images of H&E and immunohistochemistry of a *Eμ-TCL1;CXCR4^{C1013G}* animal presenting with Ki67 positive Richter-like aggressive lymphoma (scale bars: H&E overview = 200μm, H&E detailed image = 50μm, IHC detailed images = 100μm). **(D)** Representative images of aggressive lymphoma morphology in *Eμ-TCL1;CXCR4^{C1013G}* animals compared to *Eμ-TCL1* animals with symptomatic CLL requiring euthanasia. **(E)** Representative images of histiocytic sarcoma in *Eμ-TCL1;CXCR4^{C1013G}* animals. Statistical analyses were performed with Student's t test (b and c) or Mann-Whitney *U* test (d), *P < 0.05, **P < 0.01. Error bars indicate standard deviation (SD).

3.4.5 CXCR4 hyperactivation facilitates migration in B cells, especially in malignantly transformed B cells

To investigate whether the effects of CXCR4 hyperactivation on B cell leukemia and lymphoma development and dissemination are B cell-intrinsic, splenocytes of premalignant animals were isolated and assessed regarding their migratory capacity in response to CXCL12 *ex vivo*.

To this end we performed a migration assay in which cells were put into a chamber of medium lacking CXCL12, secluded to another chamber with CXCL12 rich medium by a membrane with slightly smaller pore size than the cells of interest. Hence those cells with a chemotaxis towards CXLCL12 would squeeze through the pores and were counted to determine the migratory potential. For this reason, we loaded all splenocytes and combined the migration with flow cytometry to be able to distinguish differences in the migration of subpopulations.

Strikingly CD19+CD5+ cells of *Eμ-TCL1;CXCR4*^{C1013G} showed the highest migratory potential of all analyzed cells, with a significantly enhanced migratory potential compared to *WT*, *CXCR4*^{C1013G} and *Eμ-TCL1* CD19+CD5+ cells. This is especially interesting as no increased migratory potential compared to *CXCR4*^{C1013G} could be discovered in bulk splenocytes and CD5+ T cells, which again suggests a collaboration of TCL1 and CXCR4 B cell intrinsically (Figure 14).

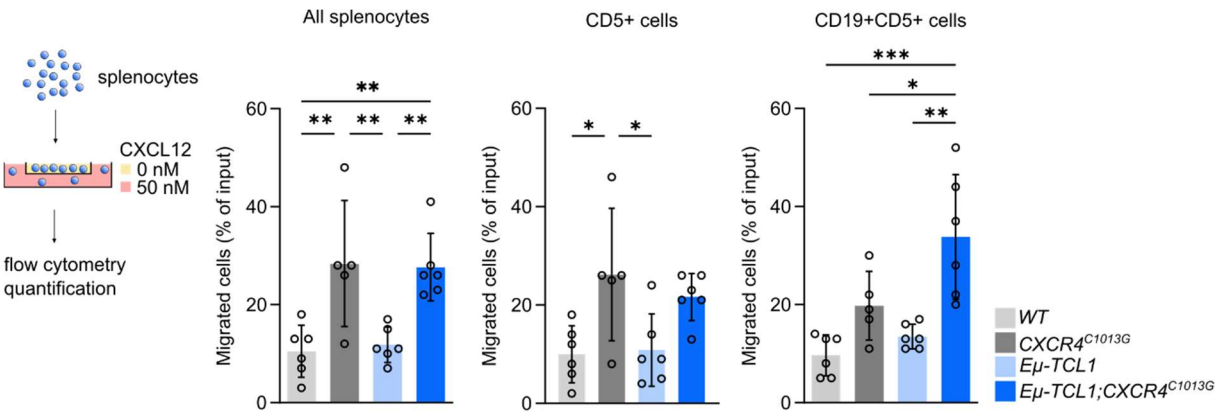

Figure 14. B cells of *Eμ-TCL1;CXCR4^{C1013G}* mice show a significantly greater migratory potential toward a CXCL12 gradient

Experimental setup and quantification for *ex vivo* transwell migration of all splenocytes, CD5+ T cells and CD19+CD5+ cells towards 50nM CXCL12 isolated from genotypes as indicated (*WT*, n = 6; *CXCR4^{C1013G}*, n = 5; *Eμ-TCL1*, n = 6; *Eμ-TCL1;CXCR4^{C1013G}*, n = 6). Statistical analyses were performed with one-way ANOVA with Tukey's correction for multiple comparisons, * P < 0.05, ** P < 0.01, *** P < 0.001. Error bars indicate standard deviation (SD).

3.5 Hyperactivating CXCR4 signaling in MYC-driven lymphoma

3.5.1 CXCR4 expression is associated with poor outcomes in DLBCL

Having seen the effects hyperactivated CXCR4 signaling induced in Eμ-TCL1-driven CLL-like disease we wanted to evaluate whether these results were also transferable to aggressive lymphoma models and biology. Beforehand we analyzed published datasets of DLBCL, the most common aggressive B cell lymphoma (Reddy et al. 2017; Chapuy et al. 2018; Morin et al. 2013). These analyses confirmed that elevated CXCR4 expression correlates with adverse prognosis in a large data set of 420 DLBCL patients (Figure 15A). Furthermore, we investigated whether we could detect recurrent mutations in CXCR4, similar to those known from Waldenström's disease. To this end we analyzed public data banks of genetic mutations in tumors and were able to prove that recurrent *CXCR4* mutations are rare, but present, in DLBCL patients (Figure 15B).

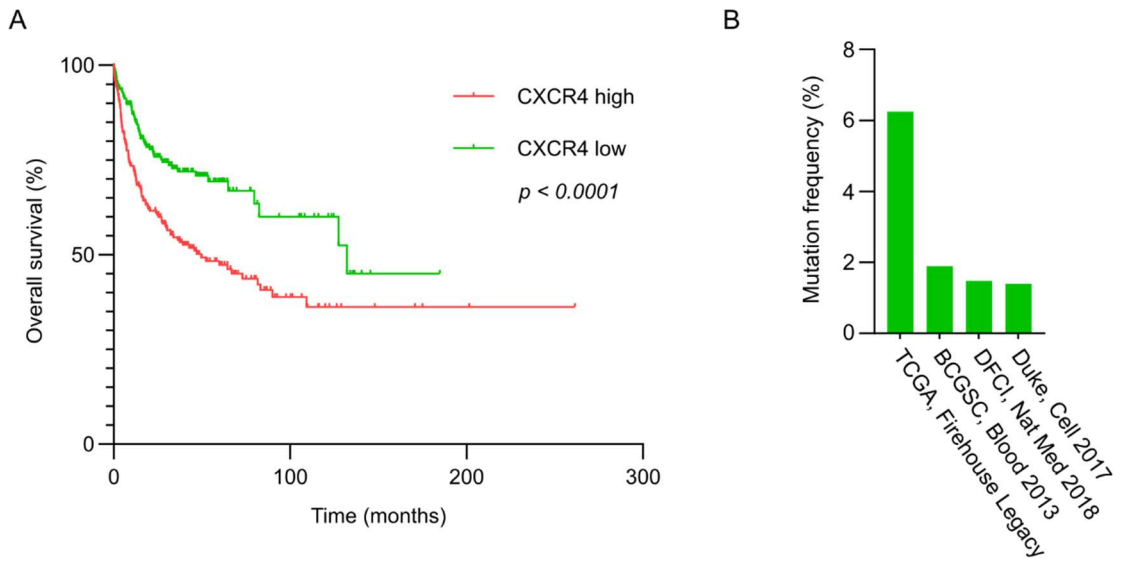

Figure 15. CXCR4 expression is associated with poor outcomes and recurrently mutated in DLBCL patients. (**A**) Kaplan-Meier survival analysis of 420 DLBCL Patients stratified by CXCR4 mRNA expression of GSE10846 (Lenz et al. 2008), risk-group maximized and analyzed with SurvExpress (Aguirre-Gamboa et al. 2013). P value of log-rank (Mantel-Cox) test is shown. (**B**) Mutation frequency of CXCR4 in DLBCL patient datasets (TCGA, Firehose Legacy, n = 48; BCGSC, Blood 2013, n = 53; CDFCI, Nat Med 2018, n = 135; Duke, Cell 2017, n = 1001) (Morin et al. 2013; Chapuy et al. 2018; Reddy et al. 2017).

3.5.2 Rationale for choosing the *Eμ-Myc* model organism

We chose the *Eμ-Myc* model to study the role of CXCR4 hyperactivation in the context of aggressive B cell lymphoma. In this model the oncogene MYC is over expressed in B cells (Adams et al. 1985) (see also 1.4.1 and 2.2.2.2). Tumors develop very early in this model and somewhat reflect features of MYC-dependent B cell biology, as seen in DLBCL and Burkitt's lymphoma. Hence, to investigate hyperactive CXCR4 activity in MYC-driven lymphomagenesis as a model of aggressive B cell lymphoma in general, we intercrossed *CXCR4*^{C1013G} with *Eμ-Myc* mice (Figure 16).

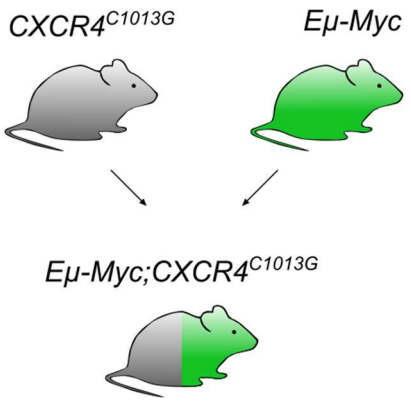

Figure 16. Generation of the *Eμ-Myc;CXCR4^{C1013G}* mouse model

Outline of breeding scheme of *CXCR4^{C1013G}* and *Eμ-Myc* mice to generate double-transgenic *Eμ-Myc;CXCR4^{C1013G}* mice.

3.5.3 Premalignant *Eμ-Myc;CXCR4^{C1013G}* exhibit more pronounced disease at a very early time point of 4 weeks

In contrast to *Eμ-TCL1* mice with a median survival of approximately one year, mice harboring the *Eμ-Myc* transgene develop symptomatic disease beginning at a very young age of 6 - 8 weeks. Thus, as we again wanted to investigate the onset of disease, we decided to sacrifice 1-month-old mice which did not yet present with symptoms.

When analyzing blood samples from these young mice, we found similarly elevated white blood cell counts in *Eμ-Myc* and *Eμ-Myc;CXCR4^{C1013G}* indicating an already present tumor development in both cohorts (Figure 17A). However, we could not detect significant differences between *Eμ-Myc;CXCR4^{C1013G}* mice and the *Eμ-Myc* controls at one month of age.

In spite of no significant differences in white blood cell count, even at this very early time point, we could already discover increased spleen weights in *Eμ-Myc;CXCR4^{C1013G}* mice compared to age-matched *Eμ-Myc, WT* and *CXCR4^{C1013G}* controls (Figure 17B).

These findings were further supported by histopathology, as we observed that the spleens of *Eμ-Myc;CXCR4^{C1013G}* mice had a more pronounced infiltration of premalignant B cells with a more extensively disrupted architecture (Figure 17C, quantification Figure 17D) very early on.

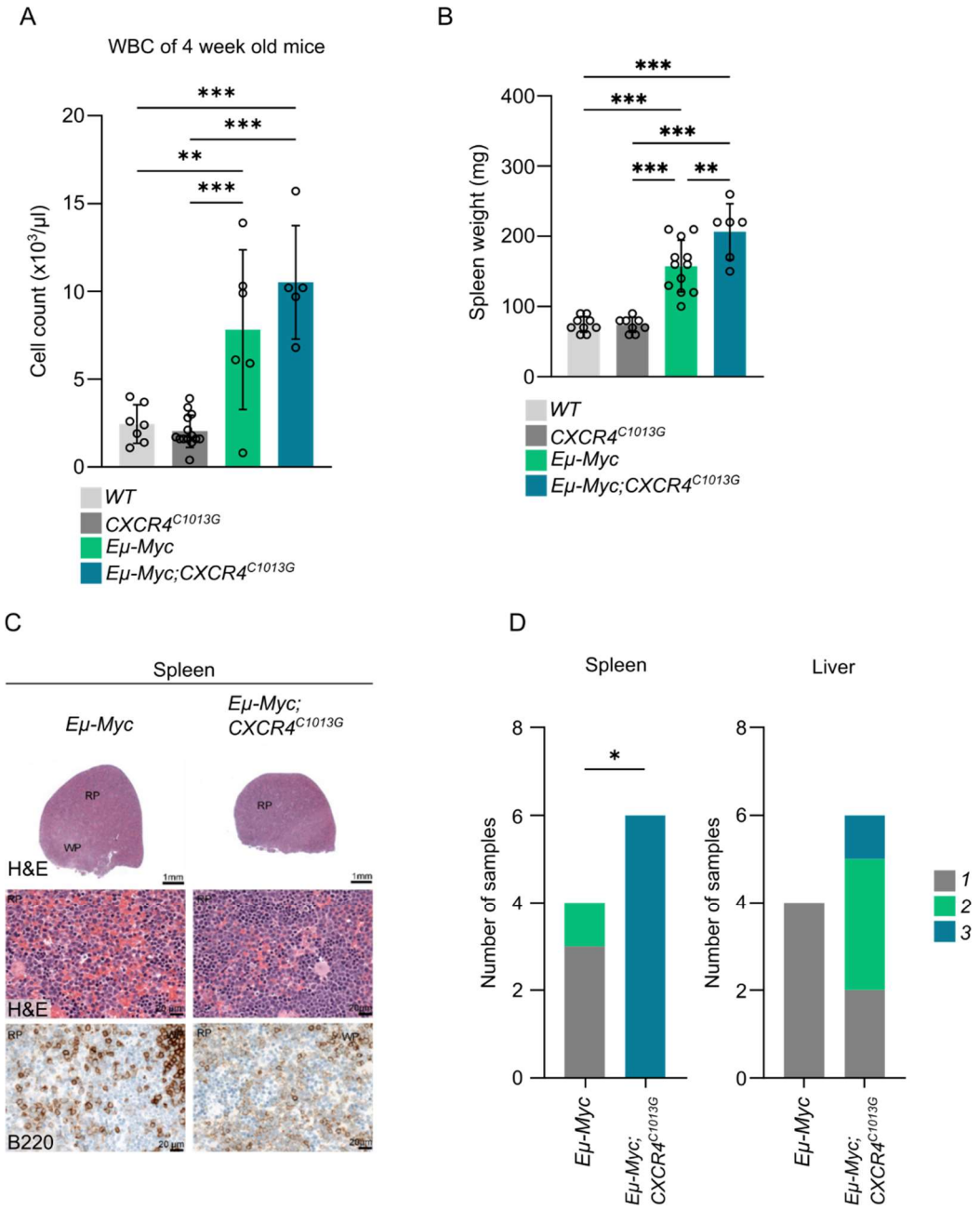

Figure 17. Characterization of 4-week-old *Eμ-Myc;CXCR4^{C1013G}* mice.

(**A**) White blood cell count (WBC) of 4-week-old mice (*WT*, n = 7; *CXCR4^{C1013G}*, n = 14; *Eμ-Myc*, n = 6; *Eμ-Myc;CXCR4^{C1013G}*, n = 5). (**B**) Spleen weight of 1 month old animals of genotypes as indicated (*WT*, n = 9; *CXCR4^{C1013G}*, n = 8; *Eμ-Myc*, n = 12; *Eμ-Myc;CXCR4^{C1013G}*, n = 6). (**C**) Representative images of H&E and immunohistochemistry of 1 month old *Eμ-Myc* and *Eμ-Myc;CXCR4^{C1013G}* mice (scale bars: overview = 1mm, detailed images: 20µm). (**D**) Quantification of histology scores (1-3) of spleen and liver from 4-week-old mice (*Eμ-Myc*, n = 4; *Eμ-Myc;CXCR4^{C1013G}*, n = 6). Scorings system as indicated in the methods section.

3.5.4 CXCR4 hyperactivation does not reduce overall survival of *Eμ-Myc* mice but induces a more infiltrative phenotype

We further investigated a cohort, which was kept until presentation of symptomatic disease. In these mice with manifest lymphoma, the *Eμ-Myc;CXCR4*^{C1013G} genotype was associated with a more aggressive infiltrative pathology, as seen in the *Eμ-TCL1* comparison. This could be demonstrated by significantly larger spleens and a higher bone marrow cell count in *Eμ-Myc;CXCR4*^{C1013G} (Figure 18A and B).

In the peripheral blood of both groups, we could see highly elevated white blood cell counts, attributed to leukemic lymphoma cells. However, similarly to the young 1-month-old mice we could not detect significant differences in the level of white blood cell counts between the two biological groups (Figure 18C).

Histopathology confirmed these findings and also fully in line with findings of the premalignant cohorts, *Eμ-Myc;CXCR4*^{C1013G} mice requiring euthanasia presented with a more aggravated splenic infiltration pattern which more extensively disrupted the physiological organ structure. Also, we could see a higher tendency towards extranodal disease, e.g. hepatic infiltration by lymphoma cells, further indicating a more invasive, extranodal phenotype of CXCR4 hyperactivated lymphoma, which we had also seen in the *Eμ-TCL1* comparison (Figure 18D and E).

Likewise, as seen in the *Eμ-TCL1* cohorts, hyperactivation of CXCR4 did not lead to a change of the immunophenotype of Eμ-Myc-driven lymphoma. In both groups we were able to detect tumors which were B220+IgM+ and such which were B220+IgM-, with no significant differences in the frequency between the two groups.

However, although *Eμ-Myc;CXCR4*^{C1013G} displayed above mentioned features resembling a more aggressive lymphoma phenotype, median survival was not altered significantly when compared with *Eμ-Myc* control mice (Figure 18D).

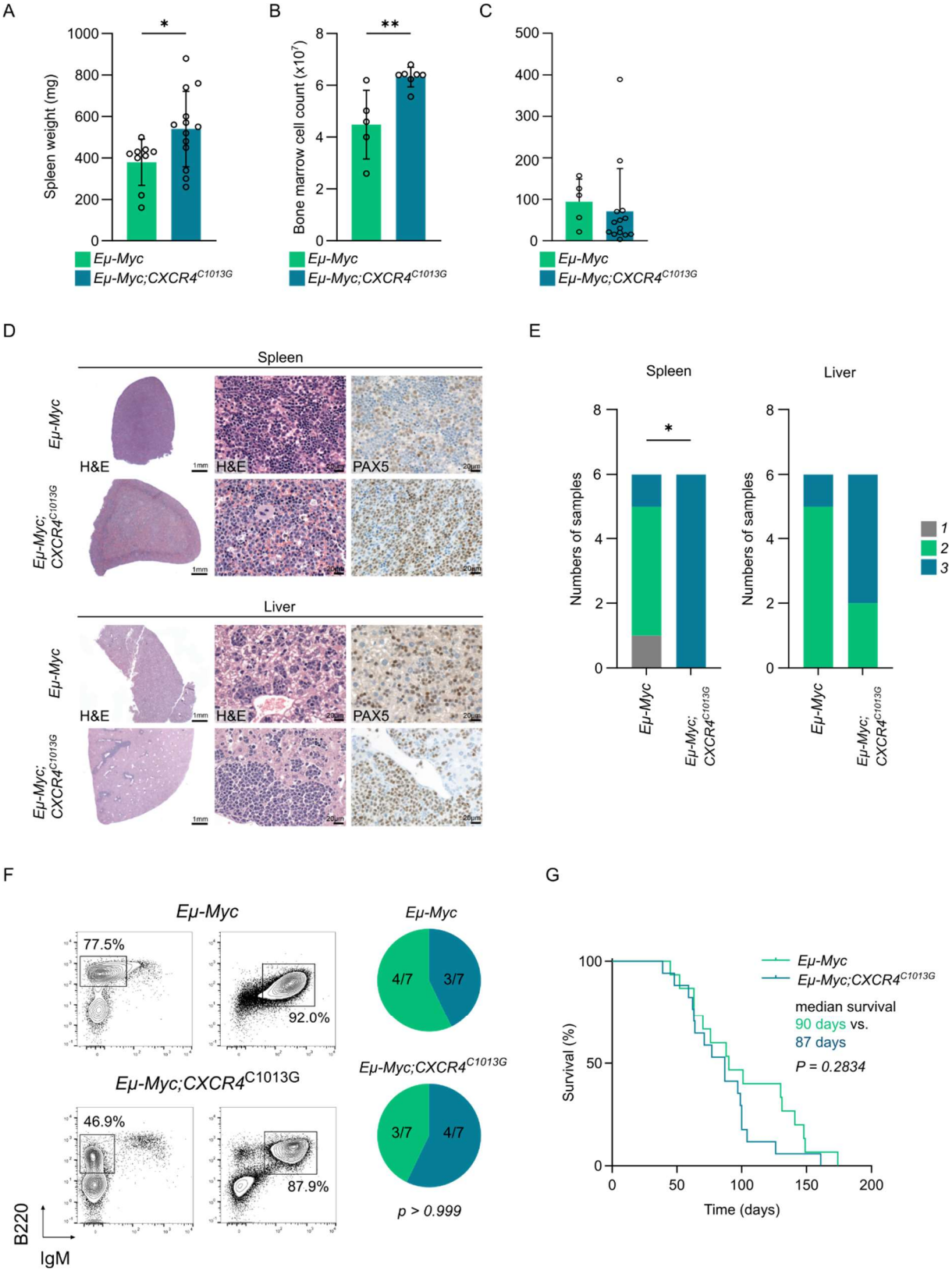
A
Spleen weight (mg)
1000
800
600
400
200
0
*
Eμ-Myc
Eμ-Myc;CXCR4C1013G
B
Bone marrow cell count (x10^7)
8
6
4
2
0
**
Eμ-Myc
Eμ-Myc;CXCR4C1013G
C
500
400
300
200
100
0
Eμ-Myc
Eμ-Myc;CXCR4C1013G
D
Spleen
Eμ-Myc
Eμ-Myc; CXCR4C1013G
H&E
H&E
PAX5
1mm
20μm
Liver
Eμ-Myc
Eμ-Myc; CXCR4C1013G
H&E
H&E
PAX5
1mm
20μm
E
Spleen
Liver
Numbers of samples
8
6
4
2
0
*
Eμ-Myc
Eμ-Myc; CXCR4C1013G
1
2
3
F
Eμ-Myc
77.5%
92.0%
Eμ-Myc;CXCR4C1013G
46.9%
87.9%
B220
IgM
Eμ-Myc
4/7
3/7
Eμ-Myc;CXCR4C1013G
3/7
4/7
p > 0.999
G
Survival (%)
100
50
0
0
50
100
150
200
Time (days)
Eμ-Myc
Eμ-Myc;CXCR4C1013G
median survival
90 days vs.
87 days
P = 0.2834

Figure 18. Characterization of *Eμ-Myc;CXCR4^{C1013G}* mice presenting with manifest lymphoma.

(**A**) Spleen weight of mice with manifest lymphoma (*Eμ-Myc*, n = 9; *Eμ-Myc;CXCR4^{C1013G}*, n = 13). (**B**) Bone marrow cell count of mice with manifest lymphoma (*Eμ-Myc*, n = 5; *Eμ-Myc;CXCR4^{C1013G}*, n = 7). (**C**) WBC of mice with manifest lymphoma (*Eμ-Myc*, n = 5; *Eμ-Myc;CXCR4^{C1013G}*, n = 14). (**D**) Representative images of H&E and immunohistochemistry of *Eμ-Myc* and *Eμ-Myc;CXCR4^{C1013G}* mice with manifest lymphoma (scale bars spleen: overview = 1mm, detailed images: 20μm, scale bars liver: overview = 1mm, detailed images = 20μm). (**E**) Quantification of histology scores (1-3) of spleen and liver from mice presenting with manifest lymphoma (*Eμ-Myc*, n = 6; *Eμ-Myc;CXCR4^{C1013G}*, n = 6). Scorings system details as indicated in the methods section. (**F**) Representative images of immunophenotyping of animals with manifest lymphoma by flow cytometry showing B220 and IgM expression of lymphoma cells (*Eμ-Myc*, n = 7 *Eμ-Myc;CXCR4^{C1013G}*, n = 7). Fractions of animals with either IgM+ or IgM- phenotype are indicated in the pie charts. (**G**) Kaplan-Meier survival curves of the indicated cohorts of mice (*Eμ-Myc*, n = 15; *Eμ-Myc;CXCR4^{C1013G}*, n = 17), median survival and P value of log-rank (Mantel-Cox) test are shown. Statistical analyses for (**A**), (**B**), (**C**) and (**E**) were performed with Student's t test, * $P < 0.05$, ** $P < 0.01$. Error bars indicate standard deviation (SD).

Summarizing, these data show that CXCR4 expression leads to an increased susceptibility for extranodal disease, while not altering immunophenotype or survival in Eμ-Myc-driven aggressive B cell lymphoma.

3.6 Hyperactivated CXCR4 is a hallmark of aggressive lymphoma biology

3.6.1 CXCR4 Surface and transcript expression are regulated by MYC

As we saw phenotypical differences in both, the *Eμ-TCL1* and the *Eμ-Myc* cohorts, but no survival differences in the *Eμ-Myc* cohorts, in contrast to the clear difference in the *Eμ-TCL1* comparison, we aimed to investigate possible reasons for these differences.

Thus, in a first step flow cytometry-based measurement of CXCR4 surface expression on tumor cells of Myc- and TCL1-driven lymphoma and compared it to healthy B cells, which we gained from healthy *WT* control animals. Here we discovered a drastically increased CXCR4 expression in *Eμ-Myc* lymphoma cells in comparison to both *WT* but also *Eμ-TCL1* lymphoma cells. *Eμ-TCL1* lymphoma cells on the other hand showed a trend toward increased CXCR4 expression compared to *WT* controls, which was however not significant. (Figure 19A). As also

elaborated in the introduction, CXCR4 and MYC expression have been linked in a previous publication in DLBCL patients (Chen et al. 2015) (also refer to 1.4.2). Hence, an explanation for the seen effects could be that CXCR4 signaling is an inherent part of MYC-driven lymphoma. Therefor we sought to evaluate more data sets to further support this hypothesis and analyzed large publicly available B-NHL patient data sets. In two data sets, for a significant number of patients MYC-translocation status was available, which indeed correlated with CXCR4 mRNA expression (Figure 19B). In the same data sets and one additional one, we could moreover see a significant correlation of MYC mRNA and CXCR4 mRNA expression (Figure 19C). Taken together these data strongly indicate MYC enhances CXCR4 expression and CXCR4 signaling may be part of the MYC oncogenic program and therefor additional hyperactivation by CXCR4^{C1013G} may be masked by an already inherently increased CXCR4 activity in *Eμ-Myc* B cells.

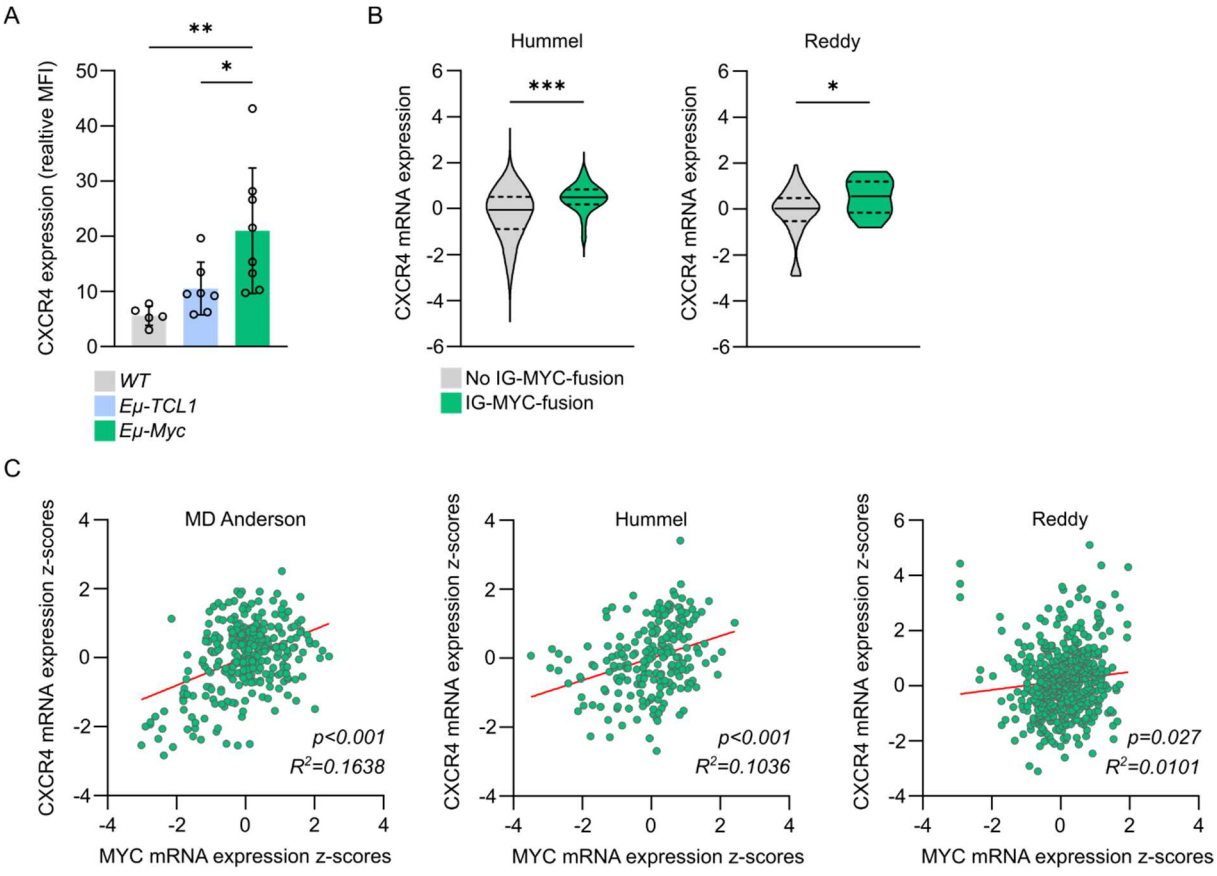

Figure 19. CXCR4 surface and transcript expression is regulated by MYC

(**A**) CXCR4 expression of tumors (Eμ-Myc, n = 8; Eμ-TCL1, n = 7) compared with healthy B cells from adult WT mice (n = 5), relative to isotype by flow cytometry. (**B**) Correlation of CXCR4 mRNA expression dependent of IG-MYC fusion status from the Hummel data set (GSE4475) (Hummel et al. 2006) (IG-MYC-fusion, n = 59; no IG-MYC-fusion n = 141, samples not annotated and samples with MYC translocations other than IG excluded) and the Reddy data set (Reddy et al. 2017) (IG-MYC-fusion, n = 12; no IG-MYC-fusion, n= 80). (**C**) Correlation of MYC mRNA and CXCR4 mRNA expression as log Z-scores relative to all samples in the MD Anderson Cancer Center data set (Ma et al. 2022) (n = 286), analyzed with cBioPortal (Cerami et al. 2012; de Bruijn et al. 2023; Gao et al. 2013), the Hummel data set (GSE4475) (Hummel et al. 2006) (n = 221) and the Reddy data set (Reddy et al. 2017) (n = 482).

Statistical analyses were performed with one-way ANOVA with Tukey correction for multiple comparisons (a), Student's t-test (b) and Pearson correlation (c), *P < 0.05, **P < 0.01, ***P < 0.001. Error bars indicate standard deviation (SD).

3.6.2 CXCR4a signature enriches in *Eμ-TCL;CXCR4^{C1013}*

To underline our hypothesis that CXCR4 signaling may potentially be part of the Myc oncogenic program, we performed an additional RNA sequencing of purified lymphoma cells (CD19-directed magnetic bead separation) from *Eμ-Myc* and *Eμ-Myc;CXCR4^{C1013G}* and *Eμ-TCL1* and *Eμ-TCL1;CXCR4^{C1013G}* lymphoma cells. Here we could see that *Eμ-Myc* and *Eμ-Myc;CXCR4^{C1013G}* lymphoma cells expressed a highly similar transcriptome dominated by a MYC signature, underscored by only 8 significantly differentially expressed pathways in a gene set enrichment analysis (Figure 20A, B and C). This was in clear difference to *Eμ-TCL1* vs. *Eμ-TCL1;CXCR4^{C1013G}* which will be outlined in detail in 3.7.

Thus, we performed a further enrichment analysis applying our CXCR4a signature of CXCR4 activation in B cells to *Eμ-Myc* and *Eμ-Myc;CXCR4^{C1013G}* and *Eμ-TCL1* and *Eμ-TCL1;CXCR4^{C1013G}* lymphoma cells. Here we saw that CXCR4a only enriched in the Eμ-TCL1 comparison but not in *Eμ-Myc;CXCR4^{C1013G}* vs. *Eμ-Myc* lymphoma cells (Figure 20D). Hence, these data further support that MYC might positively regulate CXCR4 expression, which could explain why in fully developed Eμ-Myc-driven lymphoma no additional effects of CXCR4 hyperactivation by *CXCR4^{C1013G}* could be seen on a transcriptomic level.

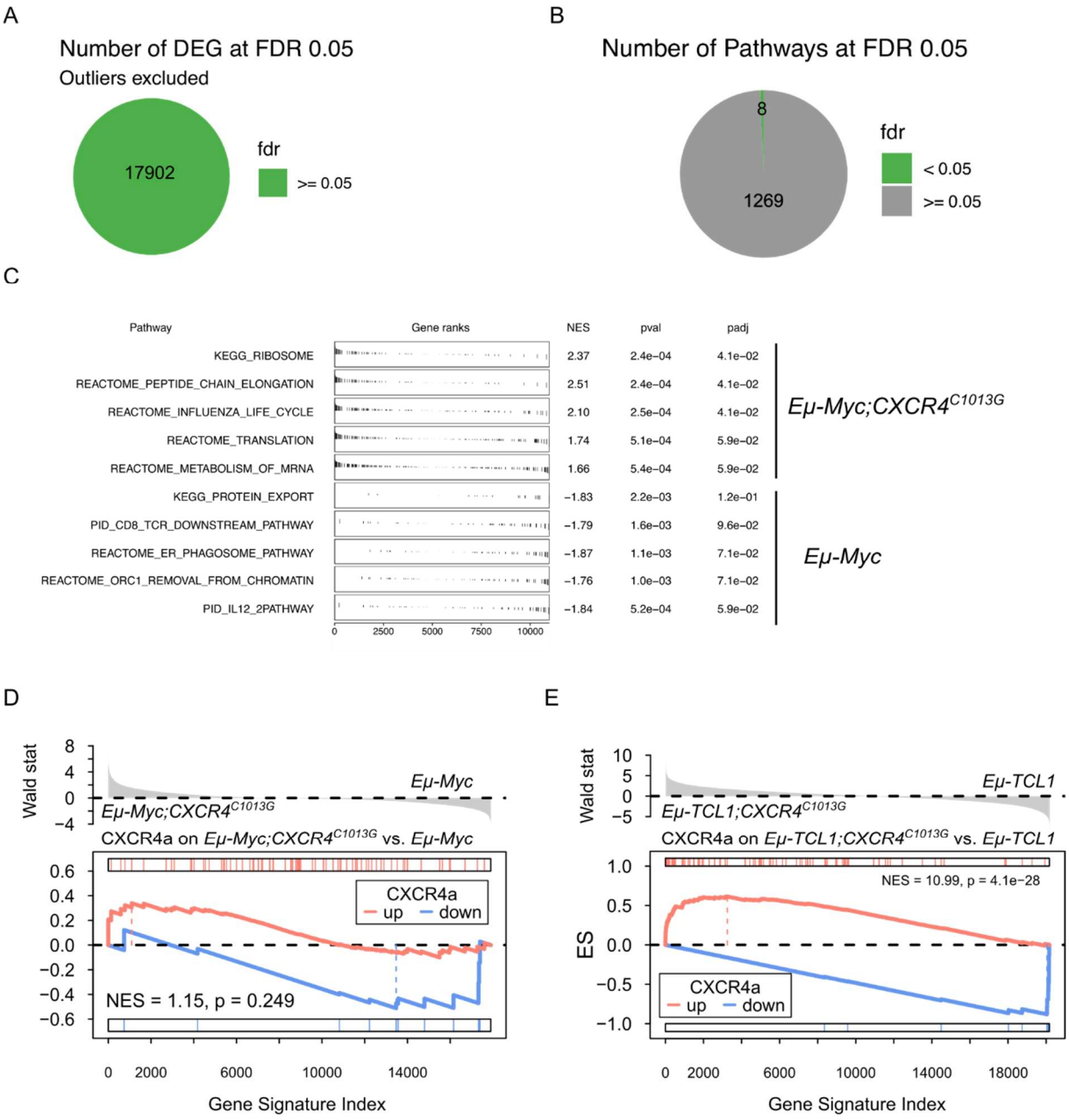

Figure 20. CXCR4a signature enriches in *Eμ-TCL;CXCR4^{C1013G}* but not *Eμ-Myc;CXCR4^{C1013G}*

(**A**) DEG in *Eμ-Myc* (n = 6) vs. *Eμ-Myc;CXCR4^{C1013G}* (n = 6). (**B**) GSEA for curated gene sets listed in MsigDB (Liberzon et al. 2011; Subramanian et al. 2005) in *Eμ-Myc* vs. *Eμ-Myc;CXCR4^{C1013G}*. (**C**) GSEA for curated gene sets listed in MsigDB (Liberzon et al. 2011; Subramanian et al. 2005) in *Eμ-Myc* vs. *Eμ-Myc;CXCR4^{C1013G}* CD19+ B cells showing normalized enrichment scores (NES) P value (pval) and adjusted P value (padj). (**D**) GSEA showing CXCR4a enrichment in *Eμ-Myc;CXCR4^{C1013G}* vs. *Eμ-Myc*. (**E**) GSEA showing CXCR4a enrichment in *Eμ-TCL1;CXCR4^{C1013G}* vs. *Eμ-TCL1*. Figure generated in collaboration with H. Carlo Maurer.

Summarizing our data, we conclude CXCR4 activation is an integrative hallmark of aggressive MYC-driven lymphoma. Therefore, we believe CXCR4^{C1013G} did not further induce a significant additional activation of CXCR4 downstream signaling activity and thus lymphoma latency and outcome, due to an already present activation via a MYC-CXCR4 axis.

3.7 The *Eμ-TCL1;CXCR4^{C1013G}* oncogenic transcriptional program

Thus, to further investigate how enhanced CXCR4 activation promotes B cell lymphoproliferation *in vivo* we concentrated on the transcriptomic profile of the *Eμ-TCL1;CXCR4^{C1013G}* model, in which we observed a significant enrichment of the CXCR4a signature.

Hence, we isolated CD19+ B cells from spleen and bone marrow of 6-week-old *Eμ-TCL1* and *Eμ-TCL1;CXCR4^{C1013G}* mice as well as respective controls and performed whole transcriptome profiling (Figure 21A).

In a first step we performed gene set enrichment analysis of curated pathways in *CXCR4^{C1013G}, Eμ-TCL1* and *Eμ-TCL1;CXCR4^{C1013G}* compared to *WT* controls and observed an overlap of deregulated pathways among these biological groups (Figure 21B). Importantly to confirm the premalignant state of *Eμ-TCL1* B cells, we were able to show pathways associated with B cell cancer biology and inflammation were enriched and DNA repair pathways were depleted in *Eμ-TCL1* compared to *WT* B cells (Figure 21C).

Aside of overlapping pathways, we also observed some pathways which were enriched specifically in *Eμ-TCL1;CXCR4^{C1013G}* B cells (Figure 21B). Among those were pathways involved in cell cycle progression (PLK1 pathway, G2M checkpoint, cell cycle checkpoints). Concordantly, pathways including p53 signaling and apoptosis (P53 pathway, P53 dependent G1 DNA damage response, apoptosis) and immune response (interferon gamma response) were depleted in *Eμ-TCL1;CXCR4^{C1013G}* B cells (Figure 21B).

Additionally, we directly compared *Eμ-TCL1* with *Eμ-TCL1;CXCR4^{C1013G}* B cells, to gain an understanding which transcriptomic changes were induced by additional CXCR4 siganling

within the Eμ-TCL1 oncogenic program and could possibly explain an accelerated lymphomagenesis and the phenotypic differences observed. Strikingly, we found the *Eμ-TCL1;CXCR4*^{C1013G} B cell transcriptome was distinctly different compared to *Eμ-TCL1* B cells. In a gene set enrichment analysis, we could see an enrichment of cell cycle progression and proliferation pathways and depletion of p53-, apoptosis-, and immune response-related pathways (overwiew of selcted pathways in Figure 21D), fully in line with the clinical presentation of the mice. Analyzing expression of individual genes, we found 2140 differentially expressed genes between premalignant B cells from *Eμ-TCL1* vs. *Eμ-TCL1;CXCR4*^{C1013G} mice. These included cell cycle genes like cyclins (Ccne1), cyclin-dependent kinase phosphatases (*Cdc25b*), mitotic regulators (*Aurkb, Prc1, Hdac6, Nek2, Mki67*), DNA repair and DNA damage response genes (*Brca2, Fanca, Rad54l*), transcripts of well-established tumor suppressor genes (*Klf6, CD82*) and positive regulators of apoptosis (*Pmaip1*) (a clustered overview of selected genes is depicted in Figure 21E). Interestingly, when we had a look at the most differentially expressed genes, multiple key components of the Plk1-Foxm1 pathway (including *Plk1* and *Foxm1* itself), the *Foxm1* target *Cdc25b* and the Foxm1 deubiquitinating enzyme *Usp5* involved in stabilization of the Foxm1 protein (Li et al. 2017), and *Myb*, which forms a complex with Foxm1 and is required for its function, were discovered. To further validate our findings that CXCR4 hyperactivation potentiates oncogenic programs we aimed for a cross-species application of our murine data on a human data set. To this end we used the Cancer Gene Census data set (Sondka et al. 2018) and two large human B cell lymphoma datasets (Chapuy et al. 2018; Reddy et al. 2017). Hence, we calculated an overlap of the list of differentially expressed genes in *Eμ-TCL1;CXCR4*^{C1013G} vs. *Eμ-TCL1* B cells with the Cancer Gene Census data bank of known regulators of oncogenic pathways and found 112 genes which were significantly differentially expressed in *Eμ-TCL1;CXCR4*^{C1013G} vs. *Eμ-TCL1* B cells were known regulators of oncogenic pathways (Figure 21F). This was further confirmed when we applied the same list of genes to the data sets of known DLBCL drivers

from two large patient cohorts (Figure 21G). In total we identified 10 DEGs which overlapped with both DLBCL datasets (outlined in Figure 21G) (Reddy et al. 2017; Chapuy et al. 2018).

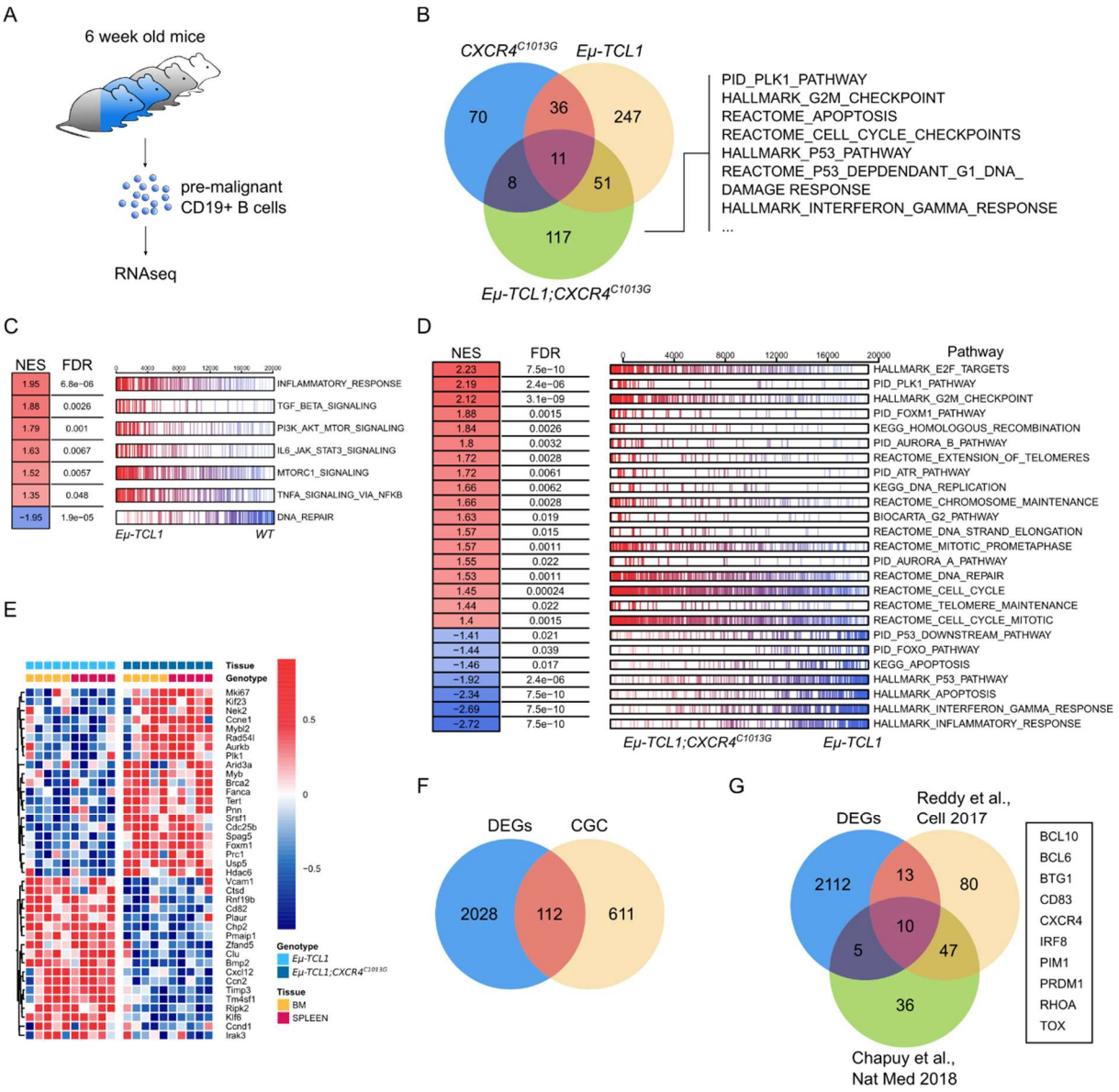

Figure 21. Co-activation of CXCR4 and TCL1 governs a distinct oncogenic transcriptional program in B cells

(**A**) Outline of experimental setup for RNA sequencing of splenic and bone marrow premalignant B cells (*WT*, n = 5; *CXCR4*^{C1013G}, n = 5; *Eμ-TCL1*, n = 5; *Eμ-TCL1;CXCR4*^{C1013G}, n = 5). (**B**) Venn diagram showing overlap of significantly enriched pathways (padj < 0.05) for curated gene sets listed in MsigDB (Liberzon et al. 2011; Subramanian et al. 2005) of indicated genotypes vs. WT B cells as determined by gene set enrichment analysis

(GSEA). (**C**) GSEA of *Eμ-TCL1* vs. *WT* CD19+ B cells showing normalized enrichment scores (NES) and false discovery rates (FDR) for curated gene sets listed in MsigDB (Liberzon et al. 2011; Subramanian et al. 2005). (**D**) GSEA of *Eμ-TCL1;CXCR4^{C1013G}* vs. *Eμ-TCL1* CD19+ B cells showing normalized enrichment scores (NES) and false discovery rates (FDR) for curated gene sets listed in MsigDB (Liberzon et al. 2011; Subramanian et al. 2005). (**E**) Selection of differentially expressed genes (DEG) with adjusted P value (padj) < 0.05 of *Eμ-TCL1;CXCR4^{C1013G}* vs. *Eμ-TCL1* CD19+ B cells. (**F**) Overlap of DEG with padj < 0.05 of *Eμ-TCL1;CXCR4^{C1013G}* vs. *Eμ-TCL1* CD19+ B cells with the Cancer Gene Census (CGC) (Sondka et al. 2018). (**G**) Overlap of DEG with padj < 0.05 of *Eμ-TCL1;CXCR4^{C1013G}* vs. *Eμ-TCL1* CD19+ B cells with DLBCL drivers in patient datasets (Reddy et al. 2017; Chapuy et al. 2018). Figures C, D and E generated in collaboration with H. Carlo Maurer.

3.8 *Eμ-TCL1;CXCR4^{C1013G}* B cells enrich a Richter's transformation signature

Having detected significant overlaps of the differentially expressed genes with patient data sets and as we observed some of our symptomatic *Eμ-TCL1;CXCR4^{C1013G}* mice experienced morphological features of Richter's transformation, we aimed to evaluate if the transcriptional program of patients with Richter's transformation were in line with the transcriptomic changes induced by hyperactive CXCR4 signaling. For this matter, we generated a gene signature from a previously published CLL data set of patients with Richter's transformation (Klintman et al. 2020). Strikingly, this "Richter-signature" enriched significantly only in B cells of *Eμ-TCL1;CXCR4^{C1013G}* mice, but not in *Eμ-TCL1* or *CXCR4^{C1013G}*. This illustrates key transcriptomic features of Richter's transformation are promoted cooperatively by CXCR4 hyperactivation and TCL1, in line with our histopathological data (Figure 22A and B).

To validate our transcriptomic data, we sought to exclude the presence of a monoclonal B cell proliferation in our purified B cell samples. To this end we performed transcriptome based clonality analysis as previously published (Shugay et al. 2015; Farmanbar, Kneller, and Firouzi 2019; Bolotin et al. 2015). Confirming our data, by this method we could rule out monoclonal B cell proliferation for both *Eμ-TCL1* and *Eμ-TCL1;CXCR4^{C1013G}* samples (Figure 23).

Summarizing our transcriptomic data provides further evidence that CXCR4 hyperactivation is associated with an aggravated tumor biology and induces a transcriptomic profile resembling features of Richter's' Transformation in cooperation with TCL1.

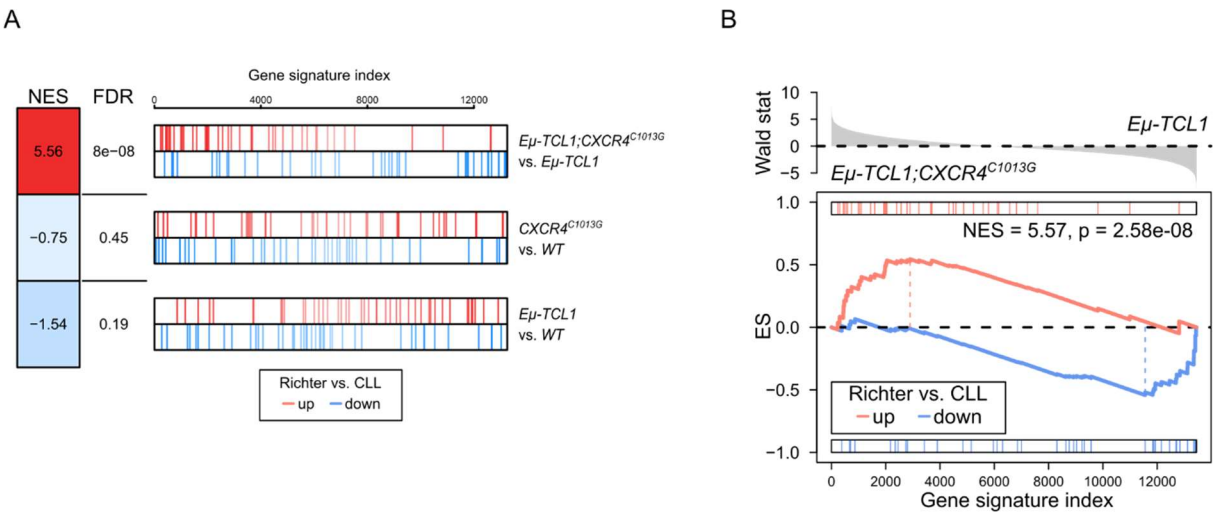

Figure 22. *Eμ-TCL1;CXCR4^{C1013G}* B cells enrich a Richter's transformation signature generated from a human patient cohort

(A) GSEA showing enrichment of a Richter's transformation signature in *Eμ-TCL1;CXCR4^{C1013G}* vs. *WT, Eμ-TCL1* vs. *WT* and *CXCR4^{C1013G}* vs. *WT* CD19+ B cells showing normalized enrichment scores (NES) and false discovery rates (FDR). (**B**) GSEA showing enrichment of a Richter's transformation signature (Klintman et al. 2021) in *Eμ-TCL1;CXCR4^{C1013G}* B cells. Figure generated in collaboration with H. Carlo Maurer.

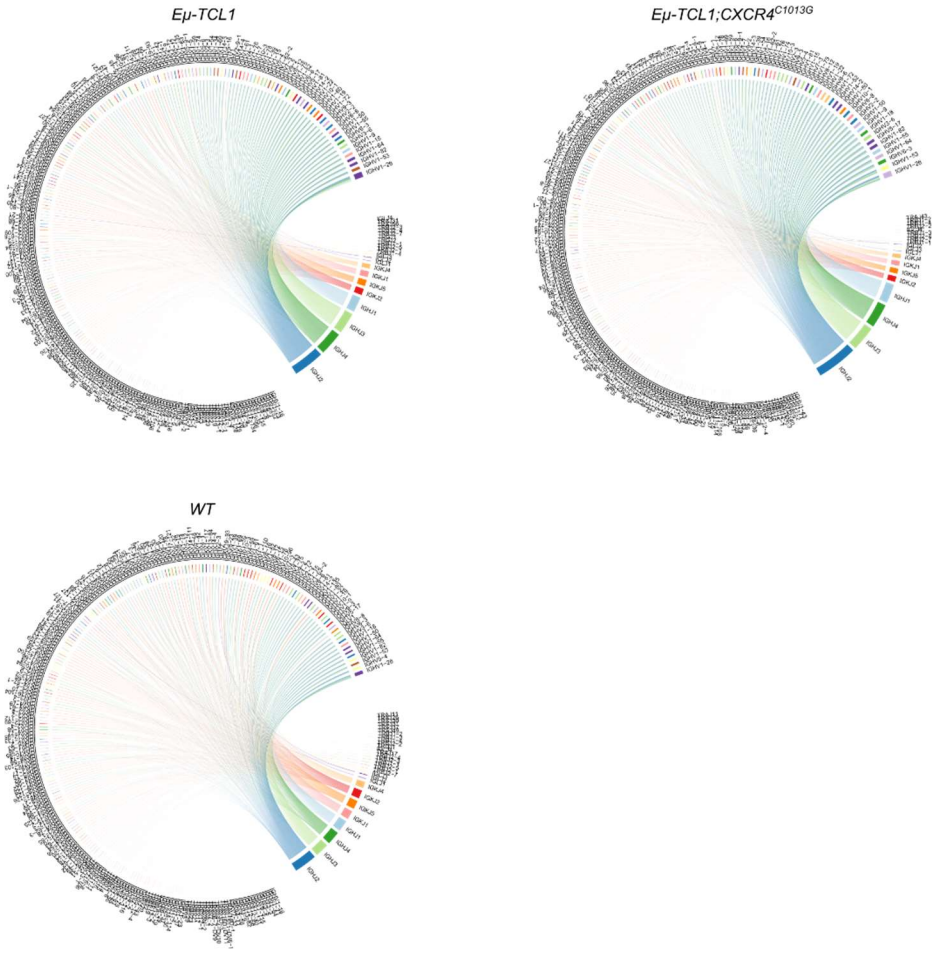

Figure 23. Transcriptomic clonality analysis of purified B cells of young premalignant mice.

Representative circos plots of V(D)J-rearrangement of CD19+ B cells of 6-week-old mice (*Eμ-TCL1*, n = 5; *Eμ-TCL1;CXCR4^{C1013G}*, n = 5; *WT*, n = 5). Figure generated in collaboration with M. Wirth.

3.9 CXCR4 induced oncogenic programs are associated with dismal clinical outcomes

To further validate our CXCR4a signature and evaluate its applicability to humans, we aimed to apply it to clinical data. As we saw greatest effects in the Eμ-TCL1 comparison, which is an established model of indolent lymphoma and especially high-risk CLL-like disease, we collaborated with Thorsten Zenz and Junyan Lu and applied our signatures to data sets of CLL with available transcriptomics. Here we stratified patients using upregulated genes of the CXCR4a signature as well as a signature generated from *Eμ-TCL1;CXCR4^{C1013G}* vs. *Eμ-TCL1*. We found that CXCR4a_high patients had significantly reduced treatment free intervals, which we termed time to treatment (TTT). Moreover, patients characterized by the *Eμ-*

TCL1;CXCR4^{C1013G} vs. *Eμ-TCL1* signature did not only have significantly reduced treatment free intervals but also reduced overall survival (Figure 24). This shows our data is transferable to clinical data and further supports our hypothesis that TCL1 and CXCR4 cooperatively accelerate lymphomagenesis and promote a more aggressive tumor biology.

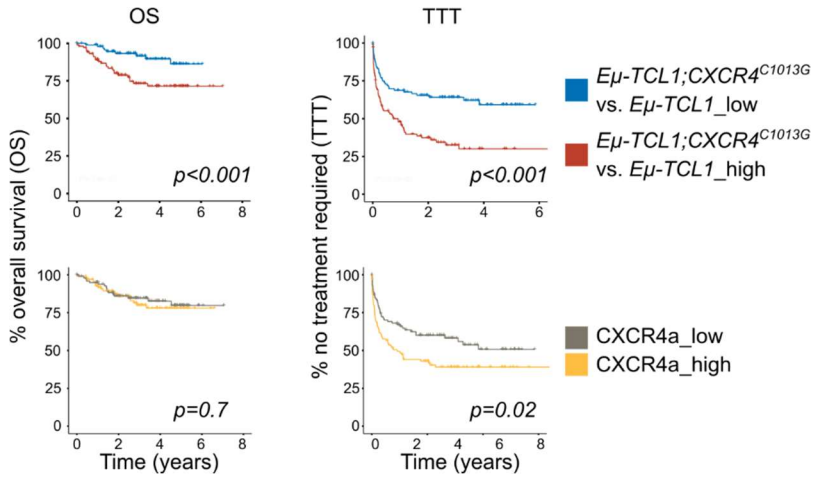

Figure 24. Overall and treatment free survival curves of CLL patients stratified by CXCR4 induced oncogenic programs

Kaplan-Meier plots of overall survival (OS) and time to treatment (TTT) in a cohort of CLL patients, for patients with high vs. low enrichment of upregulated genes from CXCR4 signatures (*CXCR4*^{C1013G} vs. *WT* and *Eμ-TCL1;CXCR4*^{C1013G} vs. *Eμ-TCL1*) (TTT *CXCR4*^{C1013G} vs. *WT*, n = 105 high, n = 103 low; OS *CXCR4*^{C1013G} vs. *WT* and *Eμ-TCL1;CXCR4*^{C1013G} vs. *Eμ-TCL1*, n = 105 in each group; TTT *Eμ-TCL1;CXCR4*^{C1013G} vs. *Eμ-TCL1*, n = 104 in each group). P-values of log-rank (Mantel-Cox) test are shown. Figure generated in collaboration with Junyan Lu.

4 Discussion

B cell non-Hodgkin lymphomas are a biologically heterogeneous group of cancers, that rank within the top 10 of most common and most lethal types of cancer in the Western world (Thandra et al. 2021). By clinical presentation they can be separated into two groups reflecting their underlying biology – aggressive and indolent B-NHLs, with the most common forms for these subgroups being DLBCL and CLL, respectively.

Previous data has associated CXCR4 with dismal outcomes in many cancers (Zhao et al. 2015; Su et al. 2005; Speetjens et al. 2009; Muller et al. 2001; Scala et al. 2005), including aggressive and indolent B-NHL (Chen et al. 2015; Moreno et al. 2015). However, all the previously available data was retrospective, correlative, or *in vitro* and no *in vivo* data investigating the effects of aberrant CXCR4 signaling on the biology of B-NHLs existed.

Hence, in this study we modeled hyperactive CXCR4 signaling by co-expressing a truncated version of CXCX4 with impaired desensitization - $CXCR4^{C1013G}$ - in the well-established tumor models of aggressive (*Eμ-Myc)* and indolent B-NHL (*Eμ-TCL1*). Here, we initially investigated the effects hyperactivated CXCR4 signaling alone induced in B cells of healthy young mice and found a vast set of differentially regulated genes predisposing B cells for leukemogenesis. Furthermore, we demonstrated hyperactivated CXCR4 signaling functions as an oncogene cooperating with TCL1 to accelerate CLL progression and development of aggressive B cell lymphoma. Moreover, we show hyperactive CXCR4 signaling induces a more aggressive and invasive tumor phenotype. Additionally, we provide evidence suggesting CXCR4 may be a key factor of MYC-driven B cell lymphoma biology. And lastly, we demonstrated a distinct oncogenic transcriptomic program in *Eμ-TCL1;*$CXCR4^{C1013G}$ vs. *Eμ-TCL1* tumor cells which when used on human data sets is associated with dismal outcomes in a human CLL cohort.

Hence, taken together the main accomplishments of this work, which will be elaborated in detail below are:

1. CXCR4 functions as a crucial activator of oncogenic pathways in B cells and prones B cells for lymphomagenesis/leukemogenesis
2. CXCR4 and TCL1 cooperatively accelerate lymphomagenesis/leukemogenesis
3. CXCR4 may be an underlying hallmark of MYC-driven lymphoma
4. Hyperactive CXCR4 signaling aggravates tumor aggressiveness in B-NHL
5. The CXCR4 hyperactivated tumor transcriptome is associated with dismal outcomes in CLL patients

4.1 CXCR4 is a crucial activator of multiple key oncogenic pathways in B cells and prones B cells for lymphomagenesis/leukemogenesis

CXCR4 is recurrently overexpressed in multiple cancers and associated with adverse outcomes (Zhao et al. 2015; Su et al. 2005; Speetjens et al. 2009; Muller et al. 2001; Scala et al. 2005). Additional to differential expression, recurrent mutations of CXCR4 are known, most importantly in Waldenström's macroglobulinemia, in which approximately a third of all patients harbor gain-of-function mutations of CXCR4 (Hunter et al. 2014). However, we demonstrated recurrent mutations are also to be found in DLBCL, even though they occur at a lower frequency. As mentioned, previous work focused on correlating elevated expression to clinical presentation and outcomes (Zhao et al. 2015; Su et al. 2005; Speetjens et al. 2009; Muller et al. 2001; Scala et al. 2005). However, gene / protein expression especially in the context of chemokine signaling not adequately reflects the complex biological processes within the cells (Busillo and Benovic 2007). We aimed to address this beforehand lack of *in vivo* data by utilizing the *CXCR4*^{C1013G} model and intercrossing it with established models of B cell lymphoma / leukemia.

Hence in a first step, we chose to validate our approach by stimulating healthy B cells of *CXCR4*^{C1013G} mice with CXCL12 and show enhanced phosphorylation of CXCR4 downstream targets AKT and ERK (Scala 2015). As the experiment was performed *in vitro* on purified B cells, ruling out effects of the microenvironment, it proves a CXCL12 induced hyperactivation

of CXCR4 signaling specifically in B cells, which is underscored by a control group of CXCR4 inhibited B cells that show no changes in downstream activity, demonstrating this effect is dependent on binding of CXCL12 to CXCR4.

In a second step, we evaluated the effects this enhanced CXCR4 signaling in B cells had on the composition of different B cell compartments in clinically healthy mice. Here we found an expansion of B1 B cells, which is important to note, as from this B cell subset malignant transformation to CLL and mantle cell lymphoma has been reported (Dono, Cerruti, and Zupo 2004).

Lastly, we performed RNA-sequencing to study the transcriptomic changes hyperactivated CXCR4 signaling evokes on healthy B cells and show B lymphocytes of *CXCR4*^{C1013G} mice render a vastly different transcriptomic profile than those of *WT* litter mates. As this transcriptomic program enriches curated pathway gene sets for chemokine signaling and inflammation it further demonstrates the applicability of *CXCR4*^{C1013G} as a model of hyperactivated CXCR4 signaling. Furthermore, as this enrichment is found in healthy B cells it suggests CXCR4 signaling might drive the B cell transcriptional program toward oncogenic processes.

Interestingly, as previously described, *CXCR4*^{C1013G} mice without addition of a further oncogenic transgene do not develop B cell malignancies (Balabanian et al. 2012). This indicates that while CXCR4 hyperactivation, as we also describe, fuels tumorigenesis in cooperation with TCL1 and hence acts as a co-driver in double transgenic mice, it does not exert enough oncogenic potential to initiate B cell malignancies alone. This may implicate that during the complex mechanisms ultimately leading to symptomatic B cell tumors, dysregulation of CXCR4 may be an additional factor contributing to malignant transformation with other oncogenes or aggravate tumor biology, when acquired later, as also described below (see 4.2. and 4.4).

Summarizing, hyperactivation of CXCR4 can be efficiently modelled by the *CXCR4*^{C1013G} model organism and induces a multitude of transcriptional alterations including several curated

oncogenic gene sets in B cells, which also redistributes different B cell compartments and prones B cells for malignant transformation.

4.2 TCL1 and CXCR4 cooperatively accelerate lymphomagenesis/-progression

Mice harboring the Eμ-TCL1 transgene are known to steadily develop leukemic disease with presence of malignantly transformed $CD19^{+}CD5^{+}$ cells in peripheral blood and lymphatic organs way ahead of symptomatic disease (Bichi et al. 2002). Strikingly, after intercrossing *CXCR4*^{C1013G} with *Eμ-TCL1* mice, we saw a dramatically accelerated lymphomagenesis and -progression with preservation of the TCL1-driven $CD19^{+}CD5^{+}B220^{dim}$ tumor immunophenotype in double transgenic mice, which implicates a cooperative mechanism of CXCR4 and TCL1 in lymphomagenesis.

Importantly, when investigating the migratory potential of these cells, we could demonstrate that B cells of *Eμ-TCL1;CXCR4*^{C1013G} mice additionally exhibited significantly increased migratory capacities. Noteworthy, the most significantly increased migratory capacity was seen in malignantly transformed $CD19^{+}CD5^{+}$ cells. This further indicates the cooperative effect of activated CXCR4 signaling and the Eμ-TCL1 transgene.

While it has previously been reported that the CXCR4-CXCL12 axis is crucial for CLL cells and their complex tumor microenvironment, especially in response to BTK inhibitors (e.g. ibrutinib) (Chen et al. 2016; Burger et al. 2000) it previously remained unclear how hyperactive CXCR4 signaling impacts the development of CLL *in vivo*. Thus, this work provides first *in vivo* evidence activated CXCR4 signaling accelerates B cell leukemogenesis in a murine model, which is most frequently used to model CLL / indolent lymphoma.

Even though with the approach used, in which mutant $CXCR4^{C1013G}$ is expressed genomically including cells of the microenvironment, the outlined data indicates by several ways that the effects seen are most likely attributed to B cell intrinsic effects. E.g., as we showed, *CXCR4* gene expression is highest in B cells, and previous data revealed CXCR4 as a pivotal regulator of B cell development and function (Allen et al. 2004; Biajoux et al. 2016; Freitas et al. 2017;

Alouche et al. 2021). Furthermore, even *in vitro*, without support of the microenvironment, B cells with hyperactivated CXCR4 signaling and especially those transformed ($CD19^+CD5^+$) cells exhibited increased migration. Moreover, besides the effects seen on B cells, the absence of effects on the T cell compartment, which did not show any significant alterations and suggests an intact T cell response, underscores the perception that TCL1 and CXCR4 act as synergistic oncogenes specifically in B cells.

Taken together, our data demonstrates for the first time *in vivo* that CXCR4 acts as codriver of leukemogenesis in cooperation with TCL1 in B cells.

4.3 CXCR4 activation may be an integrative hallmark of MYC-driven lymphoma

As hyperactive CXCR4 signaling and TCL1 synergistically drive leukemogenesis, we aimed to validate our data in a model of aggressive B cell lymphoma and chose the well-established *Eμ-Myc* model. However, unlike the observations made with *Eμ-TCL1;CXCR4^{C1013G}* mice, *Eμ-Myc;CXCR4^{C1013G}* mice did no exhibit similarly drastic changes. While premalignant mice exhibited significantly elevated WBCs and spleen weights, reflecting a more pronounced ongoing progression of tumorous disease, this did not translate to significant changes in survival.

Hence, we investigated possible explanations for the discrepancy regarding outcomes between the two models. We demonstrated elevated CXCR4 protein expression on Eμ-Myc-driven lymphoma cells by flow cytometry and showed increased CXCR4 transcript levels correlate with expression and oncogenic MYC mutations. It is noteworthy, that even though no B cell lymphoma specific data exist so far, some data shows MYC may bind and directly activate the CXCR4 promoter (Moriuchi et al. 1999). This is underscored by the transcriptomic data we evaluated from publicly available data sets, in which we demonstrate a correlation of MYC and CXCR4 expression, in B cell lymphoma patients (Ma et al. 2022; Hummel et al. 2006; Reddy et al. 2017; Cerami et al. 2012; de Bruijn et al. 2023; Gao et al. 2013). Additionally, an

increase of CXCR4 expression was seen in patient samples with translocation of *MYC* further supporting a regulation of CXCR4 by MYC in a B cell oncogenic context.

Hence it seems probable that transformed B cells, with a MYC-oncogenic program mask CXCR4 induced effects, as these are at least partly also induced by the MYC oncogenic program itself. Thus, there might not be a relevant CXCR4 hyperactivation induced acceleration of exponential tumor growth in *Eμ-Myc* animals. However, further investigations in a different experimental approach might show additional effects and are needed to demonstrate our hypothesis directly.

4.4 Hyperactivation of CXCR4 leads to a more aggressive phenotype / biology

When evaluating the histopathology of the *Eμ-TCL1;CXCR4*^{C1013G} cohort, we identified a subgroup of mice with a phenotypically more aggressive presentation of disease. These were characterized by aggravated extranodal disease and microscopic features of Richter's transformation. Strikingly, in accordance an enrichment of a patient derived "Richter-signature" enriched in the transcriptomic program of premalignant *Eμ-TCL1;CXCR4*^{C1013G} B cells. This further indicates a B cell-specific influence of CXCR4 signaling towards a more aggressive lymphoma phenotype. Intriguingly, in CLL patients with Richter's transformation, mutations in regulatory elements of *CXCR4* have recently been discovered (Klintman et al. 2020). As some data links active Akt signaling, a downstream target of CXCR4, to Richter's transformation (Kohlhaas et al. 2021), it seems plausible that Akt phosphorylation by hyperactivated CXCR4 may be a contributing factor for the aggressive lymphoma phenotype in our CXCR4 hyperactivation models, even though further investigations are needed to fully confirm this link.

To date, CXCR4 gain-of-function mutations are best studied in Waldenström's Macroglobulinemia and cell lines derived from such patients, as CXCR4 gain-of-function mutations are present in approximately a third of all WM patients (Hunter et al. 2014). Hence, previous data on these CXCR4 hyperactivating mutations was generally generated from these already transformed tumor cells (Roccaro et al. 2014; Cao et al. 2015). Yet in this study we for

the first time investigated these effects *in vivo* and demonstrated CXCR4 hyperactivation not only cooperates with the oncogene TCL1 but even aggravates tumor phenotype with some mice displaying forms of aggressive B cell lymphoma.

However, in line with known data from WM, RNA sequencing revealed elevated expression of *Prdm1* in premalignant B cells of *CXCR4*^{C1013G}. *Prdm1* is a known master regulator of plasma cell proliferation and differentiation, which was recently found pivotal for the survival and growth of WM cells by regulating EZH2 (Anderson et al. 2020; Morschhauser et al. 2020). This could be a potential link of activated CXCR4 signaling to a more aggressive proliferation in NHL and also serve as a possible target for a therapeutic approach, as there is a clinically approved EZH2 inhibitor (tazemetostat), which was recently FDA-approved for the treatment of inoperable epithelioid sarcoma following a phase II trial (Gounder et al. 2020). Similarly, tazemetostat has shown promising preliminary data in preclinical as well as phase I and phase II trials in indolent and aggressive B cell lymphoma (previously reviewed (Morin, Arthur, and Assouline 2021)).. However further data and experiments are needed to fully understand the interactions of hyperactivated CXCR4 Signaling, *Prdm1* and EZH2.

Moreover, our data shows the enrichment of multiple published data sets known to be associated with cancer in *CXCR4*^{C1013G} vs. *WT* mice but also in *Eμ-TCL1;CXCR4*^{C1013G} vs. *Eμ-TCL1*. In line we were able to show an enrichment of the CXCR4a signature in *Eμ-TCL1;CXCR4*^{C1013G} premalignant B cells. Indicating this CXCR4a transcriptomic program is significant and drives tumor progression. Together this underscores a role of CXCR4 in transformation to malignant tumor cells and growth of these.

4.5 The CXCR4 hyperactivated tumor transcriptome is associated with dismal outcomes in CLL patients

As we observed a drastically reduced overall outcome in our *Eμ-TCL1;CXCR4*^{C1013G} mice we sought to evaluate transferability to human cohorts. As described above we therein applied the transcriptomic data to a cohort of CLL patients. Both, the CXCR4a and the gene set derived

from *Eμ-TCL1;CXCR4^{C1013G}* were associated with significantly reduced time to treatment and the *Eμ-TCL1;CXCR4^{C1013G}* gene set even conferred with significantly reduced overall survival. When looking into the gene sets, CXCR4 and TCL1 combined was linked with transcriptional activation of the Foxm1-Plk1 axis and other proliferative pathways (Fu et al. 2008). Here, PI3K and Akt could potentially be the critical link connecting CXCR4 and TCL1 signaling. In line with our immunoblotting data, showing Akt phosphorylation upon CXCR4 stimulation. This may result in inhibition of Foxo3 and consequently elevated Foxm1 activity as recently published (Wang et al. 2014; Yao, Fan, and Lam 2018).

Additionally, PI3K/Akt is known to phosphorylate Plk1 which engages in a feed-forward loop with Foxm1 (Kasahara et al. 2013). Both Plk1 and Foxm1 are promising therapeutic targets in B cell lymphoma (Uddin et al. 2012; Hassan, Alinari, and Byrd 2018). A phase I study of the Plk1-inhibitor BI 2536 demonstrated activity and safety in a population of highly pretreated patients with relapsed/refractory NHL (Vose et al. 2013). In line with this we found that Myb, a known oncogene is significantly overexpressed in B cells of *Eμ-TCL1;CXCR4^{C1013G}* mice compared to their *Eμ-TCL1* littermates. Importantly Myb is pivotal for Foxm1 signaling as it is recruitment of Foxm1 to late gene promotors in the cell cycle (Sadasivam, Duan, and DeCaprio 2012; Fischer et al. 2016). Additionally, Myb-Foxm1 interaction is essential for germinal center proliferation, a site prone for malignant transformation of B cells (Lefebvre et al. 2010).

Taken together, we demonstrate that transcriptomic profiles of CXCR4 hyperactivation are associated with dismal prognosis in human cohorts of CLL. We illustrate that PI3K/AKT-Signaling and downstream mediators may be the crosslink of TCL1 and CXCR4. However, further investigations are needed to confirm these findings specifically.

4.6 Limitations of this study and our model

For most the biggest limitation of this study represents the ubiquitous expression of the CXCR4^{C1013G} truncated receptor, including the cells of the tumor microenvironment. Therefore, an acceleration of lymphoma development partially mediated by activated CXCR4 signaling in

T cells or other cell types of the tumor microenvironment known to express CXCR4 cannot safely be ruled out. However, we demonstrated in multiple aspects that the effects are attributable to B cell expression: a) We were able to enrich a CXCR4a signature derived from purified B cells, which we could show to also be enriched in purified B cells of our double transgenic *Eμ-TCL1;CXCR4*^{C1013G} mice; b) Histologically altered B cell morphology by CXCR4 hyperactivation; and c) Especially the migration experiments, in which the microenvironment was not present and CD19+CD5+ cells migrated most strongly, underline these findings. However, further experiments, e.g. in a transplantation approach would be needed to fully rule out effects of the tumor microenvironment on the data presented.

Further, as with all studies on model organisms, data may not be fully transferable to humans. Yet, we show a cross-species validation, as *Eμ-TCL1;CXCR4*^{C1013G} tumors enrich a transcriptomic signature generated from human samples of patients with Richter's transformation. Furthermore, we demonstrate that our transcriptomic CXCR4a signature is associated with dismal outcomes in a large cohort of CLL patients and moreover this is also the case for a signature derived from *Eμ-TCL1;CXCR4*^{C1013G} mice. Together these data indicate that the mechanisms are very likely transferable from our murine model organisms to humans.

5 Summary

Aberrant CXCR4 signaling has been linked to more aggressive presentation in B cell lymphomas, yet no previous in vivo data existed. Here, we crossbred a murine model of hyperactive CXCR4 signaling (*CXCR4*^{C1013G}) to established models of B cell lymphoma (*Eμ-Myc* / *Eμ-TCL1*) and identified CXCR4 as a crucial activator of multiple key oncogenic pathways. Furthermore, CXCR4 hyperactivation cooperatively accelerates tumorigenesis, promotes migration, and induces a more extranodal phenotype in Eμ-TCL1 driven lymphoma.

6 References

Adams, J. M., A. W. Harris, C. A. Pinkert, L. M. Corcoran, W. S. Alexander, S. Cory, R. D. Palmiter, and R. L. Brinster. 1985. 'The c-myc oncogene driven by immunoglobulin enhancers induces lymphoid malignancy in transgenic mice', *Nature*, 318: 533-8.

Aguirre-Gamboa, R., H. Gomez-Rueda, E. Martinez-Ledesma, A. Martinez-Torteya, R. Chacolla-Huaringa, A. Rodriguez-Barrientos, J. G. Tamez-Pena, and V. Trevino. 2013. 'SurvExpress: an online biomarker validation tool and database for cancer gene expression data using survival analysis', *PLoS One*, 8: e74250.

Alankus, B., V. Ecker, N. Vahl, M. Braun, W. Weichert, S. Macher-Goppinger, T. Gehring, T. Neumayer, T. Zenz, M. Buchner, and J. Ruland. 2021. 'Pathological RANK signaling in B cells drives autoimmunity and chronic lymphocytic leukemia', *J Exp Med*, 218.

Allen, C. D., K. M. Ansel, C. Low, R. Lesley, H. Tamamura, N. Fujii, and J. G. Cyster. 2004. 'Germinal center dark and light zone organization is mediated by CXCR4 and CXCR5', *Nat Immunol*, 5: 943-52.

Alouche, N., A. Bonaud, V. Rondeau, R. Hussein-Agha, J. Nguyen, V. Bisio, M. Khamyath, E. Crickx, N. Setterblad, N. Dulphy, M. Mahevas, D. H. McDermott, P. Murphy, K. Balabanian, and M. Espeli. 2021. 'Hematological disorder associated Cxcr4-gain-of-function mutation leads to uncontrolled extrafollicular immune response', *Blood*.

Alvarez, M. J., Y. Shen, F. M. Giorgi, A. Lachmann, B. B. Ding, B. H. Ye, and A. Califano. 2016. 'Functional characterization of somatic mutations in cancer using network-based inference of protein activity', *Nat Genet*, 48: 838-47.

Alvarez MJ., Giorgi F., and Califano A. 2014. 'Using viper, a package for Virtual Inference of Protein-activity by Enriched Regulon analysis.', *Bioconductor*.

Anderson, K. J., A. B. Osvaldsdottir, B. Atzinger, G. A. Traustadottir, K. N. Jensen, A. E. Larusdottir, J. T. Bergthorsson, I. Hardardottir, and E. Magnusdottir. 2020. 'The BLIMP1-EZH2 nexus in a non-Hodgkin lymphoma', *Oncogene*, 39: 5138-51.

Andritsos, L. A., J. C. Byrd, P. Cheverton, J. Wu, M. Sivina, T. J. Kipps, and J. A. Burger. 2019. 'A multicenter phase 1 study of plerixafor and rituximab in patients with chronic lymphocytic leukemia', *Leuk Lymphoma*, 60: 3461-69.

Armitage, J. O., R. D. Gascoyne, M. A. Lunning, and F. Cavalli. 2017. 'Non-Hodgkin lymphoma', *Lancet*, 390: 298-310.

Balabanian, K., B. Lagane, J. L. Pablos, L. Laurent, T. Planchenault, O. Verola, C. Lebbe, D. Kerob, A. Dupuy, O. Hermine, J. F. Nicolas, V. Latger-Cannard, D. Bensoussan, P. Bordigoni, F. Baleux, F. Le Deist, J. L. Virelizier, F. Arenzana-Seisdedos, and F. Bachelerie. 2005. 'WHIM syndromes with different genetic anomalies are accounted for by impaired CXCR4 desensitization to CXCL12', *Blood*, 105: 2449-57.

Balabanian, Karl, Emilie Brotin, Vincent Biajoux, Laurence Bouchet-Delbos, Elodie Lainey, Odile Fenneteau, Dominique Bonnet, Laurence Fiette, Dominique Emilie, and Françoise Bachelerie. 2012. 'Proper desensitization of CXCR4 is required for lymphocyte development and peripheral compartmentalization in mice', *Blood*, 119: 5722-30.

Balkwill, F. 2004. 'Cancer and the chemokine network', *Nat Rev Cancer*, 4: 540-50.

Becker, M., E. Hobeika, H. Jumaa, M. Reth, and P. C. Maity. 2017. 'CXCR4 signaling and function require the expression of the IgD-class B-cell antigen receptor', *Proc Natl Acad Sci U S A*, 114: 5231-36.

Beider, K., E. Ribakovsky, M. Abraham, H. Wald, L. Weiss, E. Rosenberg, E. Galun, A. Avigdor, O. Eizenberg, A. Peled, and A. Nagler. 2013. 'Targeting the CD20 and CXCR4 pathways in non-hodgkin lymphoma with rituximab and high-affinity CXCR4 antagonist BKT140', *Clin Cancer Res*, 19: 3495-507.

Benedicto, A., I. Romayor, and B. Arteta. 2018. 'CXCR4 receptor blockage reduces the contribution of tumor and stromal cells to the metastatic growth in the liver', *Oncol Rep*, 39: 2022-30.

Biajoux, V., J. Natt, C. Freitas, N. Alouche, A. Sacquin, P. Hemon, F. Gaudin, N. Fazilleau, M. Espeli, and K. Balabanian. 2016. 'Efficient Plasma Cell Differentiation and Trafficking Require Cxcr4 Desensitization', *Cell Rep*, 17: 193-205.

Bichi, R., S. A. Shinton, E. S. Martin, A. Koval, G. A. Calin, R. Cesari, G. Russo, R. R. Hardy, and C. M. Croce. 2002. 'Human chronic lymphocytic leukemia modeled in mouse by targeted TCL1 expression', *Proc Natl Acad Sci U S A*, 99: 6955-60.

Bolotin, D. A., S. Poslavsky, I. Mitrophanov, M. Shugay, I. Z. Mamedov, E. V. Putintseva, and D. M. Chudakov. 2015. 'MiXCR: software for comprehensive adaptive immunity profiling', *Nat Methods*, 12: 380-1.

Bult, C. J., J. A. Blake, C. L. Smith, J. A. Kadin, J. E. Richardson, and Group Mouse Genome Database. 2019. 'Mouse Genome Database (MGD) 2019', *Nucleic Acids Res*, 47: D801-D06.

Burger, J. A., M. Burger, and T. J. Kipps. 1999. 'Chronic lymphocytic leukemia B cells express functional CXCR4 chemokine receptors that mediate spontaneous migration beneath bone marrow stromal cells', *Blood*, 94: 3658-67.

Burger, J. A., and T. J. Kipps. 2006. 'CXCR4: a key receptor in the crosstalk between tumor cells and their microenvironment', *Blood*, 107: 1761-7.

Burger, J. A., N. Tsukada, M. Burger, N. J. Zvaifler, M. Dell'Aquila, and T. J. Kipps. 2000. 'Blood-derived nurse-like cells protect chronic lymphocytic leukemia B cells from spontaneous apoptosis through stromal cell-derived factor-1', *Blood*, 96: 2655-63.

Busillo, John M, and Jeffrey L Benovic. 2007. 'Regulation of CXCR4 signaling', *Biochim Biophys Acta*, 1768: 952-63.

Cao, Y., Z. R. Hunter, X. Liu, L. Xu, G. Yang, J. Chen, C. J. Patterson, N. Tsakmaklis, S. Kanan, S. Rodig, J. J. Castillo, and S. P. Treon. 2015. 'The WHIM-like CXCR4(S338X) somatic mutation activates AKT and ERK, and promotes resistance to ibrutinib and other agents used in the treatment of Waldenstrom's Macroglobulinemia', *Leukemia*, 29: 169-76.

Cerami, E., J. Gao, U. Dogrusoz, B. E. Gross, S. O. Sumer, B. A. Aksoy, A. Jacobsen, C. J. Byrne, M. L. Heuer, E. Larsson, Y. Antipin, B. Reva, A. P. Goldberg, C. Sander, and N. Schultz. 2012. 'The cBio cancer genomics portal: an open platform for exploring multidimensional cancer genomics data', *Cancer Discov*, 2: 401-4.

Chapuy, B., C. Stewart, A. J. Dunford, J. Kim, A. Kamburov, R. A. Redd, M. S. Lawrence, M. G. M. Roemer, A. J. Li, M. Ziepert, A. M. Staiger, J. A. Wala, M. D. Ducar, I. Leshchiner, E. Rheinbay, A. Taylor-Weiner, C. A. Coughlin, J. M. Hess, C. S. Pedamallu, D. Livitz, D. Rosebrock, M. Rosenberg, A. A. Tracy, H. Horn, P. van Hummelen, A. L. Feldman, B. K. Link, A. J. Novak, J. R. Cerhan, T. M. Habermann, R. Siebert, A. Rosenwald, A. R. Thorner, M. L. Meyerson, T. R. Golub, R. Beroukhim, G. G. Wulf, G. Ott, S. J. Rodig, S. Monti, D. S. Neuberg, M. Loeffler, M. Pfreundschuh, L. Trumper, G. Getz, and M. A. Shipp. 2018. 'Molecular subtypes of diffuse large B cell lymphoma are associated with distinct pathogenic mechanisms and outcomes', *Nat Med*, 24: 679-90.

Chen, J., Z. Y. Xu-Monette, L. Deng, Q. Shen, G. C. Manyam, A. Martinez-Lopez, L. Zhang, S. Montes-Moreno, C. Visco, A. Tzankov, L. Yin, K. Dybkaer, A. Chiu, A. Orazi, Y. Zu, G. Bhagat, K. L. Richards, E. D. Hsi, W. W. Choi, J. H. van Krieken, J. Huh, M. Ponzoni, A. J. Ferreri, X. Zhao, M. B. Moller, J. P. Farnen, J. N. Winter, M. A. Piris, L. Pham, and K. H. Young. 2015. 'Dysregulated CXCR4 expression promotes lymphoma cell survival and independently predicts disease progression in germinal center B-cell-like diffuse large B-cell lymphoma', *Oncotarget*, 6: 5597-614.

Chen, L., J. Ouyang, K. Wienand, K. Bojarczuk, Y. Hao, B. Chapuy, D. Neuberg, P. Juszczynski, L. N. Lawton, S. J. Rodig, S. Monti, and M. A. Shipp. 2020. 'CXCR4 upregulation is an indicator of sensitivity to B-cell receptor/PI3K blockade and a potential resistance mechanism in B-cell receptor-dependent diffuse large B-cell lymphomas', *Haematologica*, 105: 1361-68.

Chen, S. S., B. Y. Chang, S. Chang, T. Tong, S. Ham, B. Sherry, J. A. Burger, K. R. Rai, and N. Chiorazzi. 2016. 'BTK inhibition results in impaired CXCR4 chemokine receptor surface expression, signaling and function in chronic lymphocytic leukemia', *Leukemia*, 30: 833-43.

de Bruijn, I., R. Kundra, B. Mastrogiacomo, T. N. Tran, L. Sikina, T. Mazor, X. Li, A. Ochoa, G. Zhao, B. Lai, A. Abeshouse, D. Baiceanu, E. Ciftci, U. Dogrusoz, A. Dufilie, Z. Erkoc, E. Garcia Lara, Z. Fu, B. E. Gross, C. D. Haynes, A. Heath, D. M. Higgins, P. Jagannathan, K. Kalletla, P. Kumari, J. R. Lindsay, A. Lisman, B. Leenknegt, P. Lukasse, D. Madala, R. Madupuri, P. van Nierop, O. Plantalech, J. Quach, A. Resnick, S. Y. A. Rodenburg, B. A. Satravada, F. Schaeffer, R. Sheridan, J. Singh, R. Sirohi, S. O. Sumer, S. van Hagen, A. Wang, M. Wilson, H. Zhang, K. Zhu, N. Rusk, S. Brown, J. A. Lavery, K. S. Panageas, J. E. Rudolph, M. L. LeNoue-Newton, J. L. Warner, X. Guo, H. Hunter-Zinck, T. V. Yu, S. Pillai, C. Nichols, S. M. Gardos, J. Philip, G. Bpc Core Team, A. Project Genie Consortium, K. L. Kehl, G. J. Riely, D. Schrag, J. Lee, M. V. Fiandalo, S. M. Sweeney, T. J. Pugh, C. Sander, E. Cerami, J. Gao, and N. Schultz. 2023. 'Analysis and Visualization of Longitudinal Genomic and Clinical Data from the AACR Project GENIE Biopharma Collaborative in cBioPortal', *Cancer Res*.

Delgado, J., and N. Villamor. 2014. 'Chronic lymphocytic leukemia in young individuals revisited', *Haematologica*, 99: 4-5.

Dietrich, Sascha, Małgorzata Oleś, Junyan Lu, Leopold Sellner, Simon Anders, Britta Velten, Bian Wu, Jennifer Hüllein, Michelle da Silva Liberio, Tatjana Walther, Lena Wagner, Sophie Rabe, Sonja Ghidelli-Disse, Marcus Bantscheff, Andrzej K. Oleś, Mikołaj Słabicki, Andreas Mock, Christopher C. Oakes, Shihui Wang, Sina Oppermann, Marina Lukas, Vladislav Kim, Martin Sill, Axel Benner, Anna Jauch, Lesley Ann Sutton, Emma Young, Richard Rosenquist, Xiyang Liu, Alexander Jethwa, Kwang Seok Lee, Joe Lewis, Kerstin Putzker, Christoph Lutz, Davide Rossi, Andriy Mokhir, Thomas Oellerich, Katja Zirlik, Marco Herling, Florence Nguyen-Khac, Christoph Plass, Emma Andersson, Satu Mustjoki, Christof von Kalle, Anthony D. Ho, Manfred Hensel, Jan Dürig, Ingo Ringshausen, Marc Zapatka, Wolfgang Huber, and Thorsten Zenz. 2018. 'Drug-perturbation-based stratification of blood cancer', *The Journal of Clinical Investigation*, 128: 427-45.

Ding, L., and S. J. Morrison. 2013. 'Haematopoietic stem cells and early lymphoid progenitors occupy distinct bone marrow niches', *Nature*, 495: 231-5.

Do, H. T. T., C. H. Lee, and J. Cho. 2020. 'Chemokines and their Receptors: Multifaceted Roles in Cancer Progression and Potential Value as Cancer Prognostic Markers', *Cancers (Basel)*, 12.

Dono, M., G. Cerruti, and S. Zupo. 2004. 'The CD5+ B-cell', *Int J Biochem Cell Biol*, 36: 2105-11.

Doring, Y., L. Pawig, C. Weber, and H. Noels. 2014. 'The CXCL12/CXCR4 chemokine ligand/receptor axis in cardiovascular disease', *Front Physiol*, 5: 212.

Farmanbar, A., R. Kneller, and S. Firouzi. 2019. 'RNA sequencing identifies clonal structure of T-cell repertoires in patients with adult T-cell leukemia/lymphoma', *NPJ Genom Med*, 4: 10.

Fischer, M., P. Grossmann, M. Padi, and J. A. DeCaprio. 2016. 'Integration of TP53, DREAM, MMB-FOXM1 and RB-E2F target gene analyses identifies cell cycle gene regulatory networks', *Nucleic Acids Res*, 44: 6070-86.

Freitas, C., M. Wittner, J. Nguyen, V. Rondeau, V. Biajoux, M. L. Aknin, F. Gaudin, S. Beaussant-Cohen, Y. Bertrand, C. Bellanne-Chantelot, J. Donadieu, F. Bachelerie, M. Espeli, A. Dalloul, F. Louache, and K. Balabanian. 2017. 'Lymphoid differentiation of hematopoietic stem cells requires efficient Cxcr4 desensitization', *J Exp Med*, 214: 2023-40.

Friedman, Daniel, Drshika P Mehtani, Jennifer B Vidler, Piers EM Patten, and Robbert Hoogeboom. 2023. 'Proliferating CLL cells express high levels of CXCR4 and CD5', *bioRxiv*: 2023.12.27.573410.

Fu, Z., L. Malureanu, J. Huang, W. Wang, H. Li, J. M. van Deursen, D. J. Tindall, and J. Chen. 2008. 'Plk1-dependent phosphorylation of FoxM1 regulates a transcriptional programme required for mitotic progression', *Nat Cell Biol*, 10: 1076-82.

Gaidano, G., and D. Rossi. 2017. 'The mutational landscape of chronic lymphocytic leukemia and its impact on prognosis and treatment', *Hematology Am Soc Hematol Educ Program*, 2017: 329-37.

Ganghammer, S., J. Gutjahr, E. Hutterer, P. W. Krenn, S. Pucher, C. Zelle-Rieser, K. Johrer, M. Wijtmans, R. Leurs, M. J. Smit, V. Gattei, R. Greil, and T. N. Hartmann. 2016. 'Combined CXCR3/CXCR4 measurements are of high prognostic value in chronic lymphocytic leukemia due to negative co-operativity of the receptors', *Haematologica*, 101: e99-102.

Gao, J., B. A. Aksoy, U. Dogrusoz, G. Dresdner, B. Gross, S. O. Sumer, Y. Sun, A. Jacobsen, R. Sinha, E. Larsson, E. Cerami, C. Sander, and N. Schultz. 2013. 'Integrative analysis of complex cancer genomics and clinical profiles using the cBioPortal', *Sci Signal*, 6: pl1.

Gounder, M., P. Schoffski, R. L. Jones, M. Agulnik, G. M. Cote, V. M. Villalobos, S. Attia, R. Chugh, T. W. Chen, T. Jahan, E. T. Loggers, A. Gupta, A. Italiano, G. D. Demetri, R. Ratan, L. E. Davis, O. Mir, P. Dileo, B. A. Van Tine, J. G. Pressey, T. Lingaraj, A. Rajarethinam, L. Sierra, S. Agarwal, and S. Stacchiotti. 2020. 'Tazemetostat in advanced epithelioid sarcoma with loss of INI1/SMARCB1: an international, open-label, phase 2 basket study', *Lancet Oncol*, 21: 1423-32.

Hallek, M. 2019. 'Chronic lymphocytic leukemia: 2020 update on diagnosis, risk stratification and treatment', *Am J Hematol*, 94: 1266-87.

Hänzelmann, Sonja, Robert Castelo, and Justin Guinney. 2013. 'GSVA: gene set variation analysis for microarray and RNA-Seq data', *BMC Bioinformatics*, 14: 7.

Haribabu, B., R. M. Richardson, I. Fisher, S. Sozzani, S. C. Peiper, R. Horuk, H. Ali, and R. Snyderman. 1997. 'Regulation of human chemokine receptors CXCR4. Role of phosphorylation in desensitization and internalization', *J Biol Chem*, 272: 28726-31.

Harris, A. W., C. A. Pinkert, M. Crawford, W. Y. Langdon, R. L. Brinster, and J. M. Adams. 1988. 'The E mu-myc transgenic mouse. A model for high-incidence spontaneous lymphoma and leukemia of early B cells', *J Exp Med*, 167: 353-71.

Hassan, Q. N., 2nd, L. Alinari, and J. C. Byrd. 2018. 'PLK1: a promising and previously unexplored target in double-hit lymphoma', *J Clin Invest*, 128: 5206-08.

Herhaus, P., J. Lipkova, F. Lammer, I. Yakushev, T. Vag, J. Slotta-Huspenina, S. Habringer, C. Lapa, T. Pukrop, D. Hellwig, B. Wiestler, A. K. Buck, M. Deckert, H. J. Wester, F. Bassermann, M. Schwaiger, W. Weber, B. Menze, and U. Keller. 2020. 'CXCR4-Targeted PET Imaging of Central Nervous System B-Cell Lymphoma', *J Nucl Med*, 61: 1765-71.

Hernandez, P. A., R. J. Gorlin, J. N. Lukens, S. Taniuchi, J. Bohinjec, F. Francois, M. E. Klotman, and G. A. Diaz. 2003. 'Mutations in the chemokine receptor gene CXCR4 are associated with WHIM syndrome, a combined immunodeficiency disease', *Nat Genet*, 34: 70-4.

Heusinkveld, L. E., S. Majumdar, J. L. Gao, D. H. McDermott, and P. M. Murphy. 2019. 'WHIM Syndrome: from Pathogenesis Towards Personalized Medicine and Cure', *J Clin Immunol*, 39: 532-56.

Hippen, K. L., L. E. Tze, and T. W. Behrens. 2000. 'CD5 maintains tolerance in anergic B cells', *J Exp Med*, 191: 883-90.

Hummel, M., S. Bentink, H. Berger, W. Klapper, S. Wessendorf, T. F. Barth, H. W. Bernd, S. B. Cogliatti, J. Dierlamm, A. C. Feller, M. L. Hansmann, E. Haralambieva, L. Harder, D. Hasenclever, M. Kuhn, D. Lenze, P. Lichter, J. I. Martin-Subero, P. Moller, H. K. Muller-Hermelink, G. Ott, R. M. Parwaresch, C. Pott, A. Rosenwald, M. Rosolowski, C. Schwaenen, B. Sturzenhofecker, M. Szczepanowski, H. Trautmann, H. H. Wacker, R. Spang, M. Loeffler, L. Trumper, H. Stein, R. Siebert, and Krebshilfe Molecular Mechanisms in Malignant Lymphomas Network Project of the Deutsche. 2006. 'A biologic definition of Burkitt's lymphoma from transcriptional and genomic profiling', *N Engl J Med*, 354: 2419-30.

Hunter, Z. R., L. Xu, G. Yang, Y. Zhou, X. Liu, Y. Cao, R. J. Manning, C. Tripsas, C. J. Patterson, P. Sheehy, and S. P. Treon. 2014. 'The genomic landscape of Waldenstrom macroglobulinemia is characterized by highly recurring MYD88 and WHIM-like CXCR4 mutations, and small somatic deletions associated with B-cell lymphomagenesis', *Blood*, 123: 1637-46.

Jang, J. W., P. X. Thuy, J. W. Lee, and E. Y. Moon. 2021. 'CXCR4 promotes B cell viability by the cooperation of nuclear factor (erythroid-derived 2)-like 2 and hypoxia-inducible factor-1alpha under hypoxic conditions', *Cell Death Dis*, 12: 330.

Jiang, K., J. Li, J. Zhang, L. Wang, Q. Zhang, J. Ge, Y. Guo, B. Wang, Y. Huang, T. Yang, D. Hao, and L. Shan. 2019. 'SDF-1/CXCR4 axis facilitates myeloid-derived suppressor cells accumulation in osteosarcoma microenvironment and blunts the response to anti-PD-1 therapy', *Int Immunopharmacol*, 75: 105818.

Kasahara, K., H. Goto, I. Izawa, T. Kiyono, N. Watanabe, S. Elowe, E. A. Nigg, and M. Inagaki. 2013. 'PI 3-kinase-dependent phosphorylation of Plk1-Ser99 promotes association with 14-3-3gamma and is required for metaphase-anaphase transition', *Nat Commun*, 4: 1882.

Kashyap, M. K., C. I. Amaya-Chanaga, D. Kumar, B. Simmons, N. Huser, Y. Gu, M. Hallin, K. Lindquist, R. Yafawi, M. Y. Choi, A. A. Amine, L. Z. Rassenti, C. Zhang, S. H. Liu, T. Smeal, V. R. Fantin, T. J. Kipps, F. Pernasetti, and J. E. Castro. 2017. 'Targeting the CXCR4 pathway using a novel anti-CXCR4 IgG1 antibody (PF-06747143) in chronic lymphocytic leukemia', *J Hematol Oncol*, 10: 112.

Klintman, J., N. Appleby, B. Stamatopoulos, K. Ridout, T. A. Eyre, P. Robbe, L. Lopez Pascua, S. J. Knight, H. M. Dreau, M. Cabes, N. Popitsch, M. Ehinger, I. Martin-Subero, E. Campo, R. Mansson, D. Rossi, J. C. Taylor, D. V. Vavoulis, and A. Schuh. 2020. 'Genomic and transcriptomic correlates of Richter's transformation in Chronic Lymphocytic Leukemia', *Blood*.

Klintman, J., N. Appleby, B. Stamatopoulos, K. Ridout, T. A. Eyre, P. Robbe, L. L. Pascua, S. J. L. Knight, H. Dreau, M. Cabes, N. Popitsch, M. Ehinger, J. I. Martin-Subero, E. Campo, R. Mansson, D. Rossi, J. C. Taylor, D. V. Vavoulis, and A. Schuh. 2021. 'Genomic and transcriptomic correlates of Richter transformation in chronic lymphocytic leukemia', *Blood*, 137: 2800-16.

Knittel, G., T. Rehkamper, D. Korovkina, P. Liedgens, C. Fritz, A. Torgovnick, Y. Al-Baldawi, M. Al-Maarri, Y. Cun, O. Fedorchenko, A. Riabinska, F. Beleggia, P. H. Nguyen, F. T. Wunderlich, M. Ortmann, M. Montesinos-Rongen, E. Tausch, S. Stilgenbauer, P. Frenzel L, M. Herling, C. Herling, J. Bahlo, M. Hallek, M. Peifer, R. Buettner, T. Persigehl, and H. C. Reinhardt. 2017. 'Two mouse models reveal an actionable PARP1 dependence in aggressive chronic lymphocytic leukemia', *Nat Commun*, 8: 153.

Kohlhaas, V., S. J. Blakemore, M. Al-Maarri, N. Nickel, M. Pal, A. Roth, N. Hovelmeyer, S. C. Schafer, G. Knittel, P. Lohneis, M. Nikolic, J. L. Wiederstein, M. Franitza, T. Georgomonolis, N. Reinart, M. Herling, C. Herling, E. M. Hartmann, A. Rosenwald, W. Klapper, R. Buttner, R. Moia, D. Rossi, R. Boldorini, G. Gaidano, L. P. Frenzel, H. C. Reinhardt, J. C. Bruning, M. Hallek, M. Kruger, M. Peifer, C. P. Pallasch, and F. T. Wunderlich. 2021. 'Active Akt signaling triggers CLL toward Richter transformation via overactivation of Notch1', *Blood*, 137: 646-60.

Kolde, R. 2019. ' Pretty Heatmaps', *https://CRAN.R-project.org/package=pheatmap*.

Korotkevich G., Sukhov V., Budin N., Shpak B., Artyomov MN., and Sergushichev A. 2021. 'Fast gene set enrichment analysis', *bioRxiv*.

Landgren, O., M. Albitar, W. Ma, F. Abbasi, R. B. Hayes, P. Ghia, G. E. Marti, and N. E. Caporaso. 2009. 'B-cell clones as early markers for chronic lymphocytic leukemia', *N Engl J Med*, 360: 659-67.

Lefebvre, C., P. Rajbhandari, M. J. Alvarez, P. Bandaru, W. K. Lim, M. Sato, K. Wang, P. Sumazin, M. Kustagi, B. C. Bisikirska, K. Basso, P. Beltrao, N. Krogan, J. Gautier, R. Dalla-Favera, and A. Califano. 2010. 'A human B-cell interactome identifies MYB and FOXM1 as master regulators of proliferation in germinal centers', *Mol Syst Biol*, 6: 377.

Lenz, G., G. Wright, S. S. Dave, W. Xiao, J. Powell, H. Zhao, W. Xu, B. Tan, N. Goldschmidt, J. Iqbal, J. Vose, M. Bast, K. Fu, D. D. Weisenburger, T. C. Greiner, J. O. Armitage, A. Kyle, L. May, R. D. Gascoyne, J. M. Connors, G. Troen, H. Holte, S. Kvaloy, D. Dierickx, G. Verhoef, J. Delabie, E. B. Smeland, P. Jares, A. Martinez, A. Lopez-Guillermo, E. Montserrat, E. Campo, R. M. Braziel, T. P. Miller, L. M. Rimsza, J. R. Cook, B. Pohlman, J. Sweetenham, R. R. Tubbs, R. I. Fisher, E. Hartmann, A. Rosenwald, G. Ott, H. K. Muller-Hermelink, D. Wrench, T. A. Lister, E. S. Jaffe, W.

H. Wilson, W. C. Chan, L. M. Staudt, and Project Lymphoma/Leukemia Molecular Profiling. 2008. 'Stromal gene signatures in large-B-cell lymphomas', *N Engl J Med*, 359: 2313-23.

Lewis, R., S. Habringer, M. Kircher, M. Hefter, C. A. Peuker, R. Werner, V. Ademaj-Kospiri, A. Gable, W. Weber, H. J. Wester, A. Buck, P. Herhaus, C. Lapa, and U. Keller. 2021. 'Investigation of spleen CXCR4 expression by [(68)Ga]Pentixafor PET in a cohort of 145 solid cancer patients', *EJNMMI Res*, 11: 77.

Lewis, R., H. C. Maurer, N. Singh, I. Gonzalez-Menendez, M. Wirth, M. Schick, L. Zhang, K. Isaakidis, A. K. Scherger, V. Schulze, J. Lu, T. Zenz, K. Steiger, R. Rad, L. Quintanilla-Martinez, M. Espeli, K. Balabanian, U. Keller, and S. Habringer. 2021. 'CXCR4 hyperactivation cooperates with TCL1 in CLL development and aggressiveness', *Leukemia*, 35: 2895-905.

Li, L., D. Wu, Q. Yu, L. Li, and P. Wu. 2017. 'Prognostic value of FOXM1 in solid tumors: a systematic review and meta-analysis', *Oncotarget*, 8: 32298-308.

Li, S., K. H. Young, and L. J. Medeiros. 2018. 'Diffuse large B-cell lymphoma', *Pathology*, 50: 74-87.

Li, Y., Y. Wang, Z. Wang, D. Yi, and S. Ma. 2015. 'Racial differences in three major NHL subtypes: descriptive epidemiology', *Cancer Epidemiol*, 39: 8-13.

Liberzon, A., A. Subramanian, R. Pinchback, H. Thorvaldsdottir, P. Tamayo, and J. P. Mesirov. 2011. 'Molecular signatures database (MSigDB) 3.0', *Bioinformatics*, 27: 1739-40.

Love, M. I., W. Huber, and S. Anders. 2014. 'Moderated estimation of fold change and dispersion for RNA-seq data with DESeq2', *Genome Biol*, 15: 550.

Ma, M. C. J., S. Tadros, A. Bouska, T. Heavican, H. Yang, Q. Deng, D. Moore, A. Akhter, K. Hartert, N. Jain, J. Showell, S. Ghosh, L. Street, M. Davidson, C. Carey, J. Tobin, D. Perumal, J. M. Vose, M. A. Lunning, A. R. Sohani, B. J. Chen, S. Buckley, L. J. Nastoupil, R. E. Davis, J. R. Westin, N. H. Fowler, S. Parekh, M. Gandhi, S. Neelapu, D. Stewart, K. Bhalla, J. Iqbal, T. Greiner, S. J. Rodig, A. Mansoor, and M. R. Green. 2022. 'Subtype-specific and co-occurring genetic alterations in B-cell non-Hodgkin lymphoma', *Haematologica*, 107: 690-701.

Ma, Q., D. Jones, P. R. Borghesani, R. A. Segal, T. Nagasawa, T. Kishimoto, R. T. Bronson, and T. A. Springer. 1998. 'Impaired B-lymphopoiesis, myelopoiesis, and derailed cerebellar neuron migration in CXCR4- and SDF-1-deficient mice', *Proc Natl Acad Sci U S A*, 95: 9448-53.

Mayerhoefer, M. E., U. Jaeger, P. Staber, M. Raderer, W. Wadsak, S. Pfaff, C. Kornauth, D. Senn, M. Weber, H. J. Wester, C. Skrabs, and A. Haug. 2018. '[68Ga]Ga-Pentixafor PET/MRI for CXCR4 Imaging of Chronic Lymphocytic Leukemia: Preliminary Results', *Investigative Radiology*, 53: 403-08.

Mohle, R., C. Failenschmid, F. Bautz, and L. Kanz. 1999. 'Overexpression of the chemokine receptor CXCR4 in B cell chronic lymphocytic leukemia is associated with increased functional response to stromal cell-derived factor-1 (SDF-1)', *Leukemia*, 13: 1954-9.

Molyneux, E. M., R. Rochford, B. Griffin, R. Newton, G. Jackson, G. Menon, C. J. Harrison, T. Israels, and S. Bailey. 2012. 'Burkitt's lymphoma', *Lancet*, 379: 1234-44.

Moreno, M. J., R. Bosch, R. Dieguez-Gonzalez, S. Novelli, A. Mozos, A. Gallardo, M. A. Pavon, M. V. Cespedes, A. Granena, M. Alcoceba, O. Blanco, M. Gonzalez-Diaz, J. Sierra, R. Mangues, and I. Casanova. 2015. 'CXCR4 expression enhances diffuse large B cell lymphoma dissemination and decreases patient survival', *J Pathol*, 235: 445-55.

Morin, R. D., S. E. Arthur, and S. Assouline. 2021. 'Treating lymphoma is now a bit EZ-er', *Blood Adv*, 5: 2256-63.

Morin, R. D., K. Mungall, E. Pleasance, A. J. Mungall, R. Goya, R. D. Huff, D. W. Scott, J. Ding, A. Roth, R. Chiu, R. D. Corbett, F. C. Chan, M. Mendez-Lago, D. L. Trinh, M. Bolger-Munro, G. Taylor, A. Hadj Khodabakhshi, S. Ben-Neriah, J. Pon, B. Meissner, B. Woolcock, N. Farnoud, S. Rogic, E. L. Lim, N. A. Johnson, S. Shah, S. Jones, C. Steidl, R. Holt, I. Birol, R. Moore, J. M. Connors, R. D. Gascoyne, and M. A. Marra. 2013. 'Mutational and structural analysis of diffuse large B-cell lymphoma using whole-genome sequencing', *Blood*, 122: 1256-65.

Moriuchi, M., H. Moriuchi, D. M. Margolis, and A. S. Fauci. 1999. 'USF/c-Myc enhances, while Yin-Yang 1 suppresses, the promoter activity of CXCR4, a coreceptor for HIV-1 entry', *J Immunol*, 162: 5986-92.

Morschhauser, F., H. Tilly, A. Chaidos, P. McKay, T. Phillips, S. Assouline, C. L. Batlevi, P. Campbell, V. Ribrag, G. L. Damaj, M. Dickinson, W. Jurczak, M. Kazmierczak, S. Opat, J. Radford, A. Schmitt, J. Yang, J. Whalen, S. Agarwal, D. Adib, and G. Salles. 2020. 'Tazemetostat for patients with relapsed or refractory follicular lymphoma: an open-label, single-arm, multicentre, phase 2 trial', *Lancet Oncol*, 21: 1433-42.

Muller, A., B. Homey, H. Soto, N. Ge, D. Catron, M. E. Buchanan, T. McClanahan, E. Murphy, W. Yuan, S. N. Wagner, J. L. Barrera, A. Mohar, E. Verastegui, and A. Zlotnik. 2001. 'Involvement of chemokine receptors in breast cancer metastasis', *Nature*, 410: 50-6.

Nagasawa, T., S. Hirota, K. Tachibana, N. Takakura, S. Nishikawa, Y. Kitamura, N. Yoshida, H. Kikutani, and T. Kishimoto. 1996. 'Defects of B-cell lymphopoiesis and bone-marrow myelopoiesis in mice lacking the CXC chemokine PBSF/SDF-1', *Nature*, 382: 635-8.

Nganga, V. K., V. L. Palmer, H. Naushad, M. D. Kassmeier, D. K. Anderson, G. A. Perry, N. M. Schabla, and P. C. Swanson. 2013. 'Accelerated progression of chronic lymphocytic leukemia in Emu-TCL1 mice expressing catalytically inactive RAG1', *Blood*, 121: 3855-66, S1-16.

Odemis, V., E. Lamp, G. Pezeshki, B. Moepps, K. Schilling, P. Gierschik, D. R. Littman, and J. Engele. 2005. 'Mice deficient in the chemokine receptor CXCR4 exhibit impaired limb innervation and myogenesis', *Mol Cell Neurosci*, 30: 494-505.

Parekh, S., C. Ziegenhain, B. Vieth, W. Enard, and I. Hellmann. 2016. 'The impact of amplification on differential expression analyses by RNA-seq', *Sci Rep*, 6: 25533.

Pasqualucci, L., and R. Dalla-Favera. 2018. 'Genetics of diffuse large B-cell lymphoma', *Blood*, 131: 2307-19.

Pekarsky, Y., A. Palamarchuk, V. Maximov, A. Efanov, N. Nazaryan, U. Santanam, L. Rassenti, T. Kipps, and C. M. Croce. 2008. 'Tcl1 functions as a transcriptional regulator and is directly involved in the pathogenesis of CLL', *Proc Natl Acad Sci U S A*, 105: 19643-8.

Proudfoot, A. E. 2002. 'Chemokine receptors: multifaceted therapeutic targets', *Nat Rev Immunol*, 2: 106-15.

R-Core-Team. 2018. 'A Language and Environment for Statistical Computing.', *https://www.R-project.org/*.

Rawstron, A. C., F. L. Bennett, S. J. O'Connor, M. Kwok, J. A. Fenton, M. Plummer, R. de Tute, R. G. Owen, S. J. Richards, A. S. Jack, and P. Hillmen. 2008. 'Monoclonal B-cell lymphocytosis and chronic lymphocytic leukemia', *N Engl J Med*, 359: 575-83.

Recasens-Zorzo, C., T. Cardesa-Salzmann, P. Petazzi, L. Ros-Blanco, A. Esteve-Arenys, G. Clot, M. Guerrero-Hernandez, V. Rodriguez, D. Soldini, A. Valera, A. Moros, F. Climent, E. Gonzalez-Barca, S. Mercadal, L. Arenillas, X. Calvo, J. L. Mate, G. Gutierrez-Garcia, I. Casanova, R. Mangues, A. Sanjuan-Pla, C. Bueno, P. Menendez, A. Martinez, D. Colomer, R. E. Tejedor, J. Teixido, E. Campo, A. Lopez-Guillermo, J. I. Borrell, L. Colomo, P. Perez-Galan, and G. Roue. 2019. 'Pharmacological modulation of CXCR4 cooperates with BET bromodomain inhibition in diffuse large B-cell lymphoma', *Haematologica*, 104: 778-88.

Reddy, A., J. Zhang, N. S. Davis, A. B. Moffitt, C. L. Love, A. Waldrop, S. Leppa, A. Pasanen, L. Meriranta, M. L. Karjalainen-Lindsberg, P. Norgaard, M. Pedersen, A. O. Gang, E. Hogdall, T. B. Heavican, W. Lone, J. Iqbal, Q. Qin, G. Li, S. Y. Kim, J. Healy, K. L. Richards, Y. Fedoriw, L. Bernal-Mizrachi, J. L. Koff, A. D. Staton, C. R. Flowers, O. Paltiel, N. Goldschmidt, M. Calaminici, A. Clear, J. Gribben, E. Nguyen, M. B. Czader, S. L. Ondrejka, A. Collie, E. D. Hsi, E. Tse, R. K. H. Au-Yeung, Y. L. Kwong, G. Srivastava, W. W. L. Choi, A. M. Evens, M. Pilichowska, M. Sengar, N. Reddy, S. Li, A. Chadburn, L. I. Gordon, E. S. Jaffe, S. Levy, R. Rempel, T. Tzeng, L. E. Happ, T. Dave, D. Rajagopalan, J. Datta, D. B. Dunson, and S. S. Dave. 2017. 'Genetic and Functional Drivers of Diffuse Large B Cell Lymphoma', *Cell*, 171: 481-94 e15.

Reinholdt, L., M. B. Laursen, A. Schmitz, J. S. Bodker, L. H. Jakobsen, M. Bogsted, H. E. Johnsen, and K. Dybkaer. 2016. 'The CXCR4 antagonist plerixafor enhances the effect of rituximab in diffuse large B-cell lymphoma cell lines', *Biomark Res*, 4: 12.

Roccaro, A. M., A. Sacco, W. G. Purschke, M. Moschetta, K. Buchner, C. Maasch, D. Zboralski, S. Zollner, S. Vonhoff, Y. Mishima, P. Maiso, M. R. Reagan, S. Lonardi, M. Ungari, F. Facchetti, D. Eulberg, A. Kruschinski, A. Vater, G. Rossi, S. Klussmann, and I. M. Ghobrial. 2014. 'SDF-1 inhibition targets the bone marrow niche for cancer therapy', *Cell Rep*, 9: 118-28.

Sadasivam, S., S. Duan, and J. A. DeCaprio. 2012. 'The MuvB complex sequentially recruits B-Myb and FoxM1 to promote mitotic gene expression', *Genes Dev*, 26: 474-89.

Sanchez-Martin, L., P. Sanchez-Mateos, and C. Cabanas. 2013. 'CXCR7 impact on CXCL12 biology and disease', *Trends Mol Med*, 19: 12-22.

Scala, S. 2015. 'Molecular Pathways: Targeting the CXCR4-CXCL12 Axis--Untapped Potential in the Tumor Microenvironment', *Clin Cancer Res*, 21: 4278-85.

Scala, S., A. Ottaiano, P. A. Ascierto, M. Cavalli, E. Simeone, P. Giuliano, M. Napolitano, R. Franco, G. Botti, and G. Castello. 2005. 'Expression of CXCR4 predicts poor prognosis in patients with malignant melanoma', *Clin Cancer Res*, 11: 1835-41.

Scherger, A. K., M. Al-Maarri, H. C. Maurer, M. Schick, S. Maurer, R. Ollinger, I. Gonzalez-Menendez, M. Martella, M. Thaler, K. Pechloff, K. Steiger, S. Sander, J. Ruland, R. Rad, L. Quintanilla-Martinez, F. T. Wunderlich, S. Rose-John, and U. Keller. 2019. 'Activated gp130 signaling selectively targets B cell differentiation to induce mature lymphoma and plasmacytoma', *JCI Insight*, 4.

Shao, H., L. Xi, M. Raffeld, A. L. Feldman, R. P. Ketterling, R. Knudson, J. Rodriguez-Canales, J. Hanson, S. Pittaluga, and E. S. Jaffe. 2011. 'Clonally related histiocytic/dendritic cell sarcoma and chronic lymphocytic leukemia/small lymphocytic lymphoma: a study of seven cases', *Mod Pathol*, 24: 1421-32.

Shugay, M., D. V. Bagaev, M. A. Turchaninova, D. A. Bolotin, O. V. Britanova, E. V. Putintseva, M. V. Pogorelyy, V. I. Nazarov, I. V. Zvyagin, V. I. Kirgizova, K. I. Kirgizov, E. V. Skorobogatova, and D. M. Chudakov. 2015. 'VDJtools: Unifying Post-analysis of T Cell Receptor Repertoires', *PLoS Comput Biol*, 11: e1004503.

Siegel, R. L., K. D. Miller, H. E. Fuchs, and A. Jemal. 2022. 'Cancer statistics, 2022', *CA Cancer J Clin*, 72: 7-33.

Sondka, Z., S. Bamford, C. G. Cole, S. A. Ward, I. Dunham, and S. A. Forbes. 2018. 'The COSMIC Cancer Gene Census: describing genetic dysfunction across all human cancers', *Nat Rev Cancer*, 18: 696-705.

Speetjens, F. M., G. J. Liefers, C. J. Korbee, W. E. Mesker, C. J. van de Velde, R. L. van Vlierberghe, H. Morreau, R. A. Tollenaar, and P. J. Kuppen. 2009. 'Nuclear localization of CXCR4 determines prognosis for colorectal cancer patients', *Cancer Microenviron*, 2: 1-7.

Strati, P., and T. D. Shanafelt. 2015. 'Monoclonal B-cell lymphocytosis and early-stage chronic lymphocytic leukemia: diagnosis, natural history, and risk stratification', *Blood*, 126: 454-62.

Su, L., J. Zhang, H. Xu, Y. Wang, Y. Chu, R. Liu, and S. Xiong. 2005. 'Differential expression of CXCR4 is associated with the metastatic potential of human non-small cell lung cancer cells', *Clin Cancer Res*, 11: 8273-80.

Subramanian, A., P. Tamayo, V. K. Mootha, S. Mukherjee, B. L. Ebert, M. A. Gillette, A. Paulovich, S. L. Pomeroy, T. R. Golub, E. S. Lander, and J. P. Mesirov. 2005. 'Gene set enrichment analysis: a knowledge-based approach for interpreting genome-wide expression profiles', *Proc Natl Acad Sci U S A*, 102: 15545-50.

Susanibar-Adaniya, S., and S. K. Barta. 2021. '2021 Update on Diffuse large B cell lymphoma: A review of current data and potential applications on risk stratification and management', *Am J Hematol*, 96: 617-29.

Swerdlow, S. H., E. Campo, S. A. Pileri, N. L. Harris, H. Stein, R. Siebert, R. Advani, M. Ghielmini, G. A. Salles, A. D. Zelenetz, and E. S. Jaffe. 2016. 'The 2016 revision of the World Health Organization classification of lymphoid neoplasms', *Blood*, 127: 2375-90.

Thandra, K. C., A. Barsouk, K. Saginala, S. A. Padala, A. Barsouk, and P. Rawla. 2021. 'Epidemiology of Non-Hodgkin's Lymphoma', *Med Sci (Basel)*, 9.

Tulotta, C., C. Stefanescu, Q. Chen, V. Torraca, A. H. Meijer, and B. E. Snaar-Jagalska. 2019. 'CXCR4 signaling regulates metastatic onset by controlling neutrophil motility and response to malignant cells', *Sci Rep*, 9: 2399.

Uddin, S., A. R. Hussain, M. Ahmed, K. Siddiqui, F. Al-Dayel, P. Bavi, and K. S. Al-Kuraya. 2012. 'Overexpression of FoxM1 offers a promising therapeutic target in diffuse large B-cell lymphoma', *Haematologica*, 97: 1092-100.

Uhlen, M., L. Fagerberg, B. M. Hallstrom, C. Lindskog, P. Oksvold, A. Mardinoglu, A. Sivertsson, C. Kampf, E. Sjostedt, A. Asplund, I. Olsson, K. Edlund, E. Lundberg, S. Navani, C. A. Szigyarto, J. Odeberg, D. Djureinovic, J. O. Takanen, S. Hober, T. Alm, P. H. Edqvist, H. Berling, H. Tegel, J. Mulder, J. Rockberg, P. Nilsson, J. M. Schwenk, M. Hamsten, K. von Feilitzen, M. Forsberg, L. Persson, F. Johansson, M. Zwahlen, G. von Heijne, J. Nielsen, and F. Ponten. 2015. 'Proteomics. Tissue-based map of the human proteome', *Science*, 347: 1260419.

Varettoni, M., S. Zibellini, I. Defrancesco, V. V. Ferretti, E. Rizzo, L. Malcovati, A. Galli, M. G. D. Porta, E. Boveri, L. Arcaini, C. Candido, M. Paulli, and M. Cazzola. 2017. 'Pattern of somatic mutations in patients with Waldenstrom macroglobulinemia or IgM monoclonal gammopathy of undetermined significance', *Haematologica*, 102: 2077-85.

Vose, J. M., J. W. Friedberg, E. K. Waller, B. D. Cheson, V. Juvvigunta, H. Fritsch, C. Petit, G. Munzert, and A. Younes. 2013. 'The Plk1 inhibitor BI 2536 in patients with refractory or relapsed non-Hodgkin lymphoma: a phase I, open-label, single dose-escalation study', *Leuk Lymphoma*, 54: 708-13.

Wang, S., S. Zhang, J. Li, X. Xu, Y. Weng, M. Zheng, L. Ouyang, and F. Li. 2014. 'CXCL12-induced upregulation of FOXM1 expression promotes human glioblastoma cell invasion', *Biochem Biophys Res Commun*, 447: 1-6.

Wester, H. J., U. Keller, M. Schottelius, A. Beer, K. Philipp-Abbrederis, F. Hoffmann, J. Simecek, C. Gerngross, M. Lassmann, K. Herrmann, N. Pellegata, M. Rudelius, H. Kessler, and M. Schwaiger. 2015. 'Disclosing the CXCR4 expression in lymphoproliferative diseases by targeted molecular imaging', *Theranostics*, 5: 618-30.

Yao, S., L. Y. Fan, and E. W. Lam. 2018. 'The FOXO3-FOXM1 axis: A key cancer drug target and a modulator of cancer drug resistance', *Semin Cancer Biol*, 50: 77-89.

Zhao, H., L. Guo, H. Zhao, J. Zhao, H. Weng, and B. Zhao. 2015. 'CXCR4 over-expression and survival in cancer: a system review and meta-analysis', *Oncotarget*, 6: 5022-40.

7 Supplemental tables

Gene	Direction	Chromosome	Ensembl	Uniprot
CRABP2	up	1	ENSG00000143320	P29373
CTSE	up	1	ENSG00000196188	P14091
JCHAIN	up	4	ENSG00000132465	P01591
CHST1	up	11	ENSG00000175264	O43916
RBM24	up	6	ENSG00000112183	Q9BX46
TMEM132E	up	17	ENSG00000181291	Q6IEE7
IGLL1	up	22	ENSG00000128322	P15814
IGLL5	up	22	ENSG00000254709	B9A064
FRAS1	up	4	ENSG00000138759	Q86XX4
DNTT	up	10	ENSG00000107447	P04053
HID1	up	17	ENSG00000167861	Q8IV36
SERTAD4	up	1	ENSG00000082497	Q9NUC0
SLFN12L	up	17	ENSG00000205045	Q6IEE8
RAG2	up	11	ENSG00000175097	P55895
TMPRSS3	up	21	ENSG00000160183	P57727
FCRL6	up	1	ENSG00000181036	Q6DN72
RAG1	up	11	ENSG00000166349	P15918
SLC12A3	up	16	ENSG00000070915	P55017
P2RX3	up	11	ENSG00000109991	P56373
SERPINF1	up	17	ENSG00000132386	P36955
ANKLE1	up	19	ENSG00000160117	Q8NAG6
DERL3	up	22	ENSG00000099958	Q96Q80
DRC7	up	16	ENSG00000159625	Q8IY82
KIAA1217	up	10	ENSG00000120549	Q5T5P2
KIAA1211L	up	2	ENSG00000196872	Q6NV74
ARPP21	up	3	ENSG00000172995	Q9UBL0
VPREB1	up	22	ENSG00000169575	P12018
ADGRG3	up	16	ENSG00000182885	Q86Y34
ADAMTSL4	up	1	ENSG00000143382	Q6UY14
RHBDL1	up	16	ENSG00000103269	O75783
SMTNL2	up	17	ENSG00000188176	Q2TAL5
RAP1GAP	up	1	ENSG00000076864	P47736
RBM47	up	4	ENSG00000163694	A0AV96
ADCY6	up	12	ENSG00000174233	O43306
CAMK1G	up	1	ENSG00000008118	Q96NX5
EPS8L2	up	11	ENSG00000177106	Q9H6S3
CACNA1H	up	16	ENSG00000196557	O95180
DDC	up	7	ENSG00000132437	P20711
GPR12	up	13	ENSG00000132975	P47775
UCHL1	up	4	ENSG00000154277	P09936

RSPH1	up	21	ENSG00000160188	Q8WYR4
RGS16	up	1	ENSG00000143333	O15492
GAS7	up	17	ENSG00000007237	O60861
COL5A3	up	19	ENSG00000080573	P25940
ACKR2	up	3	ENSG00000144648	O00590
CACNA2D1	up	7	ENSG00000153956	P54289
C6orf222	up	6	ENSG00000189325	P0C671
NAV2	up	11	ENSG00000166833	Q8IVL1
RELN	up	7	ENSG00000189056	P78509
LRRC10B	up	11	ENSG00000204950	A6NIK2
EPHA2	up	1	ENSG00000142627	P29317
SAPCD2	up	9	ENSG00000186193	Q86UD0
RSPH9	up	6	ENSG00000172426	Q9H1X1
TRIM2	up	4	ENSG00000109654	Q9C040
SLC39A4	up	8	ENSG00000147804	Q6P5W5
PBX4	up	19	ENSG00000105717	Q9BYU1
ESPL1	up	12	ENSG00000135476	Q14674
HEYL	up	1	ENSG00000163909	Q9NQ87
SPAG5	up	17	ENSG00000076382	Q96R06
GFRA1	up	10	ENSG00000151892	P56159
SSPN	up	12	ENSG00000123096	Q14714
LMO7	up	13	ENSG00000136153	Q8WWI1
TIMP3	down	22	ENSG00000100234	P35625
IGFBP7	down	4	ENSG00000163453	Q16270
CXCL12	down	10	ENSG00000107562	P48061
SPARC	down	5	ENSG00000113140	P09486
KDR	down	4	ENSG00000128052	P35968
SERPINH1	down	11	ENSG00000149257	P50454
PLVAP	down	19	ENSG00000130300	Q9BX97
BGN	down	X	ENSG00000182492	P21810
CLU	down	8	ENSG00000120885	P10909
GAS6	down	13	ENSG00000183087	Q14393
SLC40A1	down	2	ENSG00000138449	Q9NP59
STAB2	down	12	ENSG00000136011	Q8WWQ8
CCR3	down	3	ENSG00000183625	P51677
COL14A1	down	8	ENSG00000187955	Q05707
KCNJ10	down	1	ENSG00000177807	P78508
EPAS1	down	2	ENSG00000116016	Q99814
CD63	down	12	ENSG00000135404	P08962
COL1A2	down	7	ENSG00000164692	P08123
CD5L	down	1	ENSG00000073754	O43866
HPGD	down	4	ENSG00000164120	P15428
AXL	down	19	ENSG00000167601	P30530

COL4A2	down	13	ENSG00000134871	P08572
VCAM1	down	1	ENSG00000162692	P19320
SERPING1	down	11	ENSG00000149131	P05155
SLC11A1	down	2	ENSG00000018280	P49279
CD163	down	12	ENSG00000177575	Q86VB7
TIMD4	down	5	ENSG00000145850	Q96H15
COL4A1	down	13	ENSG00000187498	P02462
CADM1	down	11	ENSG00000182985	Q9BY67
NAV1	down	1	ENSG00000134369	Q8NEY1
ABCC3	down	17	ENSG00000108846	O15438
ADGRF5	down	6	ENSG00000069122	Q8IZF2
SDC3	down	1	ENSG00000162512	O75056
HMOX1	down	22	ENSG00000100292	P09601
GALNT3	down	2	ENSG00000115339	Q14435
MERTK	down	2	ENSG00000153208	Q12866
ADGRE1	down	19	ENSG00000174837	Q14246
FCGR1A	down	1	ENSG00000150337	P12314
SLCO2B1	down	11	ENSG00000137491	O94956
SIGLEC1	down	20	ENSG00000088827	Q9BZZ2
STAB1	down	3	ENSG00000010327	Q9NY15
CLEC6A	down	12	ENSG00000205846	Q6EIG7
FABP4	down	8	ENSG00000170323	P15090
C1QB	down	1	ENSG00000173369	P02746
IGF1	down	12	ENSG00000017427	P05019
TBXAS1	down	7	ENSG00000059377	P24557
EPB41L3	down	18	ENSG00000082397	Q9Y2J2
C1QC	down	1	ENSG00000159189	P02747
MARCO	down	2	ENSG00000019169	Q9UEW3
TREML4	down	6	ENSG00000188056	Q6UXN2
MAFB	down	20	ENSG00000204103	Q9Y5Q3
PAQR9	down	3	ENSG00000188582	Q6ZVX9
CLEC4A	down	12	ENSG00000111729	Q9UMR7
FCGR2A	down	1	ENSG00000143226	P12318
SEMA6D	down	15	ENSG00000137872	Q8NFY4
EGFL7	down	9	ENSG00000172889	Q9UHF1
KCNA2	down	1	ENSG00000177301	P16389
TGM1	down	14	ENSG00000092295	P22735
TMEM51	down	1	ENSG00000171729	Q9NW97
SLC7A8	down	14	ENSG00000092068	Q9UHI5
MRC1	down	10	ENSG00000260314	P22897
APP	down	21	ENSG00000142192	P05067
C1QA	down	1	ENSG00000173372	P02745
CD300C	down	17	ENSG00000167850	Q08708

ZNF705A	down	12	ENSG00000196946	Q6ZN79
CSF1R	down	5	ENSG00000182578	P07333
RAB3IL1	down	11	ENSG00000167994	Q8TBN0
TGM2	down	20	ENSG00000198959	P21980
ACVRL1	down	12	ENSG00000139567	P37023
CD302	down	2	ENSG00000241399	Q8IX05
FRMD4B	down	3	ENSG00000114541	Q9Y2L6
LDLR	down	19	ENSG00000130164	P01130
SPIC	down	12	ENSG00000166211	Q8N5J4
CLN8	down	8	ENSG00000182372	Q9UBY8
MPZL1	down	1	ENSG00000197965	O95297
GPX3	down	5	ENSG00000211445	P22352
PILRB	down	7	ENSG00000121716	Q9UKJ0
PCP4L1	down	1	ENSG00000248485	A6NKN8
CPQ	down	8	ENSG00000104324	Q9Y646
CDH5	down	16	ENSG00000179776	P33151
C6	down	5	ENSG00000039537	P13671
RPS27	down	1	ENSG00000177954	P42677
CD68	down	17	ENSG00000129226	P34810
AIF1	down	6	ENSG00000204472	P55008
PTGS1	down	9	ENSG00000095303	P23219
ENG	down	9	ENSG00000106991	P17813
CAMK1	down	3	ENSG00000134072	Q14012
PILRA	down	7	ENSG00000085514	Q9UKJ1
HFE	down	6	ENSG00000010704	Q30201
TLR3	down	4	ENSG00000164342	O15455
PLA2G7	down	6	ENSG00000146070	Q13093
SIGLEC9	down	19	ENSG00000129450	Q9Y336
PLBD1	down	12	ENSG00000121316	Q6P4A8
DMPK	down	19	ENSG00000104936	Q09013
TGFBI	down	5	ENSG00000120708	Q15582
APOE	down	19	ENSG00000130203	P02649
BASP1	down	5	ENSG00000176788	P80723
SQLE	down	8	ENSG00000104549	Q14534
P2RY13	down	3	ENSG00000181631	Q9BPV8

Supplemental Table 1. The CXCR4a gene set of hyperactivated CXCR signaling in murine B cells

List of genes significantly up-/downregulated in B cells DEGs (protein coding, $p_{adj} < 0.05$; logFC > 0.5 or < -0.5), compared to *WT* controls including as well as well as designation whether they were up- or downregulated, location on which chromosome and Ensembl and Uniprot identification codes.

8 List of Figures

9 List of Tables

10 Acknowledgements

I would like to express my deepest gratitude to my primary supervisor, Professor Ulrich Keller, whose guidance, invaluable insights, and support have been instrumental throughout the entirety of this research journey. His expertise, patience, and encouragement have been truly inspiring and pivotal in shaping this thesis.

I am also deeply indebted to Stefan Habringer, who mentored me and introduced me to lab work, for his constructive feedback, thoughtful suggestions, and continuous encouragement. His guidance significantly contributed to the development of my scientific career and was pivotal to the quality and depth of this work. I would also like to thank him for his friendship aside from research and the amazing time in Munich and Berlin we shared, which I am equally grateful for.

Additionally, I would like to thank both the addiotional mentors of my thesis committee Professor Robert Oostendorp and Professor Maximilian Reichert for their insightful comments and encouragement in the committee meetings and throughout the work.

I also want to genuinely thank my colleague and later also flat mate Markus Schick, who I am profoundly grateful for his remarkable input, unfailing guidance, and steadfast friendship. His insightful discussions, be it on matters of research or private, have played an integral role in shaping the direction of my career. The two years we shared a flat in Berlin have left a footprint in my life and I will always keep this time dear to me.

Special thanks also extend to Nikita Singh, who was a great colleague and helped with many and especially large murine experiments. I will always be thankful for that help and the chats we had. It couldn’t have been done without you.

Also, I would like to thank all other members of the lab in Munich and Berlin who were part of this journey with me for scientific discussion as well as the time spent aside research.

To my beloved parents, Gabriele and Rory Lewis whose boundless love, unwavering support, and endless sacrifices have been the cornerstone of my life. Your constant encouragement

and belief in my aspirations have been a driving force. I owe everything to you and will always be in your debt.

I also extend my heartfelt gratitude to my brothers, Steven, Daniel, and Yannick, for their constant support. I am forever grateful for their presence in my life.

11 List of Publications

11.1 Articles in peer-reviewed journals

Lewis RI, Seuthe K, Lennartz S, Weber JP, Kreuzberg N, Klingel K, Bröckelmann PJ. *Case Report: Sudden very late-onset near fatal PD1 inhibitor-associated myocarditis with out-of-hospital cardiac arrest after >2.5 years of pembrolizumab treatment.* **Frontiers in Cardiovascular Medicine (2024)**

Heger JM, Mattlener J, Schneider J, Gödel P, Sieg N, Ullrich F, **Lewis R**, Bucaciuc-Mracica T, Schwarz RF, Rueß D, Ruge MI, Montesinos-Rongen M, Deckert M, Blau T, Kutsch N, Balke-Want H, Weiss J, Becker K, Reinhardt HC, Hallek M, Borchmann P, von Tresckow B, Borchmann S. *Entirely noninvasive outcome prediction in central nervous system lymphomas using circulating tumor DNA*. **Blood 8;143(6):522-534 (2024)**

Schick M, Zhang L, Maurer S, Maurer C, Isaakidis K, Schneider L, Schunck K, Rohleder E, Hofstetter J, Baluapuri A, Schergern AK, Slotta-Huspenina J, Weber J, Engleitner T, Maresch R, Slawska J, **Lewis R**, Istvanffy R, Habringer S, Steiger K, Baiker A, Oostendorp R, Miething C, Lenhof H-P, Bassermann F, Chapuy B, Wirth M, Wolf E, Rad R, Müller S, Keller U. *Actionable genetic alterations of the SUMO isopeptidase SENP6 drive lymphomagenesis and genetic instability in diffuse large B-cell lymphoma*. **Nature Communications 13, 281 (2022)**

Lewis R, Habringer S, Kircher M, Hefter M, Peuker CA, Werner RA, Ademaj-Kospiri V, Gäble A, Weber W, Wester H-J, Buck A, Herhaus P, Lapa C, Keller U, *Investigation of spleen CXCR4 expression by [^{68}Ga]Pentixafor PET in a cohort of 145 solid cancer patients*. **EJNMMI Research 11, 77 (2021)**

Lewis R, Maurer HC, Singh N, Gonzalez-Menendez I, Wirth M, Schick M, Zhang L, Isaakidis K, Scherger AK, Schulze V, Lu J, Zenz T, Steiger K, Rad R, Quintanilla-Martinez L, Espeli M, Balabanian K, Keller U*, Habringer S*. *CXCR4 hyperactivation cooperates with TCL1 in CLL development and aggressiveness.* **Leukemia 35 2895-2905 (2021)**

O'Connor T, Zhou X, Kosla J, Adili A, Garcia Beccaria M, Kotsiliti E, Pfister D, Johlke AL, Sinha A, Sankowski R, Schick M, **Lewis R**, Dokalis N, Seubert B, Höchst B, Inverso D, Heide D, Zhang W, Weihrich P, Manske K, Wohlleber D, Anton M, Hoellein A, Seleznik G, Bremer J, Bleul S, Augustin HG, Scherer F, Koedel U, Weber A, Protzer U, Förster R, Wirth T, Aguzzi A,

Meissner F, Prinz M, Baumann B, Höpken UE, Knolle PA, von Baumgarten L, Keller U, Heikenwalder M. *Age-Related Gliosis Promotes Central Nervous System Lymphoma through CCL19-Mediated Tumor Cell Retention.* **Cancer Cell 2019 Sep 16;36(3)**

11.2 Conference Contributions

Wendler J, Heger JM, Kutilina A, Knott M, **Lewis R**, Isbell LK, Valk E, Borchmann P, Schorb E, Illerhaus G. *Pre-phase treatment with rituximab and high-dose methotrexate (R-MTX) in primary and secondary central nervous system lymphoma - a retrospective multicentre study to evaluate feasibility, tolerability and efficacy in routine care*. **Jahrestagung der DGHO 2023, Hamburg (Poster)**

Heger JM, Mattlener J, Gödel P, Balke-Want H, Sieg N, Kutsch N, **Lewis R**, Ullrich F, Schwarz RF, Becker K, Weiss J, Reinhardt HC, Hallek M, Borchmann P, von Tresckow B, Borchmann S. *Peripheral blood ctDNA-sequencing enables prediction of outcomes in patients with primary central nervous system lymphoma using a dynamic risk model*. **EHA 2023 Frankfurt (Poster)**

Lewis R, Habringer S, Peuker CA, Ademaj-Kospiri V, Hefter M, Weber W, Buck A, Herhaus P, Lapa C, Keller U, *Investigation of spleen CXCR4 expression by [^{68}Ga]Pentixafor PET in a cohort of 145 solid cancer patients* **Jahrestagung der DGHO 2021, Berlin (Poster)**

Lewis R, Habringer S, Singh N, Keller U. *Aktiviertes CXCR4 Signaling akzeleriert TCL-1 getriebene Lymphomagenese / Activated CXCR4 signaling accelerates TCL-1 driven lymphomagenesis.* **Jahrestagung der DGHO 2019, Berlin (Presentation)**

12 Curriculum Vitae

The curriculum vitae has been removed from the publication for reasons of personal data protection as to TUM guidelines.